ABSTRACT

Nondestructive Evaluation of Out-of-Plane Wrinkles Within Woven Carbon Fiber Reinforced Plastics (CFRP) Using Ultrasonic Detection

William Hugh Minnie, M.S.

Mentor: David A. Jack, Ph.D.

In the automotive and aerospace industries composite materials are heavily utilized as they provide a great strength to weight ratio relative to their metallic counterparts. A drawback is they require complex manufacturing processes, and the final part performance is sensitive to internal defects. Of focus in the present study are out-of-plane wrinkles, specifically those not identifiable by visual inspection. A methodology is presented to manufacture composite laminates with intentional wrinkle defects requiring a multistage fabrication process. The manufactured parts are inspected using ultrasonic immersion scanning with full waveform capture. An automated methodology is presented in this thesis to track the wrinkle within a single lamina across the scan area resulting in a 3D plot of the wrinkle. The ultrasound data was aligned with 3D microscopy data resulting in average relative errors over all sample regions studied for the height, width, and intensity of the wrinkle of, respectively, 4.9%, 4.5% and 6.0%, with average absolute errors were 0.037 mm, 0.47 mm and 0.002, respectively.

Nondestructive Evaluation of Out-of-Plane Wrinkles Within Woven Carbon Fiber Reinforced Plastics (CFRP) Using Ultrasonic Detection

by

William Hugh Minnie, B.S.

A Thesis

Department of Mechanical Engineering

____

Paul Ro, Ph.D., Chairperson

Submitted to the Graduate Faculty of
Baylor University in Partial Fulfillment of the
Requirements for the Degree
of

Master of Science

Approved by the Thesis Committee

____

David A. Jack, Ph.D.

____

Abhendra Singh, Ph.D.

____

Ian Gravagne, Ph.D.

Accepted by the Graduate School

August 2021

____

J. Larry Lyon, Ph.D., Dean

Page bearing signatures is kept on file in the Graduate School.

TABLE OF CONTENTS

LIST OF FIGURES

LIST OF TABLES

ACKNOWLEDGMENTS

I would like to thank my wife, Erin, for all of her love, support, and encouragement throughout this process of going back to school and pursuing a graduate degree. I would like to thank my dogs, Bagby and Obi, for making me laugh when I was overwhelmed and for always being happy to see me come home.

I would like thank Dr. David Jack for giving me the opportunity to come back and join the SI'CEM group again for my graduate studies. I am thankful for your encouragement through this process, and for your guidance and direction when I was lost or confused.

I would like to acknowledge all those in the SI'CEM research group for all of their help with my research. Especially those involved with nondestructive evaluation for training me in how use our experimental set ups, software, and code needed for analysis.

I would like to thank L3 Harris for my initial research funding as I was getting started, and to thank Verifi Technologies for my current funding. Thank you both for your investment into research at Baylor University.

CHAPTER ONE

Literature Review

1.1 Introduction

The use of composite materials across the aerospace, automotive, and renewable energy industries has continually grown over recent years because of their strength to weight ratio. The strength of the composite material comes from the integration of high strength fibers and low strength polymers matrices holding the fibers together [1]. The use of two different materials to make a part leads to the need for complex manufacturing processes, such as vacuum resin transfer method (VARTM), filament winding, autoclave processing, injection molding or compression molding [1]. These complex processes lead to potential defects appearing within the composite, as for example fiber wrinkling or more specifically to this work out-of-plane wrinkling [2][3].

Detecting and characterizing out-of-plane wrinkles using nondestructive evaluation (NDE) is a concern within the aerospace industry, as can be seen from the patents by Boeing about this topic, see e.g. [2][3][4]. Wrinkles have the potential to greatly reduce the strength properties of the composites they are in [5]. One of the challenges for NDE of wrinkles is the quantification of the wrinkle dimensions of the manufactured part without destructive testing methods. Often the only option available is to section the material sample to find the wrinkle and then quantify it with microscopy [4]. This is not preferred as it damages the composite preventing it from any future use. Another difficulty of wrinkle detection is that they are hidden within the thickness of the composite and are not visually detectable by surface inspections, making it difficult to find them, see e.g. [2][3][4].

Therefore, developing a method to find wrinkles is one of the goals of this research. A second challenge is making a laminate with a controlled embedded wrinkle without any visually discernable defect. This work focuses on creation of plain weave composite laminates with embedded out-of-plane wrinkles of a known size that are unidentifiable from a surface inspection, detecting and quantifying the wrinkle using ultrasonic NDE, and then validate the ultrasound using 3D microscopy.

The main technical and scientific accomplishments of this work are as follows:

- The fabrication of composite laminates with intentional out-of-plane wrinkles of a known size
- Detection and subsequent analysis methodology for the automated 3D mapping of out-of-plane of wrinkles using ultrasonic scanning on plane weave carbon fiber composites
- Wrinkle size validation using 3D microscopy

The rest of this chapter presents a literature review about wrinkles within composite materials and how they can be detected. A discussion on the types of wrinkles and how they are characterized will be reviewed. Followed by the effect wrinkles have on reducing material properties and models to predict these reductions. A simplified approximation of how a few measured wrinkles could affect a sample composite is explored. The mechanisms for how wrinkles form and methods for fabricating composites with out-of-plane wrinkles are reviewed. Ending with a study of current nondestructive evaluation practices used for wrinkle detection with a focus on out-of-plane wrinkles.

Chapter two presents the manufacturing processes and challenges within this study. A review of the different manufacturing methods used will be discussed along with an overview of several methods tried for creating an out-of-plane wrinkle within a composite. The chapter then focus upon the new method for fabricating a consistent wrinkle using a two stage hot-press method that forms the structure in stages. Ending with the use of the 3D microscopy to validate the fabricated wrinkle size.

Chapter three discusses the NDE systems used in this study. A breakdown of the immersion scanning system and how scans are setup is covered. The data analysis implemented for ultrasound scans is reviewed. Finally, the methods for modeling the ultrasound wrinkle and comparing it to 3D microscopy will be presented.

Chapter four presents the results of the ultrasound scans compared to the 3D microscopy scans. Data from different ultrasonic transducers and different composites will be presented for validation of the method presented in this work. Comparison to similar work will be shown.

Chapter five concludes with accomplishments of this work and the future work opportunities for wrinkle investigation.

1.2 What is a Wrinkle?

In the composites world there are two main types of wrinkles that can form in laminates, in-plane and out-of-plane. For this work when the term wrinkle as it will be used is referring to a single arch within a straight line, typically an individual lamina, a graphical representation of this is seen in Figure 1.1. This representation of a wrinkle is common amongst many NDE studies and analytical strength models (see e.g., [5][6] [7] [8] [9][10]) and will be adopted in the present thesis. From the depiction of Figure 1.1 there are two main dimensions of interest, the height (h) and the width (w) of the wrinkle. The height is the equivalent of two times the amplitude A of the equivalent wave of the wrinkle

$$A = \frac{h}{2} \tag{1.1}$$

and the intensity I or severity of a wrinkle can found as

$$I = \frac{A}{w} = \frac{h}{2w} \tag{1.2}$$

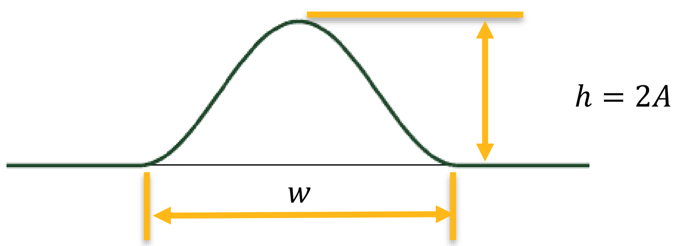

Figure 1.1, Dimensions of a wrinkle

An in-plane wrinkle represents a wave disruption or misalignment of the fibers within a lamina of a composite. These wrinkles are limited in mainly effecting the lamina they are present in,but can affect other layers too causing disturbances to occur in the surrounding lamina (see e.g., [11]). An illustration of an in-plane wrinkle can be seen in Figure 1.2. As seen in the figure the wrinkle only effects the fibers in the x_1 and x_2 directions and not in the x_3 or thickness direction.

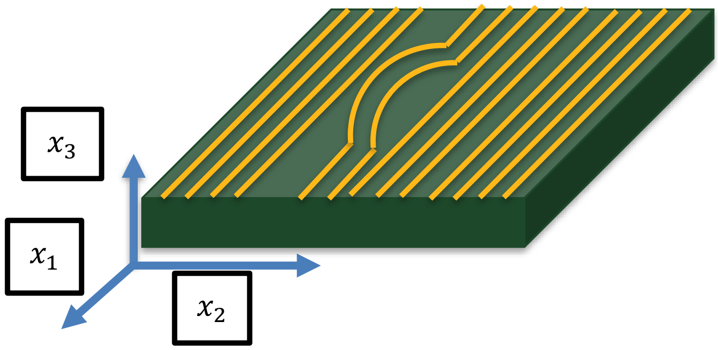

Figure 1.2, In-plane wrinkle

Out-of-plane wrinkles are waves within the thickness of a composite and typically affect multiple lamina. These types of wrinkles affect the lamina above and below them. The wrinkle will propagate through the other lamina until it is dissipated. A diagram of an out-of-plane wrinkle can be seen in Figure 1.3, where its main affects are seen in the laminates x_3 direction.

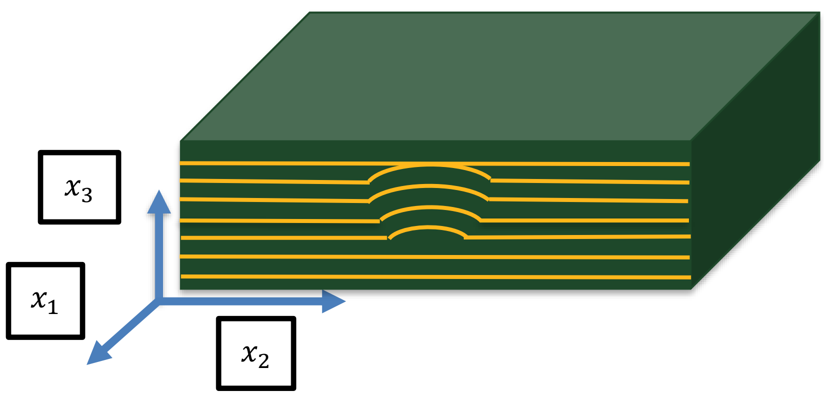

Figure 1.3, Out-of-plane wrinkle

There is another form of wrinkling called marcelling, which refers to repeating wrinkles (see e.g., [12]). A sinusoidal or cosine type wave would make this type of wrinkle. This is more common in in-plane wrinkling especially within in unidirectional fiber lamina.

For this study as mentioned earlier the main focus will be on out-of-plane wrinkles within carbon fiber composites. The goal is to fabricate a series of panels with consistent and controllable wrinkles without a visible indication of their presence, and then using ultrasonic testing and analysis of the captured waveforms quantify the height and width of the wrinkle as seen in Figure 1.1.

1.3 Effects of Wrinkles on Composite Laminates

Wrinkles in all their forms are not beneficial to composite laminates, when they are present, they can cause a weakening of the material properties. This next section will go over some of the results from other researchers on how wrinkles effect composites material properties as motivation for the need to properly characterize an embedded wrinkle and to provide insight into the required sensitivity of the non-destructive technique. This section culminates with a simple numerical demonstration of the sensitivity of the stiffness for a laminated composite with an embedded wrinkle.

1.3.1 Research on the Effects of Out-of-Plane Wrinkles

Fiber reinforced composites find their strength from the alignment of the fibers in the desired direction for loading. The fibers can all be considered as beams or rods, and as such they are stronger when they are straight with no wrinkling or bends. When wrinkles are present within laminates they induce buckling within the fibers. This preset buckling configuration weakens the composites in their loading direction, in both compression and tension loading configurations [12] [13].

In the study by Chenjun Wu *et al.*, the authors investigate the effects of a range of out-of-plane wrinkles with intensities from 0.016 to 0.037 on composite material properties [12]. The laminates they produced were all unidirectional prepregs and they used a transverse strip method to create the out-of-plane wrinkles, similar to what is seen in [14]. From the laminates that were tested their results did not show a significant reduction of the tensile strength. But for their compression strength and modulus they found a reduction of 33.0 % and 14.4 % for their highest intensity of 0.037.

The work done by Krumenacker *et al*. showed that their samples received a 30.7% reduction to the in-plane stiffness [12]. Their laminates were made of unidirectional prepregs with a corner mold using a vacuum bag method to manufacture the composite.

Pham *et al.* modeled the compressive failure of composites with waviness in both 2D and 3D models [15]. They have shown, like others, that when waviness is present it can reduce the compressive properties of composites. As the misalignment angle increases or as the intensity increases the effect on the material properties is greater, and similar results were seen in the work done by Bender *et al.* [16].

Kulkarni *et al.* did a review on the effects of fiber waviness within composite laminates looking at the effects across many material properties [10]. The authors reviewed many works done on actual samples and using analytical models, with the results they discovered in the literature showing a reduction of the material performance ranging from 10 % to 75 % based upon material system, loading configuration, and wrinkle extent. Typically, the reduction in the compressive properties of the laminates was seen to be higher than that of the tension properties.

1.3.2 Fiber Waviness Analytical Models

One of the first groups to popularize the description of a wrinkle, as shown in Figure 1.1, was Hsiao and Daniel in their work on fiber waviness [5]. They showed for their uniform waviness sample with a wrinkle intensity of 0.043, that they have about a 50 % reduction in the normalized Young's modulus in the direction of the fibers. The relative error they had between their experimental and analytical model was only 3.8 %. Their effort has served as the basis for many subsequent authors for modeling the effects of out-of-plane wrinkles on composite laminates, (see e.g. [7] [8]).

Figure 1.4 is an example the Hsiao-Daniel model incorporated in [9] comparing normalized stiffness to the intensity of fiber waviness. There are three curves representing the different directional stiffness's, red is for the fiber direction E_{11}, green is for the transverse direction E_{22}, and blue represents the vertical direction E_{33}. The loading for the model in in the E_{11} which is why this curve sees the main effects of increased fiber waviness intensity. The E_{22} is not affected by the waviness, but E_{33} with an initial loss then has an increase as the fibers become more aligned in the vertical direction.

Zhu [7] employed the Hsiao-Daniel model as a building block on modeling the effects of fiber waviness on composite laminates. In the work by Zhu, composite laminates with a uniform and a graded wrinkle is studied. Their model showed that the uniform wrinkle caused greater reduction in stiffness over that of the graded wrinkle. The graded wrinkle represented a wrinkle were the amplitude reduced linearly, instead of having uniform amplitude across the wrinkle area. The graded wrinkle represents a more realistic out-of-plane wrinkle that would be seen within a laminate, similar to the wrinkles seen in Figure 1.5.

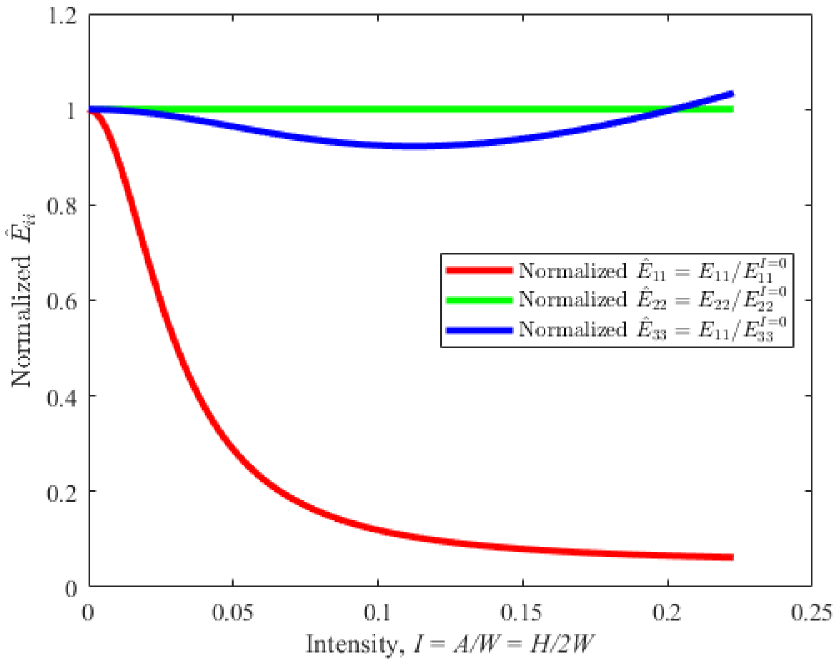

Figure 1.4, Normalized stiffness verse wrinkle intensity for unidirectional composite loaded in the fiber direction. Red is for the E_{11}, blue is for E_{22}, and green is for E_{33} [9].

The work of Takeda et al. [8] further builds on Zhu's and Hsiao-Daniel's efforts, by developing the model to incorporate different laminate layups. Zhu looked at bidirectional layups as well as unidirectional, whereas Takeda et al. considered quasi-isotropic layups and varying thicknesses. The work compared many different layups over a range of wrinkle intensities, consistently showing reductions in the stiffness in the loading direction as the wrinkle intensity increased. The results of [8] were in line with the other studies seen.

1.3.3 Approximate Stiffness Reduction of a Composite with and Out-of-Plane Wrinkle

A previous researcher, Zhang [9], used the Hsiao-Daniel model for fiber waviness predictions. Part of the code they developed will be used to make some stiffness reduction approximations.

Consider the composite in Figure 1.5, a sample of an carbon fiber composite structure provided by NDE Labs of Fort Worth, Texas, with out-of-plane wrinkles through its thickness. When using a simple inspection using a ruler on the sectioned surface for the three wrinkles shown in Figure 1.6, an approximate size and intensity of three wrinkles can be found, and the results are summarized in Table 1.1 along with the calculated intensity of Equation 1.2. The wrinkle intensity values are then taken and put into the Hsiao-Daniel model as seen in Figure 1.6. From this plot it can be seen that these wrinkles can cause a significant knock down on the stiffness in the loading direction of the composite.

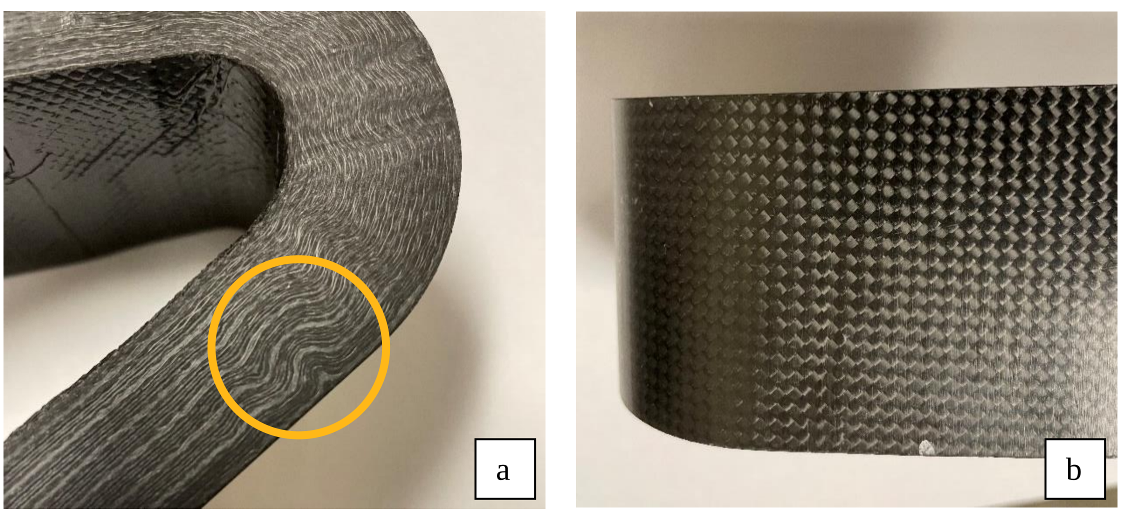

Figure 1.5, NDE Lab wing spar laminate showing out-of-plane wrinkles that are not visible on the outer surface.

Table 1.1 Approximated Wrinkle Sizes

Name	Width (mm)	Height (mm)	Intensity
Wrinkle 1	14	3	0.11
Wrinkle 2	12	3	0.125
Wrinkle 3	7	3	0.21

For clarity the model used to create the plot in Figure 1.7 comes from a model based on an entirely unidirectional composite laminate axially loaded in the fiber direction. The part in Figure 1.5 appears to be made of unidirectional fibers, but the layup is unclear. This part is of a curved geometry which is not accounted for in the model. Therefore, this is only a conservative approximation on the potential stiffness reductions caused by the out-of-plane wrinkles within the composite laminate.

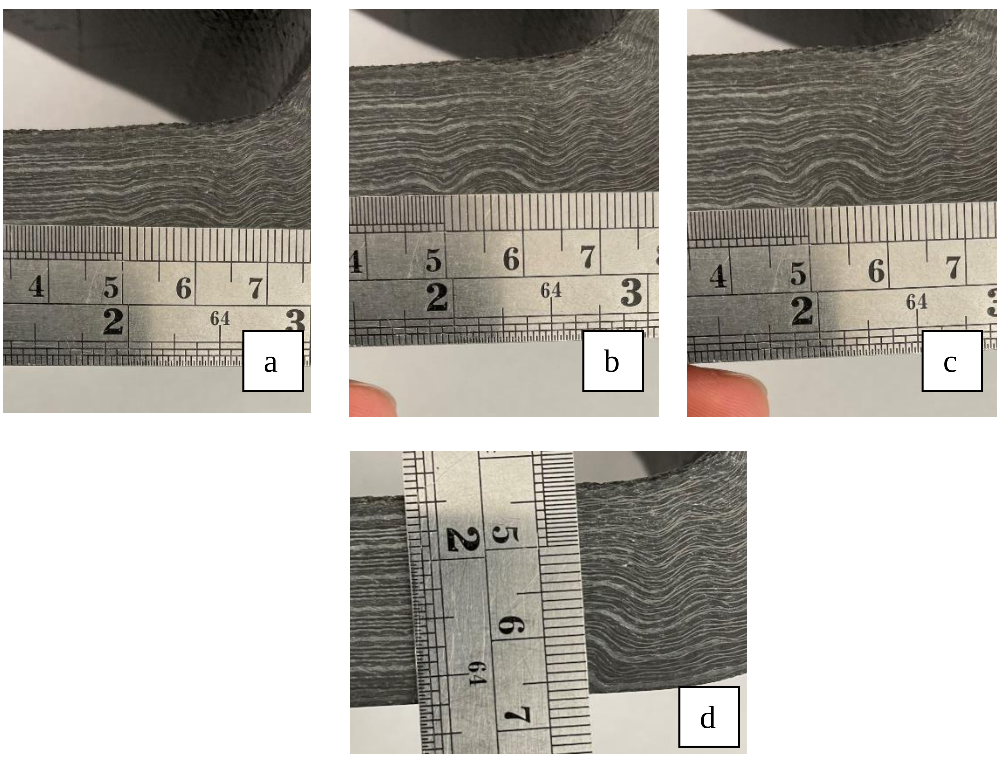

Figure 1.6, Measurement approximations for the size of three out-of-plane wrinkles, a) Wrinkle 1, b) Wrinkle 2, c) Wrinkle 3, and d) used for height approximation.

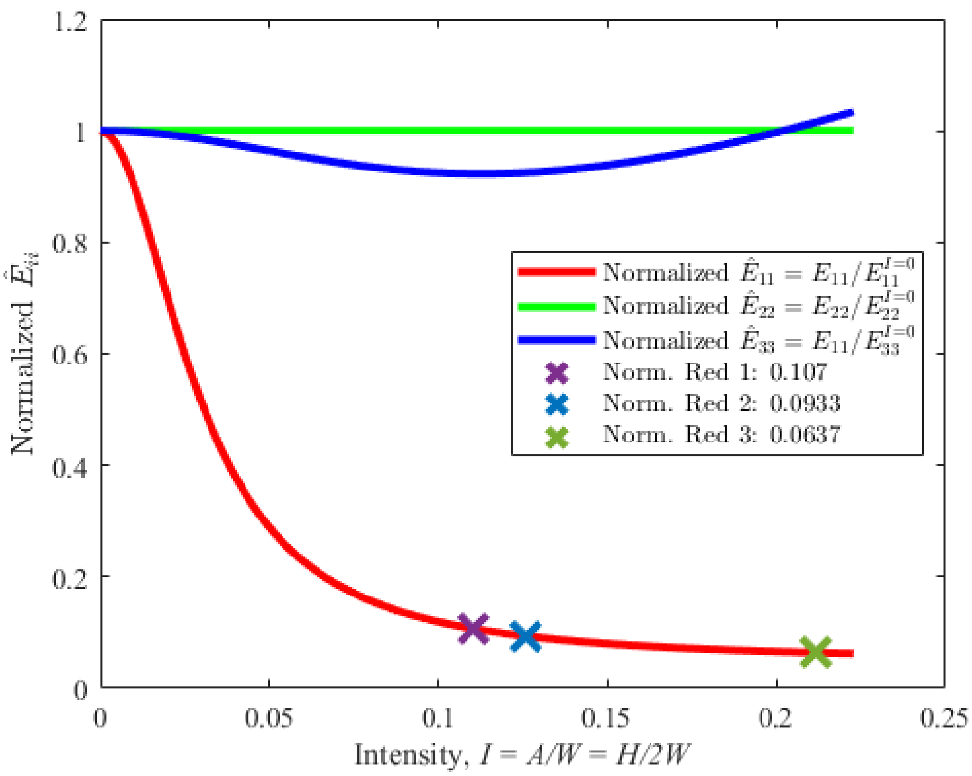

Figure 1.7, Hsaio-Daniel Normalized Stiffness with approximated wrinkle reductions based on work from [9]

1.4 How Do Wrinkles Form

Composite laminates are made up of multiple lamina of fibers whether unidirectional or woven, prepreg or dry. The stacking of lamina is a delicate process that can be done by hand or by an automated process such as composite winding. As the stacking sequence becomes more nuanced and/or the geometry more complex the introduction of wrinkles within the fiber layers is more common. The interaction of the fiber layers to one another, fibers to tools and/or the complex geometry are some of the main causes of fiber wrinkles (see e.g., [10][17][18]). An example of a part with a wrinkle is shown in Figure 1.5, with three different wrinkles shown in Figure 1.6. Notice that each of the examples are of different wrinkle intensities and formed in different regions of the part due to various processing considerations.

Wrinkles can form in multiple ways, but a way to visualize their formation can be made by thinking of a laying a blanket or towel over a bowl. As it is laid down it will not conform perfectly to the bowl, wrinkles will form as a result. An example of this with woven fiber glass lamina is found in the paper by Guzman-Maldonado *et. all* [17]. They stretched out uncoated woven fibers over an opening and slowly raised a dome mold into the fibers to see how wrinkles formed. They showed that in plane compression forces and high friction between lamina are some of the main causes of why wrinkles occur.

A similar study with dry fibers was done in [18], where instead of draping the raw fibers over a dome they used a biaxial extension test and pulled them to induce wrinkles. Pictures were taken at various displacements and image processing techniques were used to find the properties of the wrinkles. They showed that as the displacement of the lamina increased the size of the out of plane wrinkle grew as well. Another factor they discussed that caused wrinkle formation is the compression of bending layers to conform to the mold.

Hot drape forming is another common method of laminate fabrication, where lamina are heated up and then they are laid onto mold to create a laminates of complex geometry. In [19] wrinkle formation during hot drape forming over a mold to create a C-shaped laminate was investigated. They compared laying up the fibers at 20 °C and 70 °C to see how this affected wrinkle formation. Their results showed there was a reduction in wrinkles when the part was made at the elevated temperature. They believe this is the result of lower friction between plies at higher temperature because the viscosity of the resin is reduced.

Another major cause of wrinkle formation in composites comes from the shear stress between lamina. Lightfoot *et al.* [20] worked with C-shaped laminates as well but theirs were made inside of a C-channel shaped mold instead of on the outer surface. Their experiments proved that when the release film between the tool and the lamina is removed the frictional shear stress is increased. This increased shear stress reduces the potential for wrinkles to form within the laminate whether in-plane or out-of-plane wrinkles.

The process of laying up lamina for a complex composite geometry and not distorting the lamina to form a wrinkle is one of the challenges of composite manufacturing. As shown from the papers above there are a variety of factors that can cause fiber wrinkle or misalignment in composites.

1.5 The Manufacturing of Composites with Out-of-Plane Wrinkles.

One of the challenges for investigating out-of-plane wrinkles or even in-plane wrinkles within composites is intentionally placing them in a sample. Typically, in research the samples that are made are desired to be defect free. Therefore, it takes some creativity on the researchers to develop ways to intentionally add wrinkles in a controllable manner.

There have been many different methods developed for manufacturing laminates with out of plane wrinkles. One method involves using thin prepreg strips to create the wrinkle, the strips are laid across the laminate transversely to the main fiber direction [14]. Multiple strips of prepreg fibers were stacked up to create the desired wrinkle height. Some drawbacks are there can be resin rich regions or voids, and some residual stress caused by the transverse prepreg strips. Another method they developed was to create a wrinkle within a laminate with uniform thickness using a double ply drop. This meant there where two lamina that were half the length of the part, and each was placed at a different layer on opposite sides of the laminate. The result of this method was the wrinkle was an s-shape or half a wrinkle, which in relation to this study was not ideal.

The most promising form of manufacturing appeared to be a method of incorporating multiple cures to form the laminate, (see e.g. [6] [21]). This method involves either partially curing or fully curing part of the laminate to induce the wrinkle within it. In [6] a hot press was used with one plate that had a wrinkle mold to induce the out-of-plane wrinkle in the laminate during the first cure. After this first cure another set of prepreg laminas would be laid on top and would then be put back into the press for the second cure. This method did have limitations in that voids and resin rich regions would form because of the stiffness of the prepregs to form to the shape of their wrinkle.

Hsiao and Daniel did a similar method of multistage curing but theirs involved three different cures [21]. They would first partially cure the laminates in three parts. The top and bottom panels are formed flat, and the middle component contains the waviness. The three parts are then sandwiched together creating a flat laminate with a gradual waviness throughout.

As will be discussed in more detail in Chapter Two, the process of using multiple cure steps for manufacturing composites yields parts with acceptable out-of-plane wrinkles. This allows for the fabrication of laminates with wrinkles of a known size in the middle and will gradually decrease in size throughout the laminate. The result is similar to what is seen in Figure 1.5 where the wrinkle severity or intensity changes through the thickness of the laminate.

Another benefit of the multistage curing process is that it allows the wrinkle to be hidden within the thickness of the laminate. For some of the parts in [6] the bottom surface of the laminate showed the wrinkle. To enhance the industrial relevance the present research focuses on manufacturing methods to form a part with a wrinkle that is not visually detectable on the back or front surface. The reflections of the front and back surfaces are typically the strongest signals from the ultrasonic reflection wave, and any features near the exterior surface would cause an acoustic reflection thus providing a false confidence in the ability to identify a wrinkle when moving to an industrial setting. Therefore, removing any visual indication on the exterior surfaces of an interior wrinkle is desirable, as seen by the concern of Boeing, (see e.g. [2][3][4]). In addition, any fabrication method that has porosity or a resin rich region on the wrinkle plane cause an acoustic reflection that would be more easily identified but would be undesirable as these features would not be representative of the physical system being simulated.

1.6 Nondestructive Evaluation of Wrinkles Within Composites

Nondestructive evaluation (NDE) or testing (NDT) of composites has been around for many years and continues to grow as the technology improves and the use of composites becomes more common. In relation to wrinkle detection within composite materials the main technologies used for detection are eddy current (see e.g., [22][23][24]), computed tomography (CT) (see e.g. [10] [25] [26]), and ultrasonics (see e.g., [6] [25] [26] [27]). The need to detect wrinkles and the ability to quantify their respective intensity and relative orientation direction as a function of spatial location is a growing concern within industry (see e.g., [2][3][4]).

The focus of this thesis is the use of ultrasonic NDE to find and characterize out-of-plane wrinkles. The current section presents a review of select existing NDE techniques for wrinkle detection within composites. Many of the current works reviewed for this research involved using unidirectional prepregs to make their laminates, there were a few using woven laminates which is the focus of this work.

1.6.1 Non-ultrasonic Nondestructive Evaluation (NDE) of Composites with Wrinkles.

Eddy current technology has been used to investigate wrinkles within composite materials and the main success with this technology has been with detecting in-plane fiber waviness (see e.g., [22][23] [24]). One of limitations for detecting in-plane waviness is that the eddy current coils need to be in-line with the fiber direction for the best result. The work done by Mizukami, was able to detect out-of-plane waviness and could find the peak of it in the complex plane with about 2 % relative error but was not able to quantify the size of the wrinkle.

Computed tomography (CT) X-ray scanning provides the ability obtain highly detailed scans at a resolution of ~500 nm [28], which can easily detect individual carbon fibers composite materials [1]. The limitation of the technology is that it is expensive, time consuming and not practical for work in the field. In regard to out-of-plane wrinkle research the technology is being used as a means to validate other NDE methods, (see e.g. [10] [25] [26]).

1.6.2 Ultrasonic Nondestructive Evaluation of Composites with Wrinkles

Nondestructive evaluation of composites using ultrasound is a topic of interest among researchers, see e.g. ([6][26] [29]-[35]) A range of ultrasonic transducer styles have been used such as single element, phased array, and laser ultrasound. These works have mainly focused on the investigation on wrinkles within unidirectional composite panels. Though some have considered woven composites as in [29] where orthogonal plain weave composites were characterized using ultrasound. Zardan [30] studied satin weave composites with ultrasound and determined beam deviation off the wrinkle was important to take into account when investigating wrinkles.

The ability to characterize the size of wrinkles is mixed within the ultrasound literature. For example, the works in [26][31][32][33] and [34], have shown the ability to detect out-of-plane wrinkles but did not show any qualitative characterization of the wrinkles.

Zhang's work dealt with investigating thick composites with out-of-plane waviness [31]. They used single element immersion probes to perform their ultrasonic scans with a time corrected gain to improve the signal through the laminate. In [32] the authors use laser ultrasound to investigate composites with out-of-plane wrinkles. They showed that when a moving average is applied to a scan area it flattens out the wrinkled zone. To improve the resolution around the wrinkle a tilt filter was developed which is a form of localized averaging between a-scans, resulting in greater wrinkle clarity. Again, both of these studies performed a qualitative identification of the wrinkle, i.e., wrinkle detection, but did not quantify their results or compare the quantified geometry against a known sample.

In [33] ultrasonic scans of both in-plane and out-of-plane wrinkles were processed using the 2D fast Fourier transform (2D FFT). Their results showed a good qualitative detection of the wrinkles within c-scan and b-scan images, even within an 18 mm thick laminate.

The work in [34] investigated composites with out-of-plane wrinkles that were manufactured with unidirectional carbon fiber along with layers of woven glass fibers. They performed scans on these laminates using an ultrasonic phased array with a 16-element aperture and captured sectoral scans from 7°, 0°, and -7°. The results show some definition because of strong reflections from the glass lamina in their samples but were not able to identify the start and end of the wrinkle within their scans. This prevented them from being able to quantify the size of the wrinkle within their laminate samples.

Nelson *et al.* [26] investigated the use of the instantaneous phase of the ultrasonic data in inspecting a composite with out-of-plane wrinkles. They then applied structure tensor analysis to the phase data to find the angles of the lamina. The angles that were found were then overlaid on top of a CT image of the laminate being studied. From their results they were able to find the angle of the wrinkles present which they state is critical for understanding how the composite is weakened, but there were not results provided within the work [26] to demonstrate the accuracy of their method nor a quantification as to the accuracy of the method compared against the provided CT data.

The study in [25] investigates the effects of resin layer thickness from different composite defects on the ultrasound signal. The signal is viewed in three different ways, instantons amplitude, instantaneous phase, and instantaneous frequency. In regard to wrinkles it was found that in the areas where the wrinkle causes the layers to be thinner the instantaneous amplitude and frequency signals are larger. Then in the areas where the layers are further apart the responses of the signals are lower. For the instantaneous phase signal the layer thickness of the plies can cause the resonance mode to change. From their research they have found that when the when the signal is in the first resonance mode out-of-plane wrinkle identification is easier. Similar work was shown in [35] and [36] that applying the Radon transform to the instantaneous phase signal allows for the angle of the wrinkle waviness to be found, and for modeling simulations approximated an uncertainty of 0.25° +5%.

In the work by Pain *et al.* a 5 MHz 64 element phased array transducer was used to scan composites with out-of-plane wrinkles [27]. For their scans they focused on postprocessing the captured waveforms to provide the best results, the main techniques incorporated were the total focusing method (TFM) and average scattering. TFM is considered to be one of the best methods for image postprocessing (see e.g., [37]), it allows for individual pixel focusing across an entire image for a given array of elements. In their work [27] they looked at the amplitude and phase using TFM on their wrinkled composites and were able to detect the presence of a wrinkle. They did not do any quantification as to the dimensions of the wrinkle using the ultrasound results but did use microscopy to show the size of the detected wrinkle having an intensity of 0.017 to 0.18. The average scattering matrix technique was used to investigate the effects of the reflection waves off of the wrinkle within the laminates. This method showed descent results with detecting the presence of waviness within a part, but again it was not shown to quantify it.

The work of [6] studies three ultrasound techniques through the use of phased array incorporating the full-matrix capturing (FMC) with total-focusing method (TFM) or FMC/TFM, Olympus' OmniScan MX2 phased array system, and immersion scanning with a single focused transducer. Similar to the method of TFM described above, FMC/TFM uses a custom firing sequence, where one element fires and then all of the elements receive. This is done for the entire array of elements, the TFM post processing is applied to enhance the image. The OmniScan, a commercial phased array system, is a common system used in industry. For the scans presented in [6], they used 2.25 MHz and 5 MHz frequencies, except for the FMC/TFM which used a 2.5 MHz element instead of a 2.25 MHz.

Larrañaga-Valsero *et al.* [6] investigated a range of unidirectional carbon fiber composites with out-of-plane wrinkles, one unique sample had alternating layers of woven fiber glass for every five layers of carbon fiber. The results for the ultrasound scans are shown in [6] as instantaneous amplitude and phase b-scans. From other work within the same research group (see e.g., [38]) quantifying the max angle of the wrinkle is considered to be the most critical dimension of the wrinkle in regards to its effect on the composites material properties. Larrañaga-Valsero *et al.* were able to measure all of the parameters of the wrinkles as seen in Figure 1.1 with good accuracy to their actual measurements. The measurements were made using an electric ruler on the b-scan that were investigated. Table 1.2 presents the average relative and absolute errors form the samples in [6]. These results will be considered more in Chapter Four as an approximate comparison to the results found in this study since the material systems used are different.

Table 1.2. Average Relative and Absolute Error for samples in [6]

	Relative Error (%)	Absolute Error
Height	10.8	0.575 mm
Width	13.5	5.75 mm
Intensity	16.3	0.013

The study of out-of-plane wrinkles is an area of interest to many researchers, and as can be seen from above it is a challenging problem. There have been many different approaches presented here on how to detect and quantify wrinkles with different NDE techniques. One of the current struggles within this area of work is the ability to accurately characterize out-of-plane wrinkles. This work will present a post processing technique for ultrasound scans for the characterization of out-of-plane wrinkles. The avg relative error for the height, width, and intensity was 4.92 %, 4.45 % and 6.04 % respectively and the average absolute error was 0.0366 mm, 0.4717 mm and 0.0021 respectively.

CHAPTER TWO

Materials and Experimental Setup

2.1 Introduction

The following chapter presents the sample fabrication of carbon fiber laminates with an intentional out-of-plane wrinkles, including several alternative methods, along with the experimental quantification of the surface of the wrinkle using high-resolution 3D microscopy. This characterized surface from each of the fabricated parts will be used in Chapter 4 as part of the validation of the results obtained from the ultrasound scans.

2.2 Carbon Fiber Material System Selection

Carbon fiber laminates can be manufactured in many ways and using variety types of fibers. In this work dry 3K plain weave carbon fibers from ACP Composites, SKU number W-CF-6.0-PW-50-P, are used in the fabrication of the composite laminates. The weight and dimensions of the dry fabric are provided in Table 2.1. The resin system used in this work is the Pro-Set Infusion Epoxy Resin 114 (INF-114) and the Pro-Set Infusion Epoxy 211 Hardener (INF-211). The the mix ratio is 3.65 to 1 resin to hardener, and the cure cycle is eight hours at room temperature followed by at eight hours at 82° C. The manufacturing methods used in this research involve a hybrid multi-step method that uses a combination of vacuum assisted resin transfer molding (VARTM), a wet layup with VARTM and wet layup with hot press. All tooling surface use Partall® Hi-Temp Mold Release Wax as the release agent.

For the wet layup process a programmable hot press is used to aid in the laminate curing. The hot press used in this research is a Carver AutoFour/1512-PL, H with a minimum applied load of 4448 N (1,000 lb_f) and max applied load of 133 kN (15 Tons). The target pressure that was used for the system was 276 kPa (40 psi), which is converted to a load value in pounds for use by the press controller. The setpoint force will be dependent on the on the dimensions of the laminate being manufactured and can be obtained from the pressure as,

$$F = \sigma A \tag{2.1}$$

where F is the setpoint force, σ is the desired stress, and A is the cross-sectional area of the laminate. The press plates are 305 mm (12 in.) by 305 mm (12 in.), so any laminate created will need to be smaller than these dimensions.

At the onset of the study, it was unclear as to the proper pressure to apply to the laminates. Initially a 483 kPa (70 psi) pressure was imposed on the laminates but was determined to be too high because of the displacement of the fibers and the resin on the edge of the laminates. The pressure was lowered to 414 kPa (60 psi) with reasonable results, but the parts were considered too thin because of layer shifting of the lamina and large displacement of resin and fibers at the edges. In parallel to studying manufacturing of the woven laminates and similar study was undertaken using unidirectional carbon fiber prepregs, 14706 high modulus by Rock West Composites The manufacturer recommended a pressure of 40 psi for the similar material system, and it was found during preliminary studies as part of this research that this pressure produced acceptable quality parts for both the unidirectional laminates and the wet-layup woven fabrics. Thus, no further work was performed to optimize the laminates based upon density or wet-out.

Table 2.1 Carbon Fiber Material Properties

Fiber Weave	Fiber Type	Tow Thickness (mm)	Weight, oz/yd^2	Fiber Tow size	Count Wrap x Fill
Plain Weave	Dry Fibers	~2	6.08	3K	13 x 13

2.3 Laminate Fabrication Manufacturing Methods

2.3.1 Vacuum Assisted Resin Transfer Molding (VARTM)

The vacuum assisted resin transfer molding (VARTM) manufacturing process is often used by industry to produce high quality composites with minimal tooling and consumable costs (see e.g., [39]). The VARTM process involves using a vacuum pump to draw the resin system over dry fibers similar to that shown in Figure 2.1. In this study the dry carbon fiber fabrics are placed upon an aluminum tooling surface, which allows smooth glossy finish on one side of the part.

The tool is prepared with Partall® Hi-Temp Wax, typically three coats worth, across the entire tooling surface. This is done by applying the wax with a clean dry cloth, waiting 1-2 minutes, and then wiping the wax off with a second clean dry cloth. The edges of the tooling surface are then cleaned with acetone to provide a clean and wax free surface for the application of the vacuum sealant tape to be applied. The sealant tape is used to provide the seal between the vacuum bag and tooling when creating the vacuum pressure on the part.

The inlet and outlet tubes are then placed on the tooling surface as can be seen in Figure 2.1. The tubes going from the mixed resin to the tool, and from the tool to the waste jar are clear 6.35 mm (0.25 inch) PVC tubing. These tubes are held down in place on the tool using gum tape and are placed just slightly wider than the width of the part.

With the PVC tubes in place, slotted spiral tubing is pushed into each tube to allow the resin to flow quickly across the surface of the laminate. The spiral tubing needs to be close to the sides of the lamina to avoid the bag pressing onto the surface between the infusion tube and the laminate thus preventing resin flow.

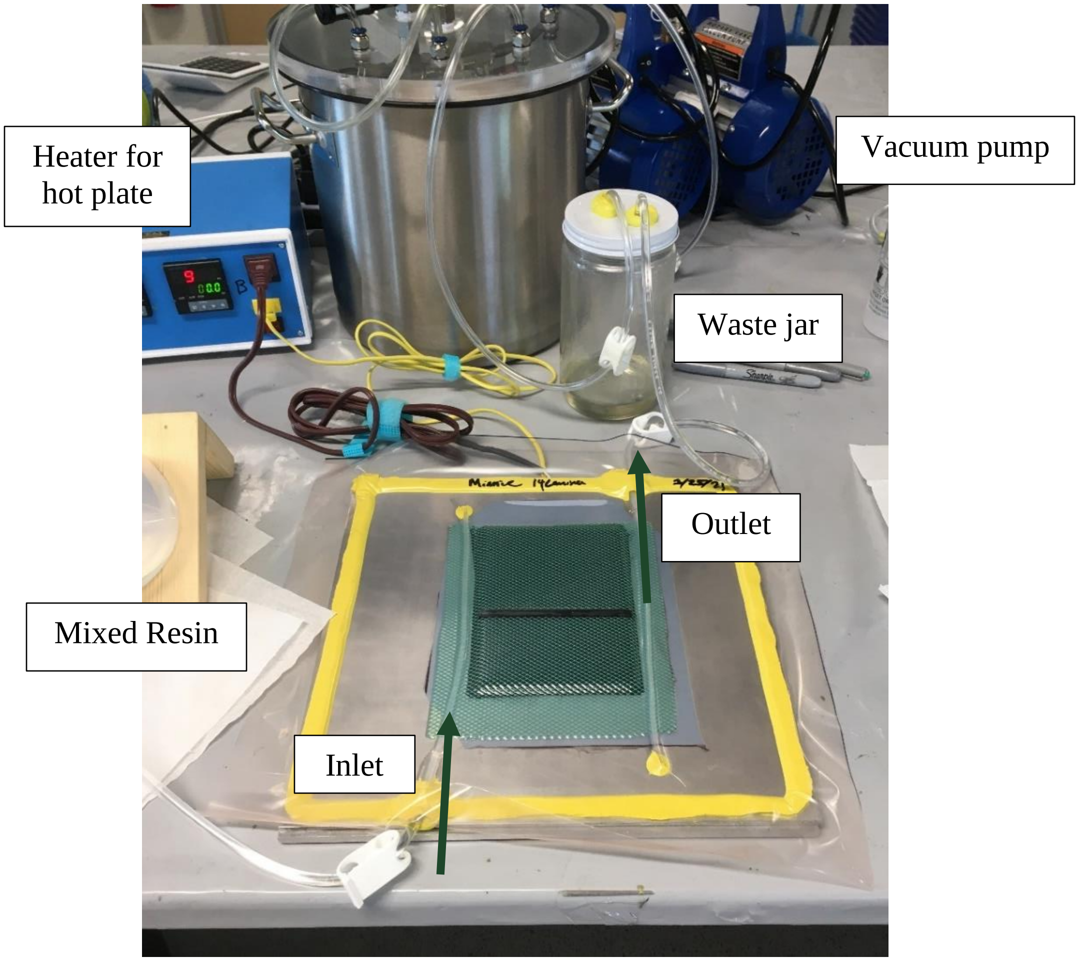

Figure 2.1, Example of a laminate being manufactured using the VARTM method

Once the inlet and outlet tubes are in place, the individual lamina are placed on the tool surface one at a time at various orientations until the desired stack is completed. The peel ply and infusion mesh are then placed on top of the lamina stack. These allow for resin to flow over the top surface of the fibers during infusion and then soaking downward into the part, instead of the need to flow exclusively within the densely packed region of the weave. The peel-ply is porous to the resin in the liquid form, and upon the completion of the cur the peel ply does not adhere to the resin and it allows for relatively easy removal of the bagging material after the part has been cured. The final step is to place the vacuum bag over the entire tool as seen in Figure 2.2. Vacuum is then pulled on the part and any leaks are addressed before infusion.

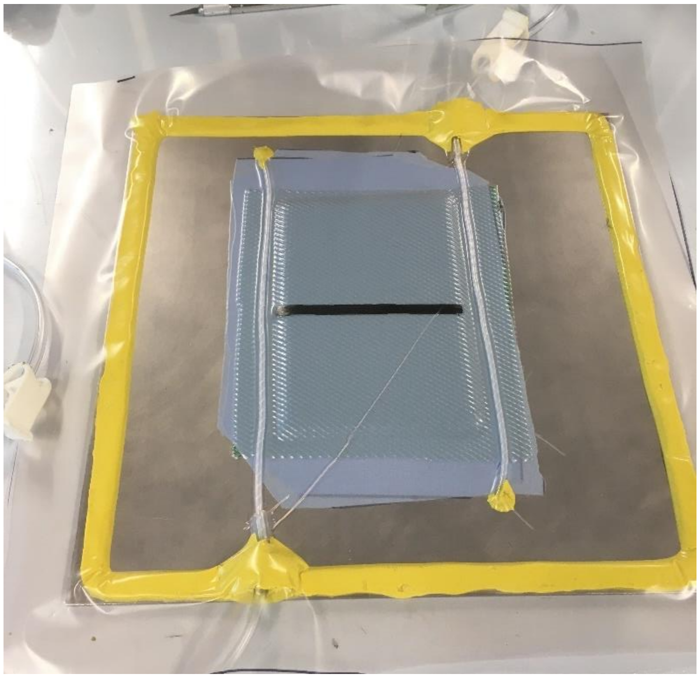

Figure 2.2, The carbon fiber laminate after bagging, prior to infusion while inspecting for any leaks within the vacuum seal.

The vacuum sealed tool with the dry carbon fiber fabric is placed on a heated plate to warm up the tool and the fibers. This will reduce the viscosity of the resin during infusion allowing for complete wet-out of the fiber tows along with complete infusion of the part. The hot plate is set to 100 °F, and the vacuum sealed tool is placed on the hot plate until equilibrium is achieved, typically this is done in 30 minutes.

The resin is mixed using a FlackTech automated mixer. The mixing ratio is 3.65:1, resin to hardener. The mixer initially spins the resin at 800 RPM for 30 seconds and then ramps up to 1500 RPM for 4 minutes and 30 seconds. During the high RPM phase, the mixer pulls vacuum. This process mixes the resin and hardener uniformly and removes the majority of the air within the mixture. Once the resin has been mixed it has an approximate working time of 30 minutes for the infusion process after this time the resin begins gelation, and the increasing viscosity will prevent the resin from flowing. After gelation occurs the part is placed in a programmable convection oven for the curing cycle, during which time vacuum is maintained. The cycle begins with an eight-hour room temperature cure at approximately 22 °C. The convection oven is then set to ramp to 82 °C over a one hour period and then held at 82 °C for eight hours. At the completion of the 8 hour elevated cure, the part is convection cooled within the oven, removed from the oven, and then debagged.

2.3.2 Wet Layup

The second manufacturing method used in this work is wet layup with an applied vacuum pressure and the wet layup process with the programmable hot press. The vacuum bagging and the hot press both serve to reduce the resin mass fraction. The wet layup involves manually applying the resin on to the dry carbon fiber fabric, in this study this was performed using a disposable paint brush. The fibers are then placed on the same aluminum tooling used for the VARTM process, to provide a smooth glossy finish on the part.

The wet layup process starts in a similar manner to the VARTM process. The tool has to be prepped with the Partall® Hi-Temp Wax to prevent the part from sticking.

Again, three layers of wax are applied. A layer of gum tape is placed around the edge of the aluminum tool this is to prevent spillage of the resin and to provide a means to apply vacuum pressure.

The resin is mixed using the FlackTech mixer using the same settings as in the VARTM study. The resin is then applied to the tool surface using a brush prior to the first lamina being placed. After each lamina is placed, the resin it is lightly pressed into the fibers manually using a roller or by hand, this helps to compact the layers. Then a new coat of resin is brushed onto the lamina. This process is repeated until each of the lamina have been placed according to the desired stacking sequence and a final layer of resin is brushed onto the top of the last lamina.

The next step of the process involves removing excess resin, which can be done using vacuum, a press, or a combination that includes pulling vacuum while placing the part within the hot press. For either method using vacuum pressure the laminate requires at least one outlet tube as demonstrated in Figure 2.3a. Once the vacuum bag has been placed over the part, vacuum is pulled on the part and the vacuum seal is inspected and any leaks are addressed. The part is then placed either in the oven or the hot press for the duration of the curing process. One alternative used for some parts in the present study involves the placement of a second aluminum tool in lieu of the peel ply and infusion mesh on top of the last wet layup layer, as seen in Figure 2.3b. Then placing the bagged double tooled composite panel into the programmable hot press. This latter technique is done to provide a smooth and flat tool surface on both sides of the laminate while maintaining a uniform thickness. This double tooling approach could be performed with vacuum pressure only, but no panels using this alternative method were fabricated in the present study. When manufacturing with the hot press the laminate should sit out for six hours prior to subjecting the laminate to the applied load of the hot press, this allows for the resin to approach gelation greatly reducing the viscosity of the resin. This provided acceptable results without disrupting the fiber layup in the processed parts. More on this step will be discussed in the following section.

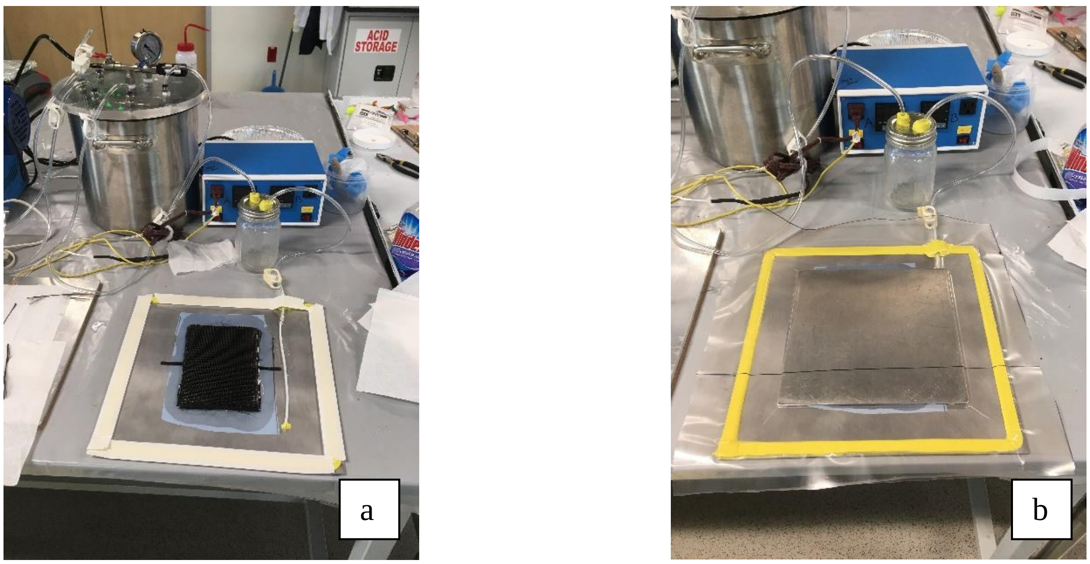

Figure 2.3, Wet-layup panels. a) Wetted lamina prior to the placement of the vacuum bagging material, and b) wetted laminate with aluminum tool showing double tooling method of fabrication.

2.3.3 Hot Press Manufacturing Challenges

Manufacturing composites with the hot press was one of the challenges of this study, as mentioned earlier there were difficulties in figuring out the correct pressure to reduce fiber distortion and misalignment. The resin system used for making laminates in this study is designed for infusion methods of fabrication and not wet layup, which means the mixed resin has a lower viscosity at the beginning of the cure cycle ideal for resin infusion methods such as VARTM. This characteristic of the resin system would cause the mixed resin ooze out of the sides of the laminate resulting in distortions of the fibers and the laminates being thinner than desired. Figure 2.4 shows an example of a laminate with excessive resin leakage resulting in a distorted part and fiber layup.

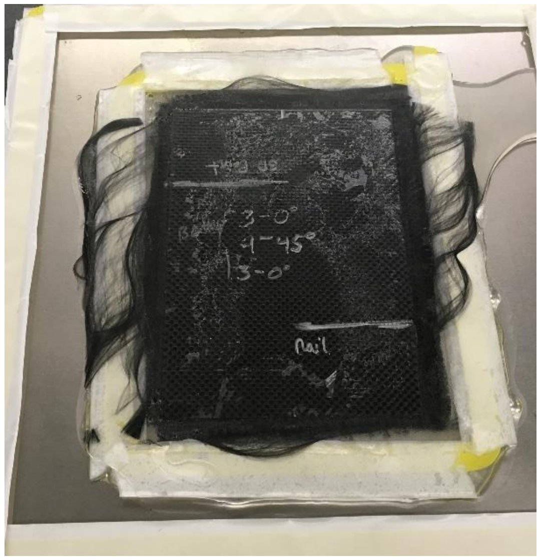

Figure 2.4, Fiber distortion from hot press manufacturing when gelation is not taken into consideration.

In order to overcome the high resin flow, the laminates were not placed in the press immediately after the last layer was laid up in the wet layup process. Instead, the initial gelation process was allowed to progress allowing the polymer chains to extend during the initial b-stage curing thus increasing the viscosity of the resin. Waiting for the full eight hours of gelation to occur would inhibit resin flow when pressed. Based upon some early studies six hours was found to be an appropriate delay prior to subjecting the panel to the applied load from the hot press. A panel with a four hour delay to allow for gelation was prepared, but as shown in Figure 2.5a the result was not satisfactory.

Figure 2.5b shows the result of the six hour delay providing a drastic reduction in the spillage of the resin and less fiber distortion from the sides of the lamina. As a means to approximate part quality for the hot press a simple thickness comparison was done for the two samples in Figure 2.5. Within the VARTM process a laminates approximate final thickness should be close to the number of lamina times the dry thickness. The result for the two parts was the six hour delay part was more in line with the results from the VARTM approximation check. Adding to the confidence of method of using the gelation delay time.

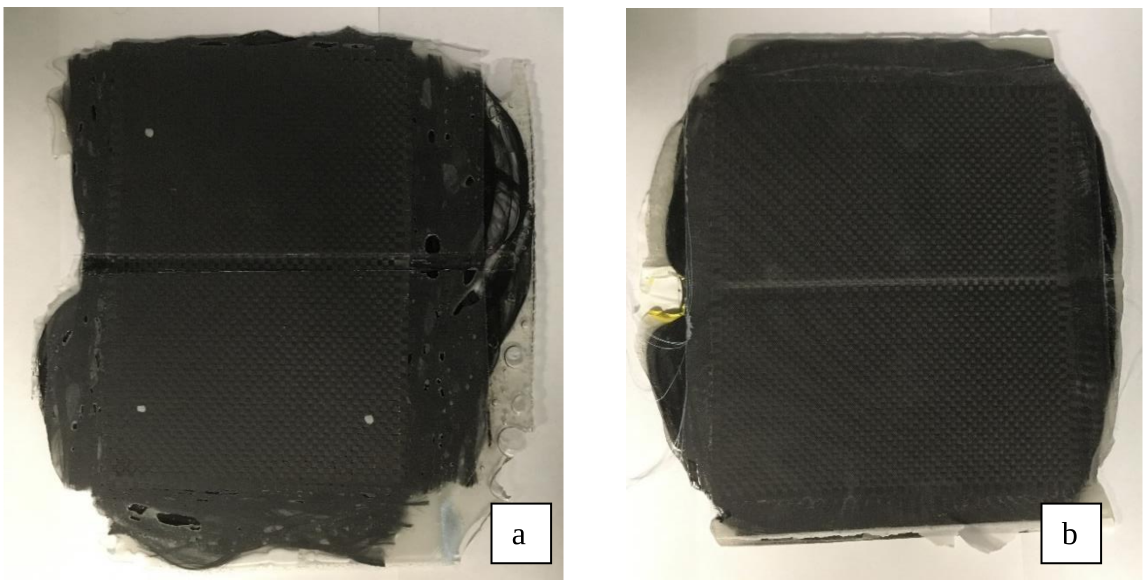

Figure 2.5, a) is the laminate made with the four hour start delay, and b) is the six hour start delay

Another benefit of the gelation delay is less fiber/lamina movement. Figure 2.6 is unidirectional lamina made during the testing phase for this study. This laminate had no delay and a 414 kPa (60 psi) pressure was used, as can be seen in the yellow box in the figure there was significant layer shifting of the lamina.

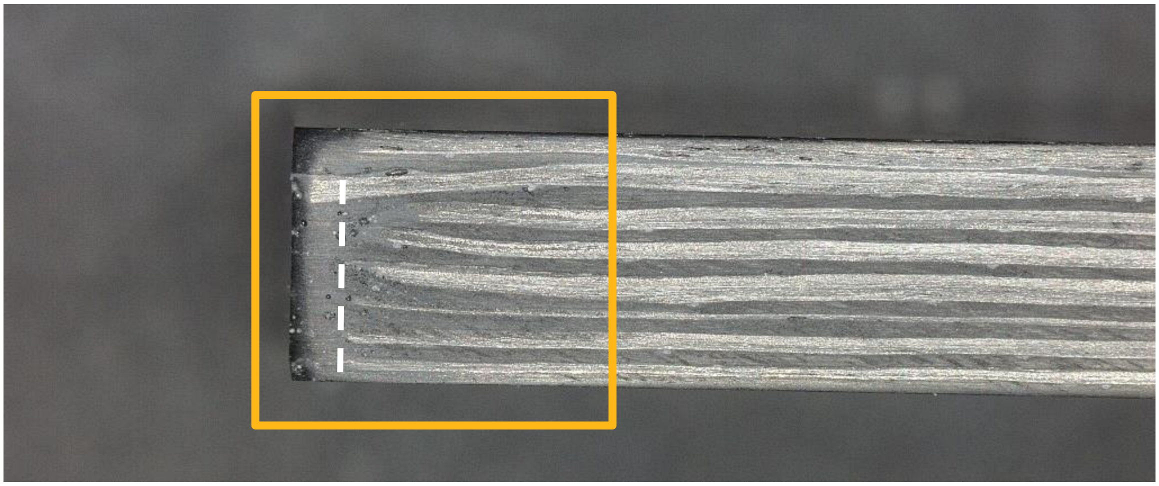

Figure 2.6, Unidirectional laminate made in the hot press with significant layer shifting.

*2.4 Manufacturing Out-of-Plane Wrinkle*s

The next step in the fabrication process was to create a method for making controlled and intentional out-of-plane wrinkles within a laminate. In this section several methods are discussed for the fabrication of an internal out-of-plane wrinkle within a laminate, each trying to simulate, in a controlled fashion, the wrinkle depicted in Figure 1.5 of the wing spar. There were three main criteria for creating a wrinkle within a composite laminate. The first is to be able to create a simple wrinkle geometry as discussed in Chapter One, which is a single wave or bump as seen in Figure 1.1. The second criteria is to have a way to quantify the wrinkle to validate the ultrasound methodology presented as part of this thesis. The third criteria is to fabricate a wrinkle that is not detectible from a visual inspection of a surface.

2.4.1 Single Step Fabrication

The first method of fabrication presented is in Figure 2.7, which uses a simple fold in one lamina method to create the wrinkle, similar work was done [27]. The method works well using the VARTM process, but successful parts were not able to be created using the wet layup process. In the VARTM process tape can be used to hold the dry fabric in place to form the fold/wrinkle, whereas with wet layup no tape was found to hold the wrinkle in place.

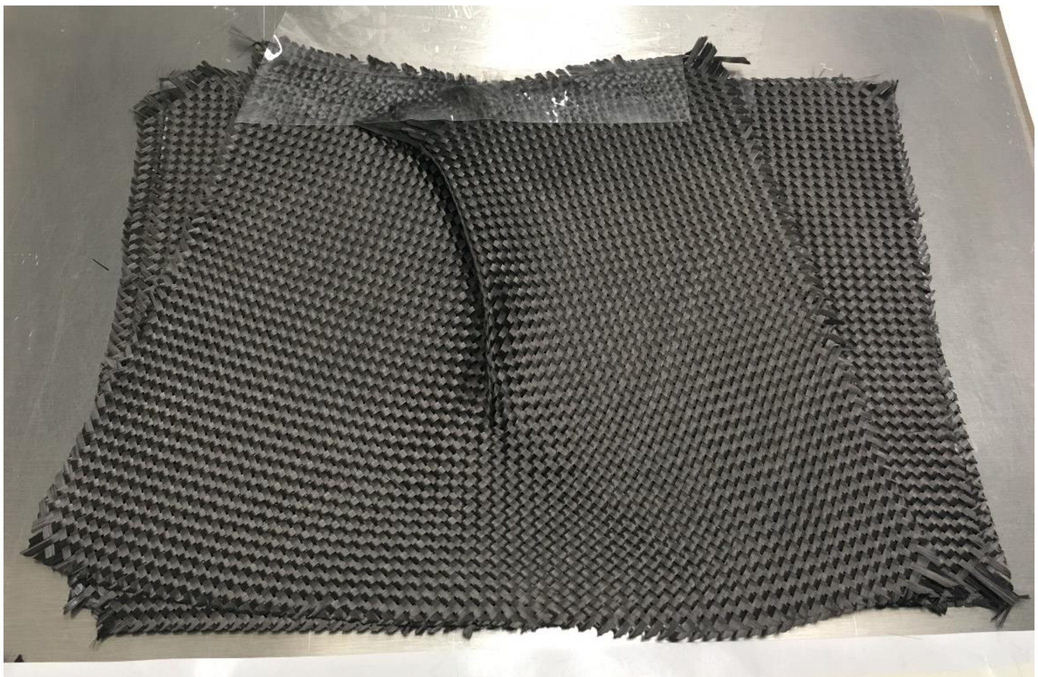

Figure 2.7, Example of creating a fold in one lamina to induce an out-of-plane wrinkle

Although this method allowed for the formation of a wrinkle, there was no method found to yield geometrically consistent wrinkles, either in the size or placement within the fabricated laminate. In addition, there was not a clear way to quantify the wrinkle to validate its size, apart from a computed tomography (CT) scan or sectioning the sample for microscopy. This method also requires a significant number of lamina within the laminate on either side of the wrinkle to allow for a smooth exterior part surface. The primary advantage of the fold method is that is allows for the creation of a wrinkle without the need to fabricate the laminate in two cure steps introduced in later sections.

An alternative method for wrinkle formation studied in the present work is based upon the method introduced in Wang *et al.* [14]. In [14], the authors create a wrinkle in multiple ways, of note is the use of a thin-strips of a second material, such as additional strips of pre-preg, in a transverse direction across a laminate. These additional strips created a raised section within the laminate resulting in a wrinkle being formed as more lamina are laid on top. This method has the advantage of using the same material system within the laminate as the surrounding lamina, but due to the cross-ply orientation the region around the wrinkle will have a different density than that of the surrounding plies. Resulting in an increased acoustic mismatch between lamina causing an increased acoustic reflection.

In the present study dry woven fabrics are used instead of prepreg unidirectional lamina Therefore, the insertion of thin strips of dry tows to form a wrinkle was not able to be successfully completed in the present study. The woven material will separate and fall apart when cut into strips on the order of the tow width itself.

An alternative is to replace the prepreg strips with small half cylindrical shaped pure resin insert, created using a polytetrafluoroethylene (PTFE) mold as seen in Figure 2.8. These resin mold inserts were placed within the laminate to fabricate out-of-plane wrinkles before using the VARTM process to infuse the full composite. As noted in Figure 2.9 there are significant issues with the formation of the wrinkle around the resin rich insert. As noted in Figure 2.9a there is a propensity to have poor resin infusion surrounding the insert. Parts without porosity can be fabricated as noted in Figure 2.9b, but care must be taken during fabrication to ensure complete resin infusion by increasing the infusion time.

Figure 2.8, PTFE mold used to create solid resin wrinkle inserts.

Although the part has wrinkles within the lamina, there is a clear wrinkle within the part based upon inspection of the bagging surface as it is no longer parallel to the tooling surface, as observed in Figure 2.9. To allow for parallel surfaces where one would be unable to visually identify a sub-surface wrinkle, a significant number of lamina would be required making the fabricated part inconsistent with the real world scenario trying to be simulated. Therefore, this method is not considered a viable option for creating wrinkles within laminates.

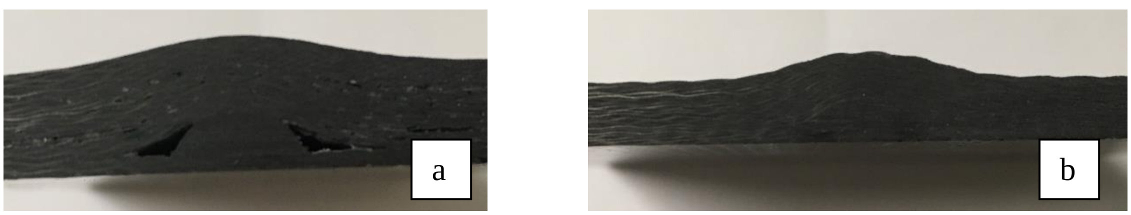

Figure 2.9, Laminates made using the resin insert mold method. a) has poor infusion around the mold, b) has better infusion.

2.4.2 Two Step Fabrication VARTM and Hot Press

A new method is presented in this section that results in a consistent and repeatable out-of-plane winkle within the laminate. This method does not require an inserted object, that can lead to an artificial acoustic reflector, nor does it use a lamina fold. This method is based upon the work from Larrañaga-Valsero and Smith [6] where they fabricate a wrinkle in their part using a two-stage process with a hot press and aluminum tooling. They used a partial arc to create the wrinkle within the first half of the laminate and then cured the laminate. After curing of the first laminate, a second set of prepregs are placed on the laminate with the surface wrinkle and a complete laminate is generated with an embedded wrinkle.

This two-step process is extended in the present work using a hybrid VARTM method with the hot press. The results generate an embedded wrinkle without the use of an additional material component within the part. Instead of using aluminum tooling to create the wrinkle as was done in [6], various objects with curved surface were placed outside of the peel-ply during the curing of the first laminate. An initial proof of concept panel is presented using a nail and simple polylactic acid (PLA) 3D printed object placed on the surface of the laminate outside of the peel ply to create the wrinkle as shown in Figure 2.10. Figure 2.10a shows the placement of the nail and the PLA wedge within the bagging material, but behind the peel-ply prior to curing. Figure 2.10b shows a cured composite with the two wrinkles created using the method shown in Figure 2.10a. It was observed that the use of PLA was not appropriate as the glass transition temperature, about 60 °C, is below that of the cure temperature for the resin. This resulted in the PLA wedge deforming during manufacturing. The nail worked well, but its high degree of curvature was not desirable for the simulated wrinkle and a wedge is preferred with a low degree of curvature.

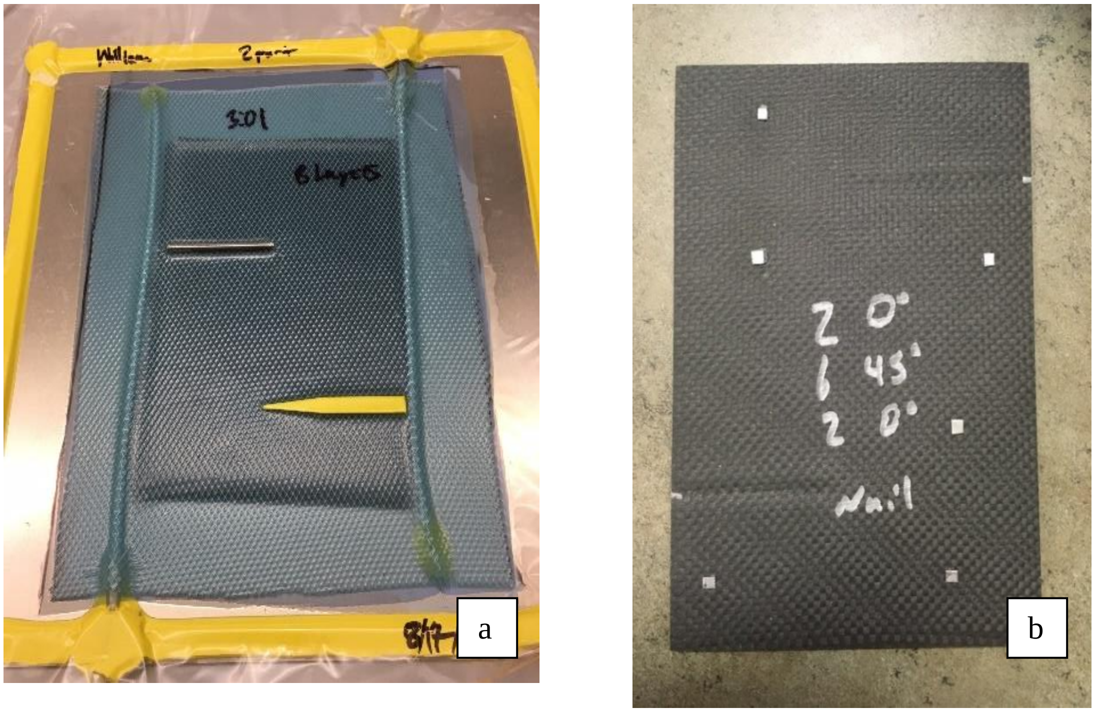

Figure 2.10, The two figures are not of the same laminate, a) shows the process of using a nail and PLA wedge to create the wrinkles in the laminate, b) shows a cured laminate using this fabrication process.

The second generation of parts were fabricated using polycarbonate (PC) 3D printed wedges on an Ultimaker S5. PC is both stronger than PLA and has a glass transition of 160 °C which is greater than the laminate curing temperatures utilized. The benefit of using 3D printed molds is that it allows for the potential of a variety of wrinkle sizes to be easily manufactured and investigated. For this study a single wedge size was fabricated to have a height of 0.762 mm, a width of 6.35 mm and a radius of 7.0 mm. An example of the CAD cross section and the printed mold are shown in Figure 2.11. Using the description of wrinkle intensity from Equation (1.2) is I=0.762/(2*6.35)=0.06, a moderately small wrinkle, but still significant if considered on in approximation with the Hsiao-Daniel plot in Figure 1.6 plot approximation.

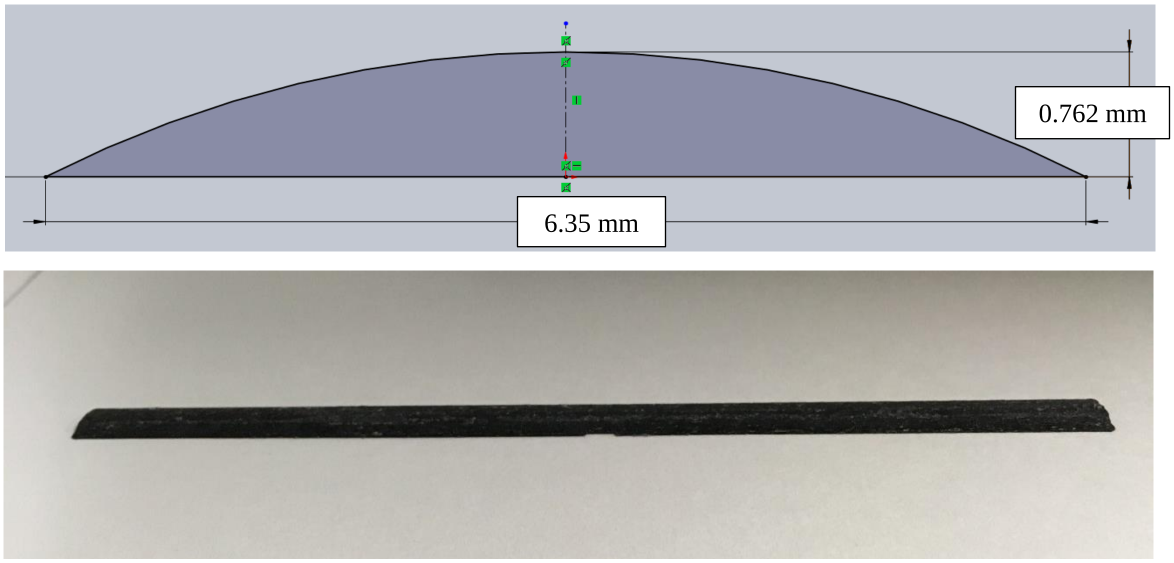

Figure 2.11, CAD image of the cross section of the wrinkle mold, and printed sample of wrinkle mold.

Once the first half of the laminate is formed with the surface wrinkle, the wedge is removed from the surface and discarded. The second stage of the process is to place the wrinkle/bag surface of the first stage part on top of a new stack wet layup lamina. The new combined stack will have another tool placed on top of them before being placed in the hot press where a second cure cycle will be performed. This is similar to the process shown by Larrañaga-Valsero *et al.* the one main difference is the part created for this study is flat on both sides [6]. Figure 2.12 shows the side profile with uniform thickness and no visible wrinkle of one the parts made using this method. The result of this is the method is that the wrinkle is not visually detectable to the eye when looking at either of the surfaces similar to that of the challenges currently being encountered in industry [2][3][4].

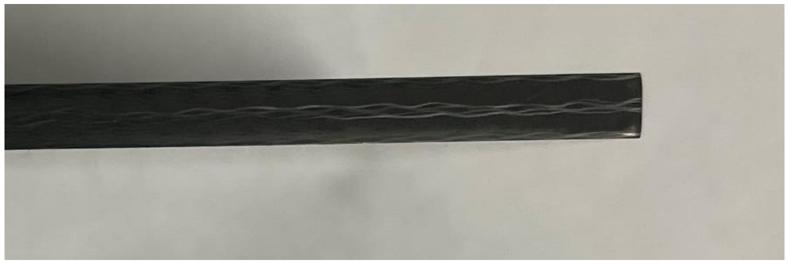

Figure 2.12 Finished side view of laminate made using the VARTM and hot press method, showing uniform laminate thickness.

There are some drawbacks of this method. First is that this method creates a ripple affect around the main wrinkle. Instead of a single wave/bump there were often three identifiable waves with two small wrinkle/bumps forming on the sides of the main wrinkle as seen in Figure 2.13. These additional bumps are in the opposite direction than the main wrinkle but would cause additional signal distortion from the ultrasonic method to yield a false sense of confidence. The other drawback of this method is the use of VARTM and hot press manufacturing methods causing a mismatch in the part density between the two processes. Thus, a decision was made to for all laminates to be fabricated with either exclusively the VARTM method or the programmable hot press. Due to the ability for more consistent parts, the use of the hot press was selected as the preferred method and is used for the final analyzed samples.

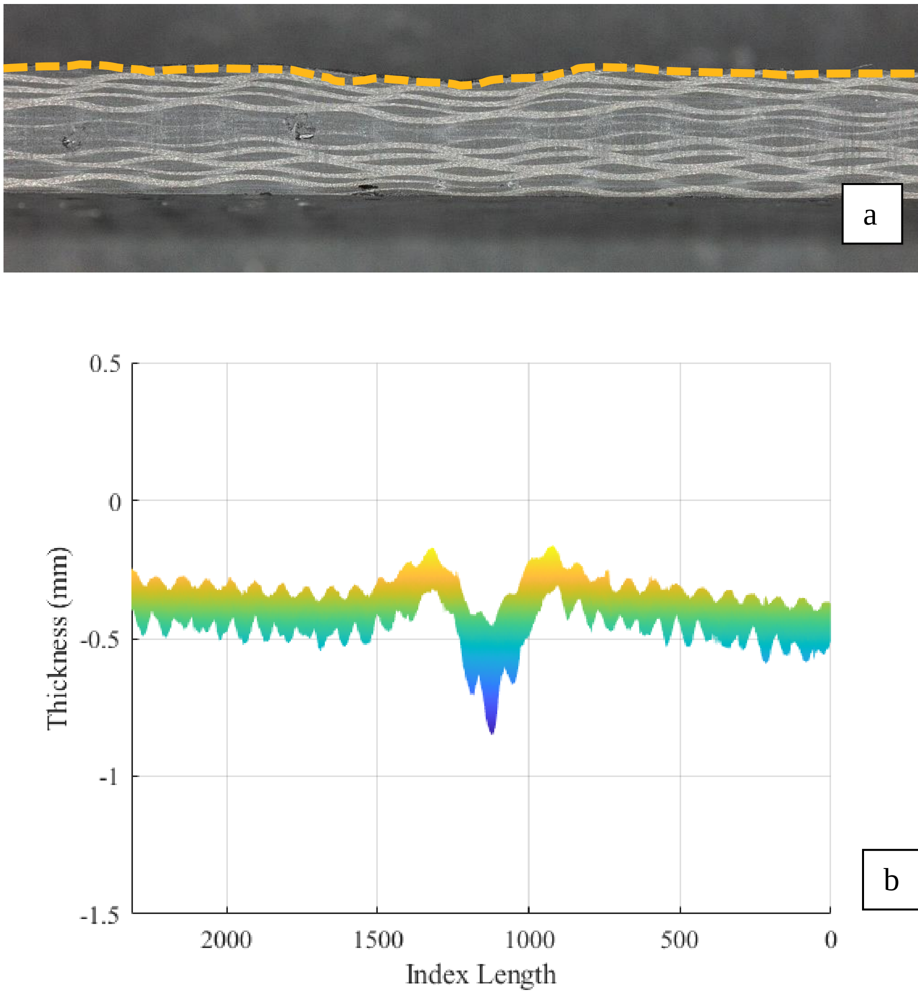

Figure 2.13, a) The effect of a mold used to induce a wrinkle during VARTM fabrication resulting in a ripple effect, b) the 3D microscope surface plot showing the ripple effect of the wrinkle in a).

2.4.3 Two-Step Fabrication of an Embedded Wrinkle Using a Programmable Hot Press

The two-step hot press manufacturing method induces the wrinkle during the first cure. The second stage takes the first cured half and places it on top of a stack of wet layup lamina, wrinkle side down, to provide uniform thickness and to hide the wrinkle. This results in a consistent part with an embedded wrinkle without any visible surface blemishes or indications of an internal wrinkle. In addition, there is no acoustic reflection at the interface between the top and bottom laminate as the holding pressures are identical between the various stages of curing of the laminates.

The initial lamina are wetted as described previously and placed on an aluminum tool and left at room temperature for six hours to allow for gelation. A sheet of peel ply fabric is laid on top of the stack wetted lamina to both prevent the lamina from sticking to the second aluminum tool and to provide a rough unfished surface to allow for the subsequent laminate build-up after the first cure. Figure 2.14 shows a schematic representation of the first cure stage cycle. Figure 2.15a shows the layup of the wet fibers resting before being placed in the hot press prior to gelation. Observe in Figure 2.15d that the plate is also covered with aluminum foil to prevent any debris from landing on the top surface.

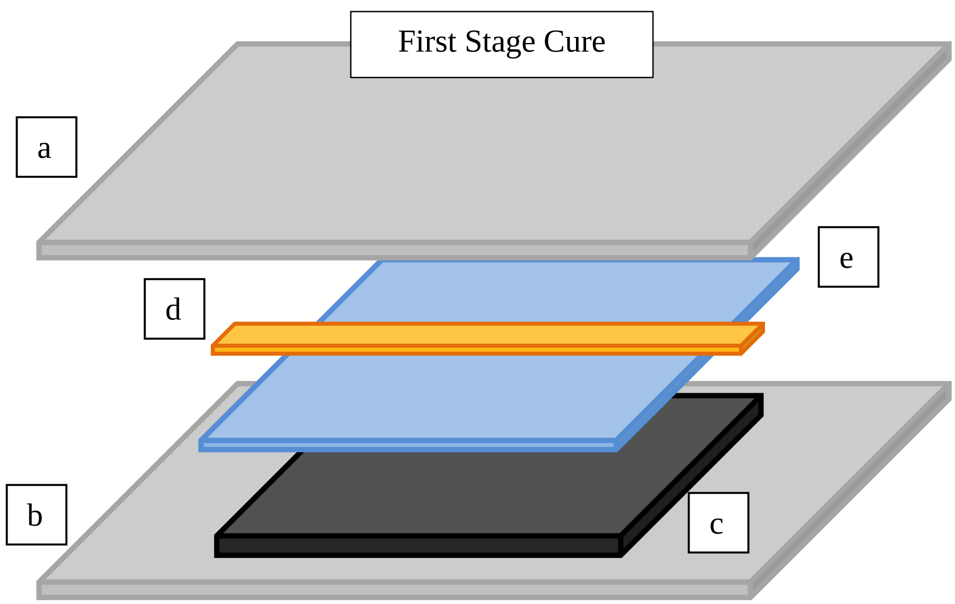

Figure 2.14, This is a schematic of the first stage curing cycle. a) and b) are the top and bottom tooling respectively, c) is the wetted lamina, d) is the wedge mold for the wrinkle, and e) is the peal ply layer.

The polycarbonate wedge is adhered to the top tooling plate using gum tape as seen in Figure 2.15b. This allows the wrinkle to be pressed into the unfished side of the laminate being made as shown in Figure 2.15c. After the six hour wait time the top tooling plate is placed on the wetted carbon fiber fabric stack and placed into the hot press for the elevated temperature cure cycle.

Once the cure cycle is completed the parts are removed from the press. Figure 2.16a shows the laminate after curing prior to the peel ply being removed and the wrinkle can be clearly seen across the middle of the part. Figure 2.16b shows the tool surface of the laminate and the effects of the wrinkle are not visible on the surface as desired.

Prior to the second stage of the fabrication, the surface is characterized geometrically for later validation. This is done using a Keyence 3D 3100 laser microscope. This process is fully discussed in the following section, but the primary purpose of capturing the 3D surface of the wrinkle is to allow for the comparison of the true wrinkle surface with that of the surface obtained through the presented ultrasonic methodology. To allow the coordinate systems to be aligned between the data set obtained using 3D microscopy and the ultrasonic study, three markers are placed on the surface as shown in Figure 2.17. The 5 mm by 3-4 mm markers are made from a 0.127 mm (0.005 in) thick polytetrafluoroethylene (PTFE) sheet. These markers will appear as a surface displacement on the 3D microscopy and as acoustic reflectors for the ultrasonic signals. They are not used to calibrate or identify the wrinkle surface, but only for a coordinate system alignment for validation purposes.

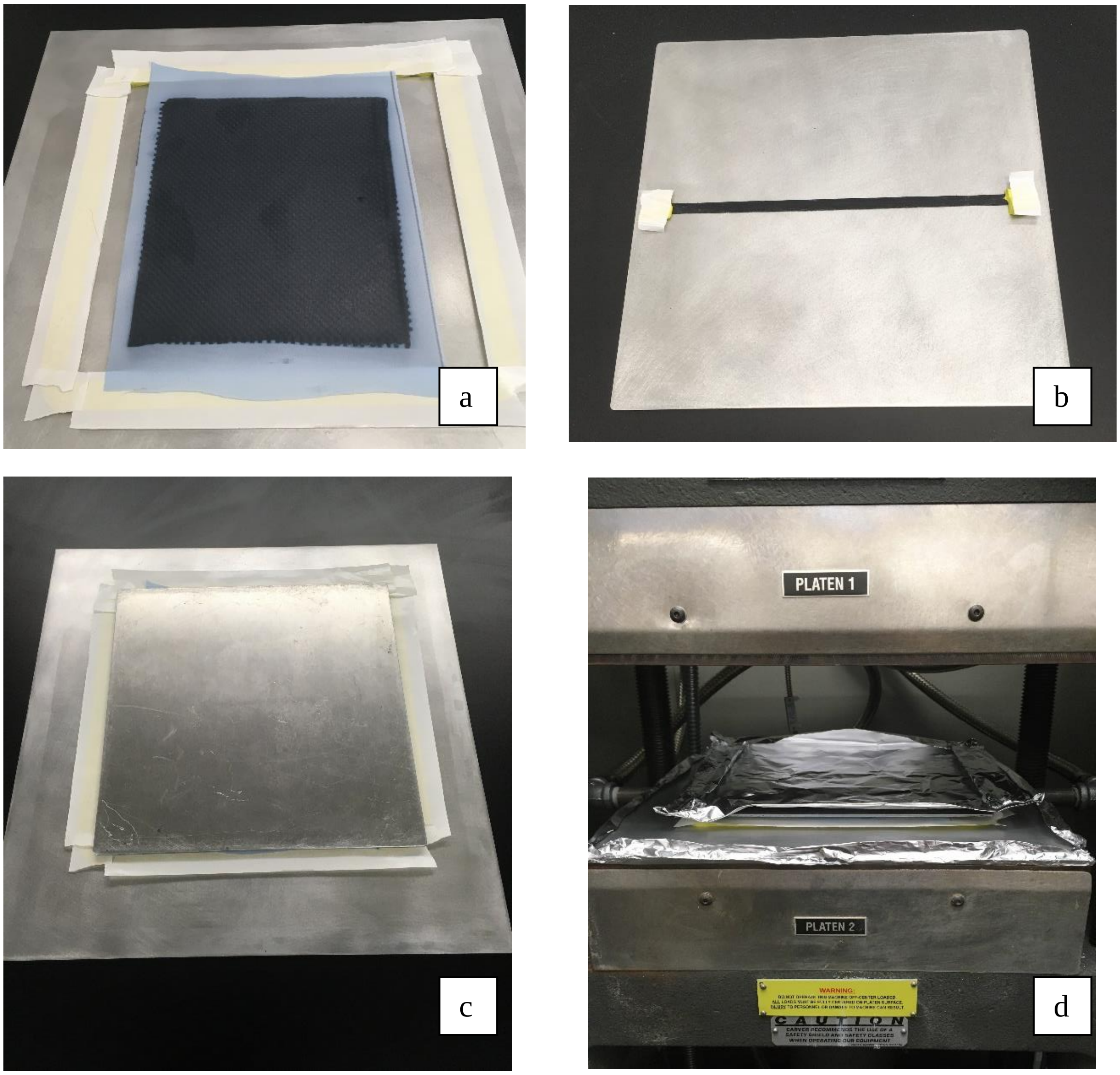

Figure 2.15, a) wetted lamina during six hour delay, b) top tool with wrinkle mold attached, c) top tool placed on wetted lamina, d) tools placed in the hot press.

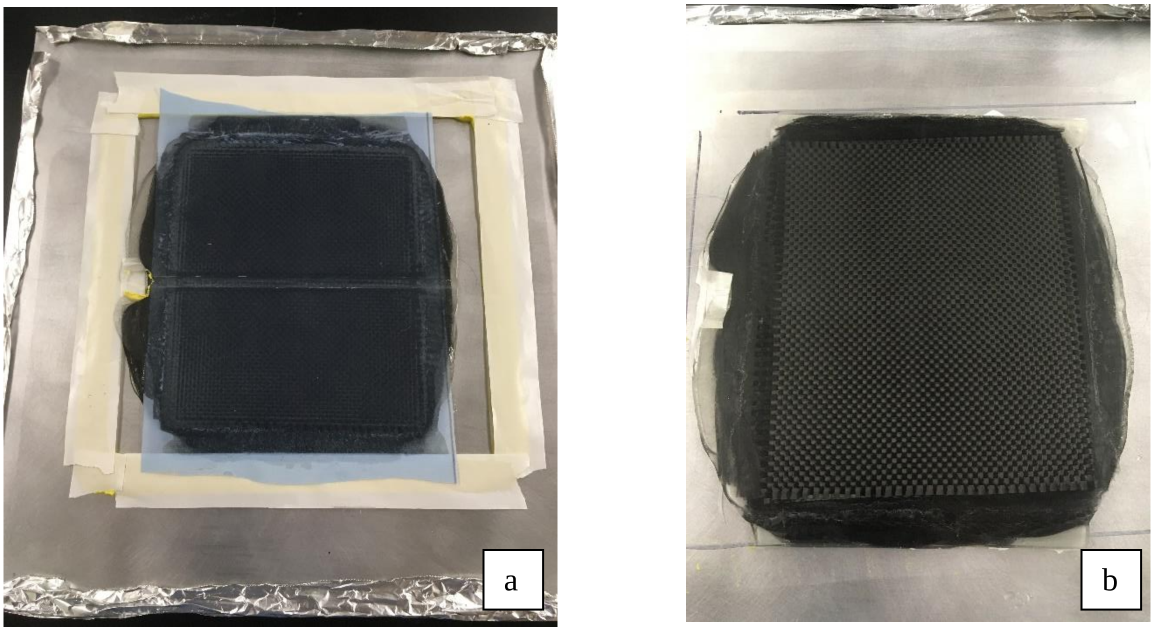

Figure 2.16, a) laminate after the top tool is removed and the peel ply still on, b) tool surface of the laminate with no visible wrinkle.

After the 3D surface is captured using 3D microscopy, the part fabrication is continued to add additional lamina to cover up the wrinkle following the schematic in Figure 2.18. Wetted carbon fiber lamina are placed directly onto a new tool surface as shown in Figure 2.19a. The lamina are allowed to come to gelation as was done with the first stage cure. After the delay for gelation the first stage laminate with the wrinkle is placed on top of the wetted lamina, as shown in Figure 2.19b. Once the cured part is in place, an aluminum tool is placed on it and then the combined composite structure is placed into the hot press to cure the new lamina.

Again, a double tooling method is used, but this time without any peel ply on the surface of the upper tool. Figure 2.20a shows the panel after being removed from the hot press. The edges of the laminate are then cut using a wet band saw with a diamond tipped grinding blade and the resulting panel is shown in Figure 2.20b. Observe that there is no visual indication of the underlying wrinkle in the part.

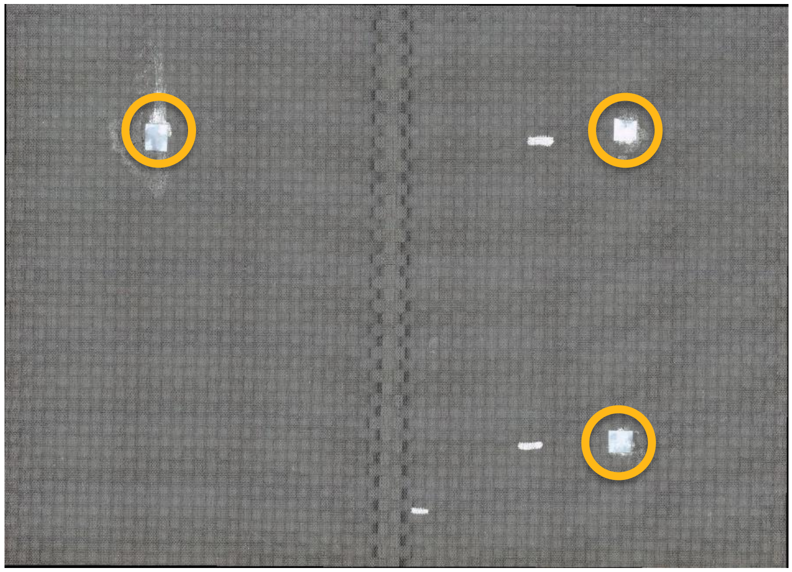

Figure 2.17, This is an image of the midplane of the laminate after the first cure using the Keyence microscope. The three white PTFE markers have been placed and can be seen on the surface and are highlighted by yellow circles.

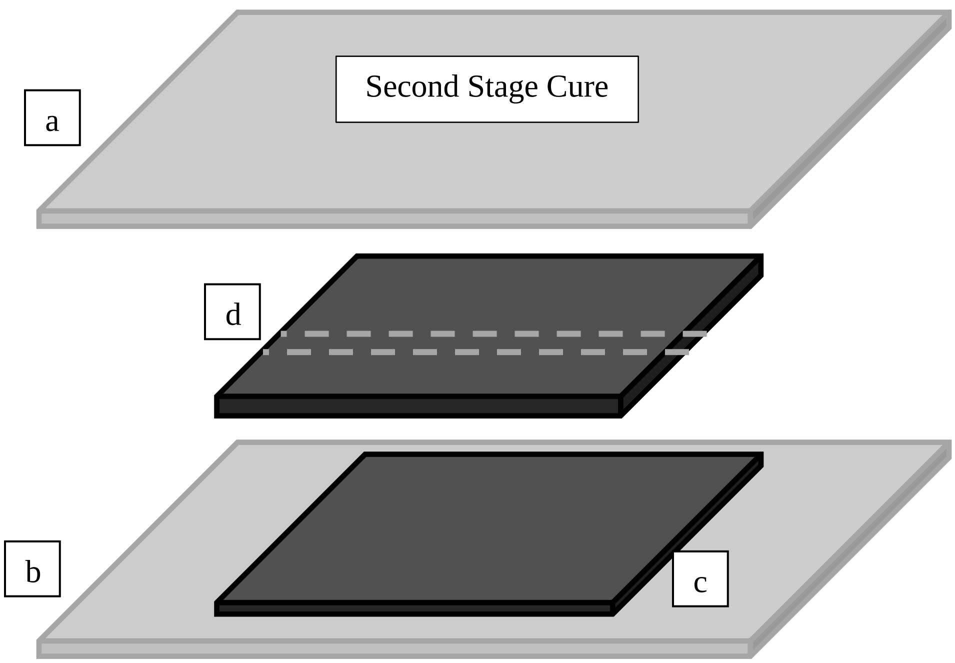

Figure 2.18, Schematic of the stacking sequence for the second cure cycle. a) and b) are the top and bottom tooling respectively, c) is the new stack of wetted lamina, and d) is the first stage cured laminate with an out-of-plane wrinkle, the wrinkle region is in gray dashed lines.

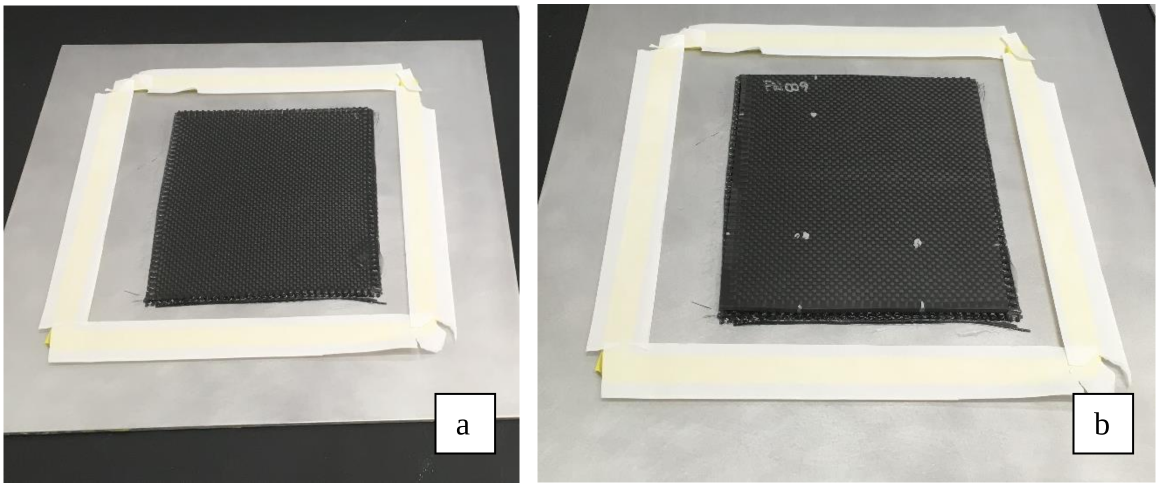

Figure 2.19, a) wetted lamina for the second stage cure during the six hour delay for gelation, b) the first stage cured laminate placed onto the new wetted lamina before being placed in the press.

The layup used for this study was composed of 18 lamina of 3K tow, plain weave carbon fiber fabric, with each lamina being placed in the 0°/90° orientation. The first cured laminate consists of 14 lamina and the full laminate has an additional 4 lamina. The reason for the nonsymmetric halves is that the 14 lamina allow for the wrinkle to propagate through more of the thickness of the laminate without the ability to identify from a surface visual inspection.

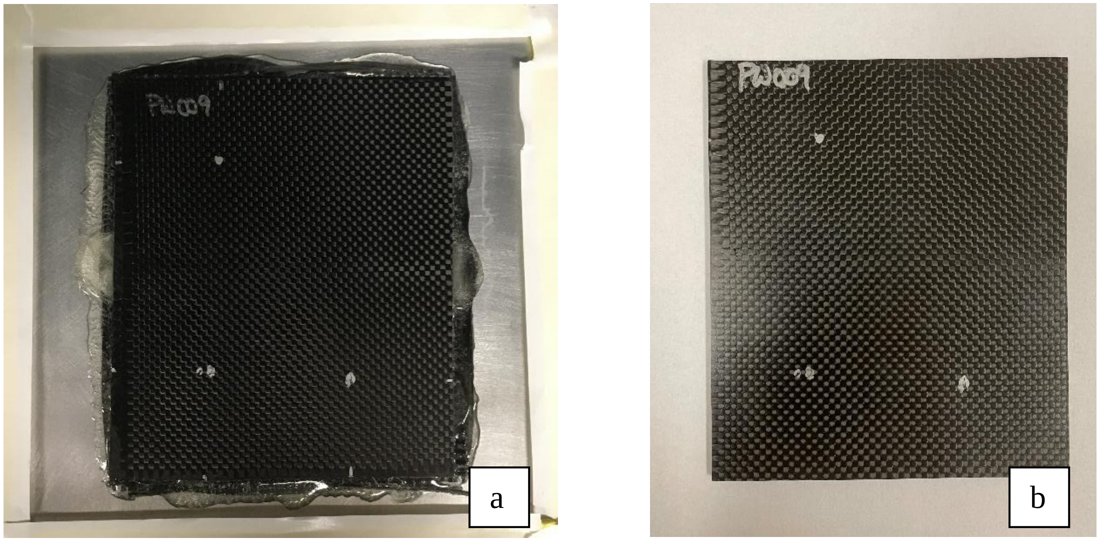

Figure 2.20, a) laminate after the second cure in the hot press, b) edges of the laminate are cleaned using wet band saw.

Keyence Microscope Scanning

Validation of the size of the wrinkle seen by the ultrasound scanning is difficult to do without using computed tomography (CT) scanning or some form of destructive testing of laminate to investigate it with microscopy. Therefore, to quantify the wrinkle put into the laminate a Keyence 3100 3D microscope is used to measure the mid plane of laminate prior to the second cure stage.

The 3D microscope can scan an object and provide a detailed height map of its surface. This method is thus applied to the mid plane of the laminate between the two stages. The 3D microscope provides a detailed image of the height and width of the laminate. An example surface plot from the 3D microscope is shown in Figure 2.21. The wrinkle is observed to be approximately 0.76 mm deep and is seen by the blue region occurring in the middle of the scanned region. The three points on the surface of the plot correspond to the three 0.127 mm thick PTFE markers that were added to the mid plane and will be used to align the microcopy images with the ultrasonic analysis data sets in the following chapter.

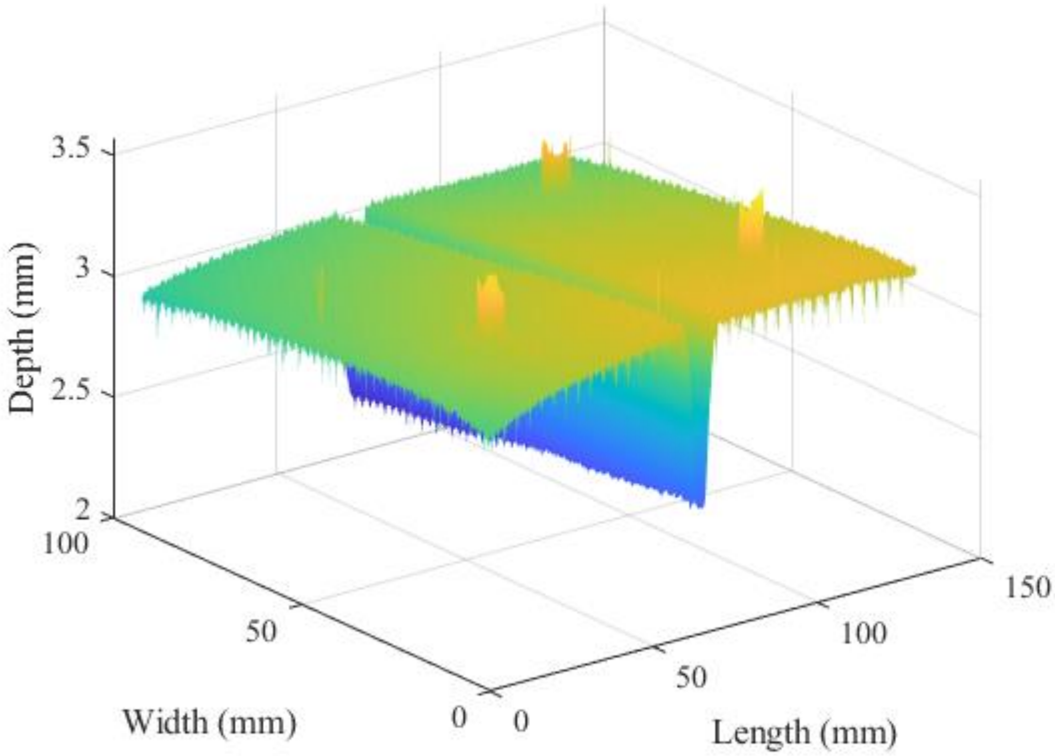

Figure 2.21, Height map of midplane of the lamina using the data collected from 3D microscope.

CHAPTER THREE

Ultrasonic Scanning and Analysis

3.1 Introduction

The following chapter will go over the basic principles of ultrasound being used in this work, the equipment used, and the different types of scans being investigated. The base codes used to analyze the ultrasound data has been developed by other researchers within the Baylor Sic'em Research group and are built upon in the present study. The prime advancement in the software is the analysis out-of-plane wrinkles, the methodology of which will be discussed in this chapter. The base method relies upon the previous work of bond line detection work by Blandford [40][41] and extends the previous method to track individual lamina as they undulate across a wrinkle.

3.2 Scanning Method and Transducers

The ultrasonic scanning method used in this work is immersion scanning within a water tank using pulse echo scanning with either a single element transducer or a focused beam phased array transducer. Pulse/echo is a method of ultrasonic scanning using a single transducer to send out a sound wave and use the same transducer to receive the reflection [42]. The single element transducers used are Olympus spherically Point Target Focused (PTF) immersion probes, which means the face of the element is concaved allowing the ultrasound waves to provide a maximum response from a small focal point for the given focal length [43]. The transducers are available over a range of frequencies. Based upon early studies as part of this research, the 10 MHz probe was found to identify sufficient through thickness resolution while maintaining sufficient signal strength at deeper depths within the laminate.

For the focused transducers used in this work they were both 10 MHz Olympus Videoscans with nominal focal lengths of 38.1 mm (1.5 in). One was a 12.7 mm (0.5 in) element diameter, with an actual focal length of 40.36 mm (1.589 in) and a model number of V311-SU-F1.5IN-PTF. The other had a 6.35 mm (0.25 in) diameter element with an actual focal length of 39.19 mm (1.543 in) and a model number of V312-SU-F1.5IN-PTF.

The phased array transducer used in this study was an Olympus 10 MHz 64 element linear phased array transducer with a 0.5 mm pitch between elements. The length of the transducer is 32 mm, and the width is 5 mm. Phased array works differently than single element transducers, especially focused ones. A phased array is essentially an array of flat front transducers placed in an ordered pattern. For the current phased array system, the elements are spaced in a linear line with a 0.5 mm pitch. This line element array allows for large areas of a part to be scanned quickly. Simulated focusing can be achieved with this type of transducer by firing the elements at various time intervals creating a focused wave, or what is known as “electronic beam forming” [44]. This can be visualized using a five-element aperture, meaning five elements/transducers are used to create a single a-scan as shown in Figure 3.1. The simulated focus wave is generated by first firing the outer elements, 1 and 5, followed by the next two outer elements, 2 and 4, and finally the middle element, 3, fires. The elements then receive the signal back in the same order as they were fired with the same nanosecond delays between receiving on the elements. Due to the high speed of sounds for the materials being investigated along

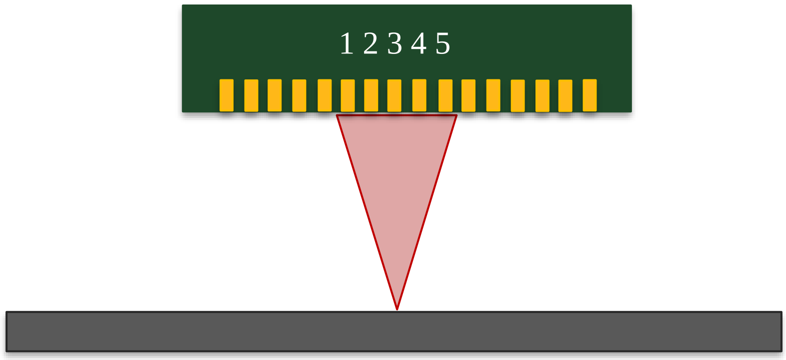

Figure 3.1, Phased array firing sequence for focused beams

with the short distances between elements, the delays between firings are on the order of nanoseconds. In addition, the number of elements in the aperture can be adjusted to provide different results, such as when more elements are used the a-scans produced become distorted from the greater number of scans being used to create the signal. Alternatively, the element firing sequence can be adjusted to create a wave that fires at an angle instead of straight down. These permutations are not investigated in this study, but some future possibilities are discussed in the future work potential presented in Chapter Five.

3.3 Immersion Scanning System

The scanning is performed using a custom immersion scanning system fabricated by researchers at Baylor University and is shown in Figure 3.2. The system consists of two Velmex Bi-slides to move the transducer in the index and scanning directions. These Bi-slides are placed on a frame above a water filled tank containing the part being scanned. A Velmex X-slide is used in a vertical configuration to control the transducer’s height above the part allowing the focal point of the transducer to be adjusted. A rotational stage is mounted onto the vertical X-slide for curved composites and can be observed in Figure 3.2. The rotational stage is not used in this work but could be used to extend the present study to curved composite systems.

Two Velmex motor controllers control the four motorized stages of the system. Inside the tank is an acrylic plate, seen in Figure 3.2 to level the part before a scan is taken. The author was part of the team to modify this stand to have three points of contact instead of four, speeding up the process to level the part. On top of the acrylic plate there are blocks used to raise the part being scanned off the plate creating a water gap between the back wall of the part and the acrylic. The transducer's signal is powered by the Olympus Focus PX pulser receiver and the transducer settings are adjusted using Olympus' Focus PC software.

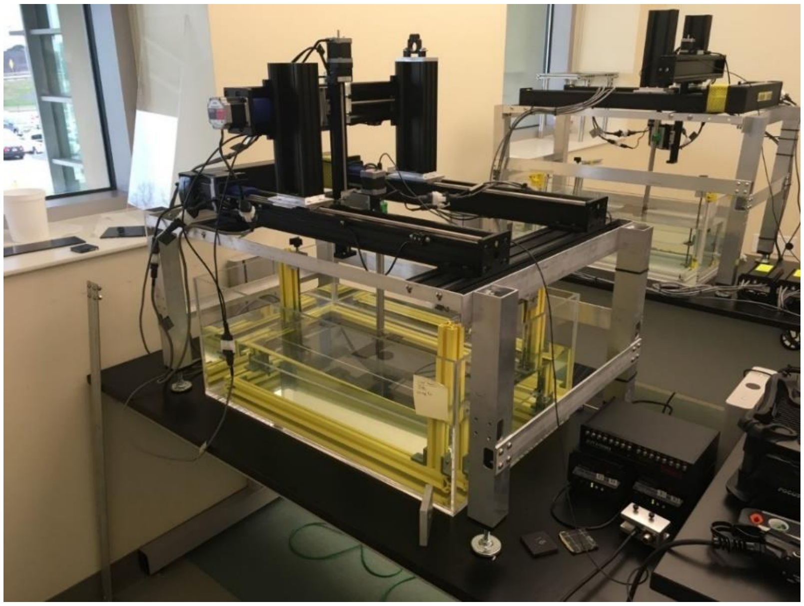

Figure 3.2, Ultrasonic immersion scanning system

The immersion scanning system's motors are controlled by a MATLAB script created by members of the laboratory. The script communicates through the serial port of the computer to controls the motion of each individual motor on the desired scanning path. The timing of the transducer firing is controlled using the Focus PC software that communicates with the encoders to identify the current position of the various motor controllers. The transducer is prescribed to move in a raster pattern over the desired part taking an a-scan every 0.2 mm in line with previous researchers identifying features smaller than the 3K tow of the laminate (see e.g., [29][26][31]). A diagram of the raster pattern can be seen in Figure 3.3, the long leg is the scanning direction, and the short steps are the 0.2 mm index steps between scanning passes. The pattern repeats until the desired index length of the scan is reached. In order to accurately control the capturing of the a-scans in the scanning direction at every 0.2 mm interval a linear encoder is used. The encoder reads a magnetic strip along the scanning direction X-slide, which allows it to accurately track the scanning position. For the index direction an encoder was not used because Focus PC can increment the index distance based on a pulse from a motor. Every time the index motor moved Focus PC added 0.2 mm to the index direction.

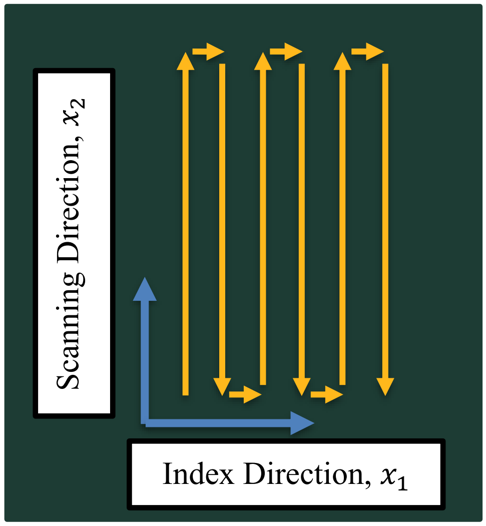

Figure 3.3, Raster pattern of the ultrasonic transducer during immersion scanning

3.3.1 Ultrasonic Scanning Settings

The scan settings for the system were controlled using Olympus' Focus PC software as mentioned above. The scan settings had to be adjusted for each scan based on the transducer type and frequency. The sampling rate for this system is set to 100 MHz for all scans that were taken within this work. The settings that were adjusted for each individual scan are the gain, pulse width, start time and range. The gain required is typically lower for low frequency transducers and higher for high frequency transducers. The gain is often difficult to select properly because of the tradeoff of higher gain to signal accuracy and the amplification of electrical noise. In addition, when the gain is raised higher aspects of the signal can be amplified to a point where the data gets cutoff or clipped from being recorded. Typically, with most of the scans within this work there will be 1-4 maximum and minimum peaks that will be clipped as a result of the gain value chosen. The higher gain values are used to counter the attenuation of the ultrasound signal through thicker parts being scanned. One side effect of higher gain is the signal to noise ratio increases reducing the scan quality at deeper depths within parts.

Alternatively, one could select the time corrected gain option to improve the signal at deeper depths and reduce clipping of the signal. This option was used for some of the scans done in this work. This process raises the gain at certain points within the reflection wave, allowing the for different parts of the signal to be made stronger. The benefit is that it allows an overall reduction in the total gain needed for a scan and a more uniform scan resolution.

The pulse width P_w for each transducer is typically defined as a function of the transducer frequency f (see e.g., [45]) as

$$P_w = \frac{500}{f} \tag{3.1}$$

where the transducer frequency f is in units of MHz and the resulting pulse width is in units of nanoseconds. The P_w for all testing is set to 50 nanoseconds for each of the various 10 MHz transducers used in the study.

The start time and range are some of the critical settings for capturing the ultrasound signal, both are measured microseconds (μs). The start time is the value for where the user wants to start recording data, typically this value would be about 1 μs before the onset of the signal. The range is how many μs that are to be recorded, a typical length for this would be about 1 μs past the end of the signal. The length of this value is dependent on the width of the part being scanned. A thicker part will have a larger range, and a thinner part have a shorter range.

For the work in this study the transducers were focused on the front wall of the part being scanned. The process for doing this varied between single element focused transducers and phased array transducers. For the focused transducers the focal length given by the manufacture had to be converted to microseconds to align it properly in Focus PC. As mentioned earlier the transducers being used have a nominal focal length of approximately 38.1 mm (1.5 in) and the actual focal lengths can be found in the previous section. The actual focal length is used to find the time of flight of the signal to the front surface of the laminate. This determines the start time for recording the signal during a scan.

The material depth at which to focus within the part, $M_D$is determined as (see e.g., [43]),

$$M_D = t_p \frac{p_f}{100} \tag{3.2}$$

where p_f is the percentage of focus within the part and t_p is the thickness of the part. Equation (3.2) is used to define the depth into the part to focus upon. When the focal point is set to the front surface of the part, the materials depth is $M_D = 0$. The water path W_P is then defined as (see e.g., [43])

$$W_P = F_l - M_D \frac{c_{sample}}{c_{water}} \tag{3.3}$$

where F_l is the focal length of the transducer in water, c_{sample} is the speed of sound of the material, and c_{water} is the speed of sound of water. The signal has to travel from the transducer to the surface of the laminate and back, so the full distance traveled in the water is $2W_P$. This distance can be converted to signal time by dividing by the speed of sound of the medium, in this case water, to find the total time of flight, ToF, required for the signal onset to focus at a material depth M_D is expressed as

$$ToF = \frac{2\, W_P}{c_{water}} = \frac{2}{c_{water}}\left(F_l - M_D \frac{c_{sample}}{c_{water}}\right) \tag{3.4}$$

The time of flight is often expressed in terms of microseconds, and the transducer's vertical position must be adjusted until the time of flight from Equation (3.4) is obtained during scanning to properly focus the acoustic wave. For example, if the ToF is 54 μs, vertical offset of the transducer would be adjusted until the first major peak of the signal would be set to this position. In practice, a tolerance of ± 0.5 μs was found to yield similar results and is used throughout this work. The start time for signal capture is set to 1 μs before the ToF, i.e. 53 μs for $ToF = 54$ μs. In Figure 3.4 the horizontal axis time scale is not relative to the initial pulse of the signal, but time $t = 0$ corresponds to the start of the data collection, 53 μs after the initial voltage pulse on the transducer initiating the acoustic wave. Notice the first reflection wave from the top surface of the part occurs approximately 1 μs after the start of the data collection and the back wall occurs at about 4 μs. into the data. For this scan the total range is 6 μs providing a little less than 2 μs of unnecessary data where there are only acoustic echoes present in the signal. Notice that the whole signal for the part is about 3 μs.

In this work all of the transducers are focused on the front or top surface of the laminate, one reason for this is it provides consistency for scans and easily set up. Based upon personal communications with several industry experts it is common to focus on the front wall of a thin carbon fiber laminate. Alternatively, there were suggestions to focus on the back wall of the part, but in the present study this was not considered as the scan quality obtained was sufficient as will be demonstrated by the results. The issue of the optimal focal position is left to future researchers such as existing studies that utilize the mid-plane of the part for the focal plane (see e.g., [6] [26]) using Equation (3.2).

Focusing a phased array transducer provides more signal flexibility than that of a single element focused transducer. The single element has a fixed focal distance and produces a single high-quality signal with a good signal to noise ratio and tight control over transducer bandwidth. Conversely, the phased array focal distance is varied through by offsets in time between the firing of individual elements. The phased array is composed of a series of flat front style transducer, and it can be focused by firing different elements at different times to create a focused beam as discussed in Section 3.2. There are limitations on the focal distance depending on the number of elements used in the aperture to create the focused wave. The more elements used the greater the focal distance can be, fewer elements allow for shorter focal lengths to be used. When setting up the phased array in Focus PC a calculated near field is given, typically the part being scanned should be past the near field. This will limit the number of transducers and the actual focal length.

The first step for focusing the phased array is to choose the number of elements for the aperture, then the focal height can be adjusted. For Focus PC, the aperture and focal height are properties that are chosen before the transducer is put into focus. For a phased array the focal point of the signal is defined to occur at 0 microseconds. Therefore, in a similar manner as described above for the single element transducer the phased array transducer is adjusted to where the onset of the signal would be at +/- 0.5 μs of 0.

The start and range would be determined in a similar way as described above. The start would be about 1 μs before the onset of the signal and the range would be about 1 μs after the end of the signal. Figure 3.5 is a sample a-scan from the phased array transducer, similar to the one in Figure 3.4. The front wall of the signal begins at approximately 1 μs and the back wall is at 4 μs. There is about 1 μs on the front and back end that is unnecessary data being collected.

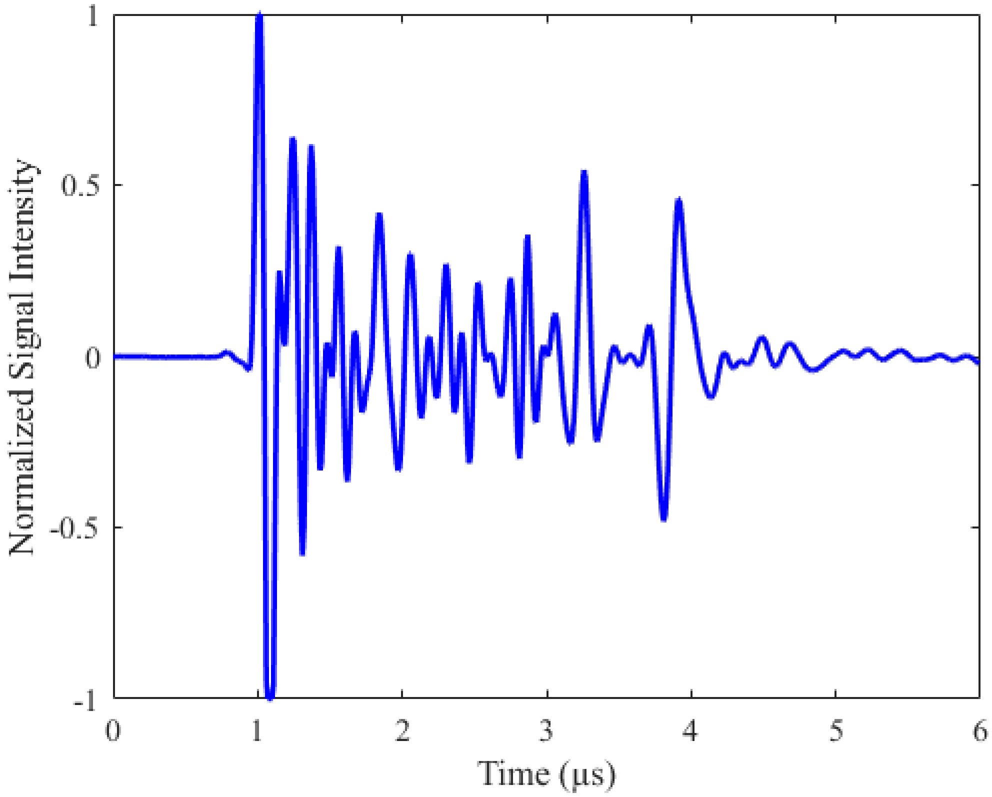

Figure 3.4, Representative a-scan of a carbon fiber laminate of the normalized signal intensity as a function of time, using a single element transducer.

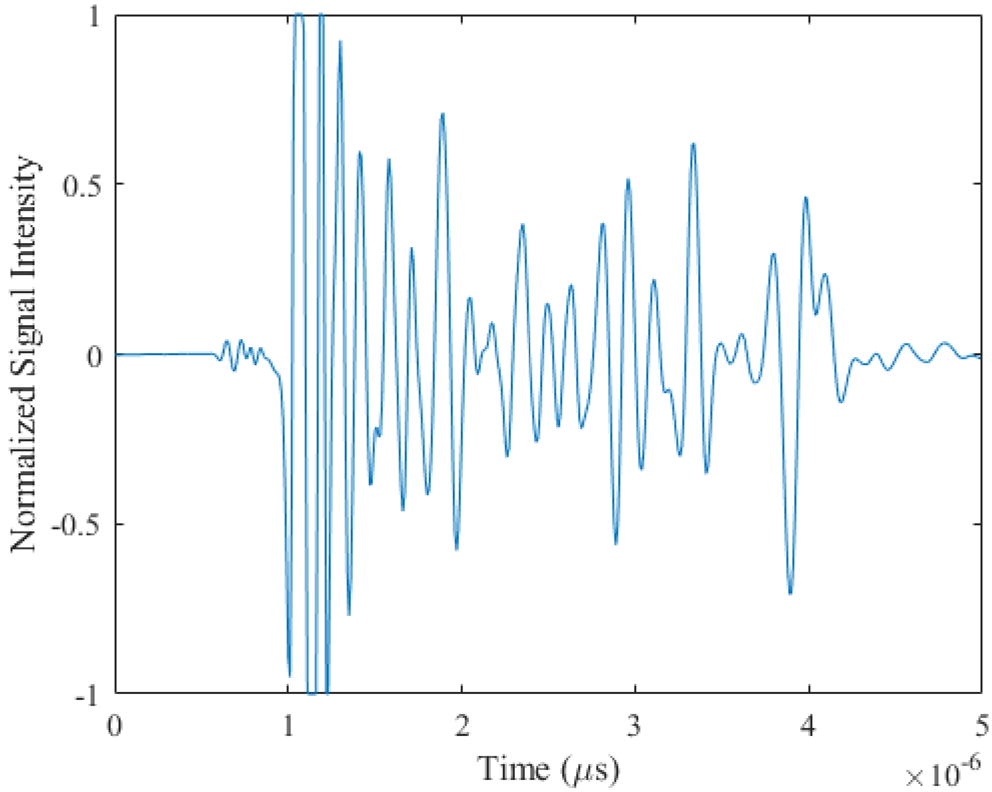

Figure 3.5, Representative a-scan of a carbon fiber laminate of the normalized signal intensity as a function of time, using a phased array transducer.

3.4 Ultrasonic Scans

For investigating the out-of-plane wrinkles three main types of figures are generated from the ultrasonic scanning data: a-scans, b-scans and a form of a c-scan. In the present study, the resulting c-scan is termed a *3D lamina plot* as it is essentially a snapshot of a single lamina. The a-scans and b-scans are used to generate the lamina plot, the process for this will be discussed below for a single example and are discussed in detail in Chapter Four.

The a-scan represents the basic building block of ultrasound analysis. In this work because of the use of pulse/echo transducer configurations the a-scan represents the sound wave reflection through the material as a single planar location on the surface of the part and they typically appear as that of Figure 3.4 and 3.5 [42].

The b-scan is a slice of the thickness of a part being scanned, it is an image generated by combining a series of a-scans into a single matrix, with the horizontal axis representing the spatial location of the a-scan and the vertical dimension corresponding to the depth into the part [42]. This latter dimension of depth into the part is often expressed in units of microseconds based upon the reflection wave return to the emitting transducer but is easily converted to a unit of depth through the speed of sound of the material being studied. The resulting b-scan is an image that creates a slice of the part being investigated, such as that of the laminated composite shown in Figure 3.6. From the image one can observe the individual lamina within the composite denoted by the horizontal lines. In general, the transition between lamina will result in a high (red) and then a low (blue) wave. Note that the horizontal lines are not smooth, nor are they anticipated to be so, as the physical lamina of the woven composite itself is not smooth but on the order of 2 mm will undulate with each successive carbon fiber tow. An analogy is that the b-scan represents a slice of a layered cake, which when cut exposes the individual layers of the cake. Combinations of multiple b-scans will be the main data sets used in this study to characterize out-of-plane wrinkles. These types of scans are conducive to identifying the presence out-of-plane wrinkles that are present and then will be analyzed to quantify the wrinkle size. As observed in Figure 3.6 there is a wrinkle present between 50 and 60 mm along the scan axis that appears to initiate in the top quarter of the part and can be seen to increase in height as one goes deeper into the laminate stack.

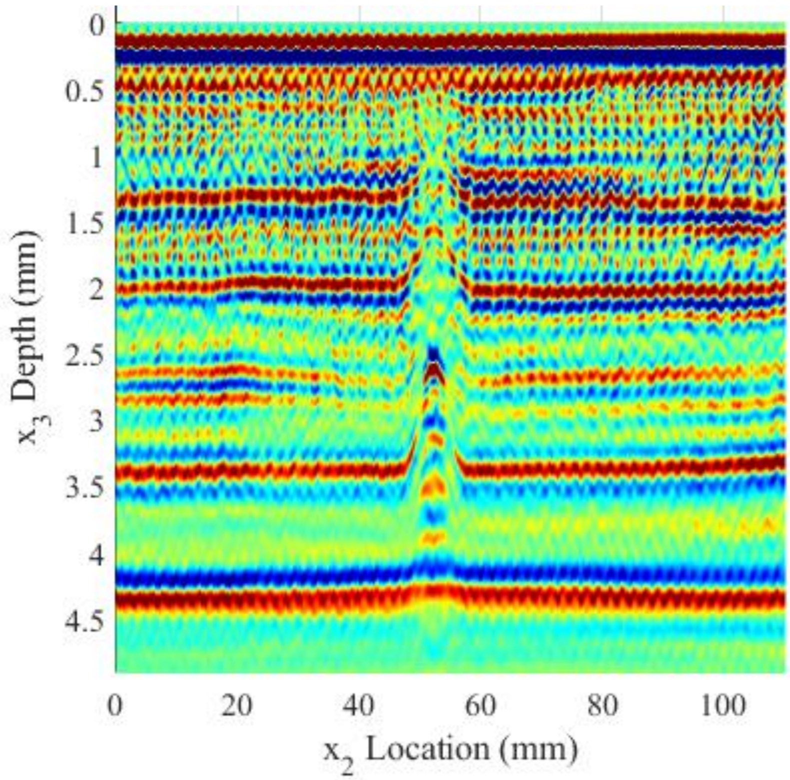

Figure 3.6, Sample b-scan plot from a composite with an out-of-plane wrinkle

When all of the a-scans are collected from an entire scan area a three-dimensional array of can be built. From this array time gates can be used to find the intensities across the scan area at a given time depth [42]. Figure 3.7 is for a gated time depth below the top surface of the laminate. In this figure the undulations of the fiber tows can be seen across the scan area. These scans are useful within nondestructive evaluation but were not considered helpful for this current study.

The last type of figure generated for this work, and the key scientific contribution of this research, is a 3D ultrasonic lamina plot of the surface morphology of an individual lamina as shown in Figure 3.8 and 3.9. The full mathematical details for how this plot is generated is provided in Section 3.4.1. Unlike the c-scan which is of a fixed depth or some integral value over a range of depths, the surface morphology shows the vertical position of an individual feature within the composite, even if it changes in depth. This contrasts with the c-scan that typically looks at a single depth position and shows the all the varying intensities at this depth. The surface morphology plot is generated by tracking the high intensity of a lamina's acoustic reflection in a set of a-scans across a scan area. This allows for tracking of internal features that change in the vertical direction within the composite structure. Previously this approach was employed by Blandford [40][41] to study the variation of the thickness of the bond line between two composite panels. This can be seen for the top and bottom of the adhesive planes in a bonded composite in Figure 3.8 (Figure B.12 from [40]). In this present thesis, the previous algorithms are modified to track the height changes of the wrinkle through a single lamina and an example of a captured wrinkle within a composite panel is shown in Figure 3.9, the model development to create this image is provided in the following section.

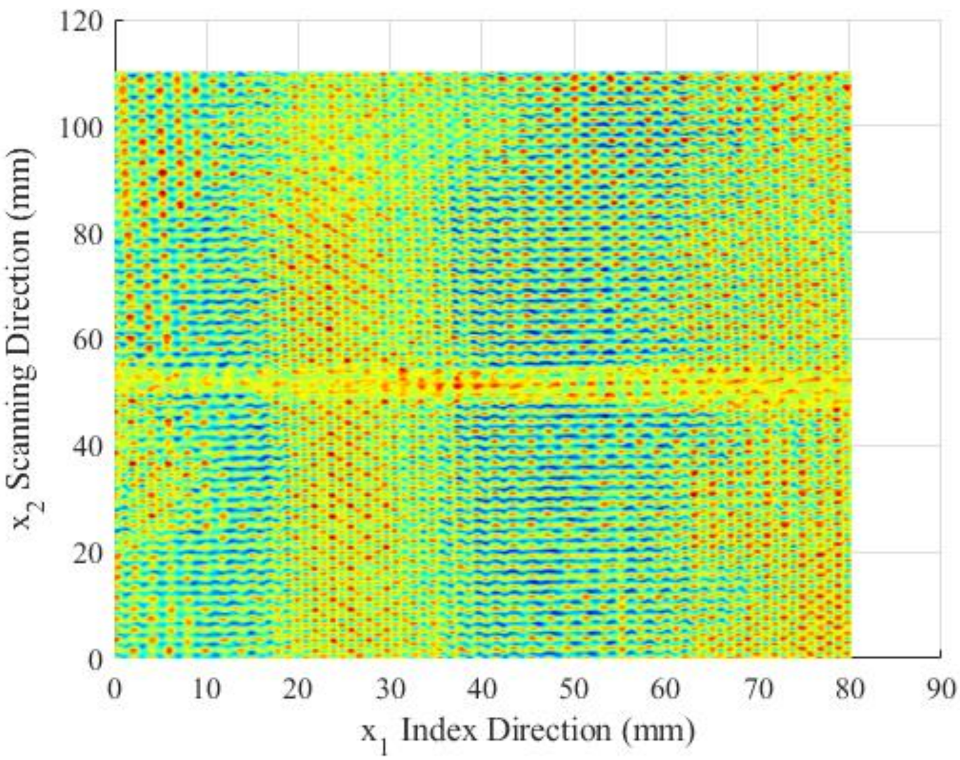

Figure 3.7, A sample c-scan plot of a woven composite with a wrinkle present. The undulations of the weave can be clearly seen.

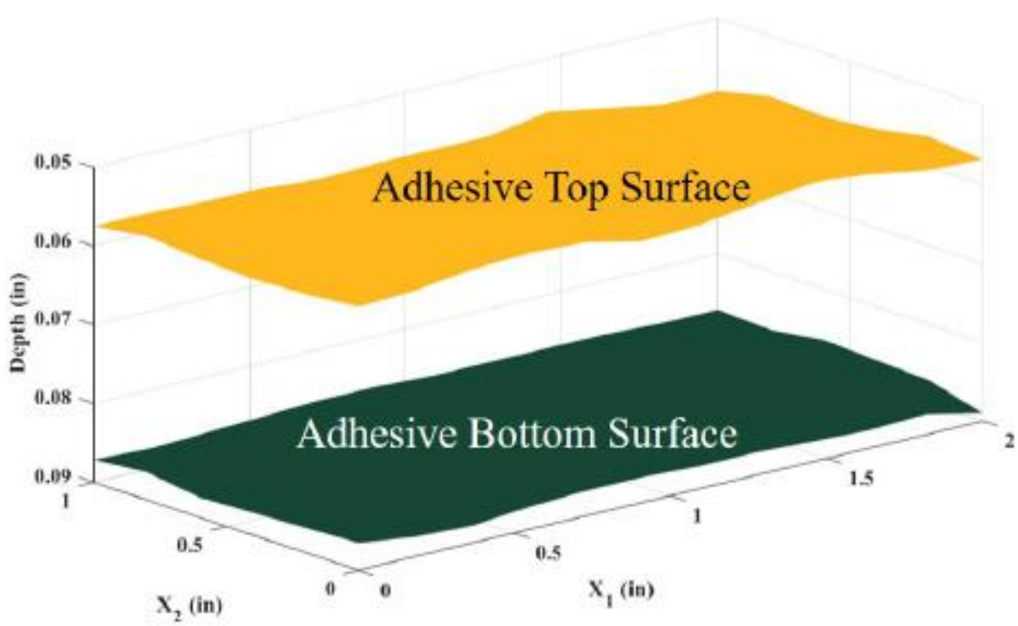

Figure 3.8, Example bond line thickness plot created by Ben Blandford [40].

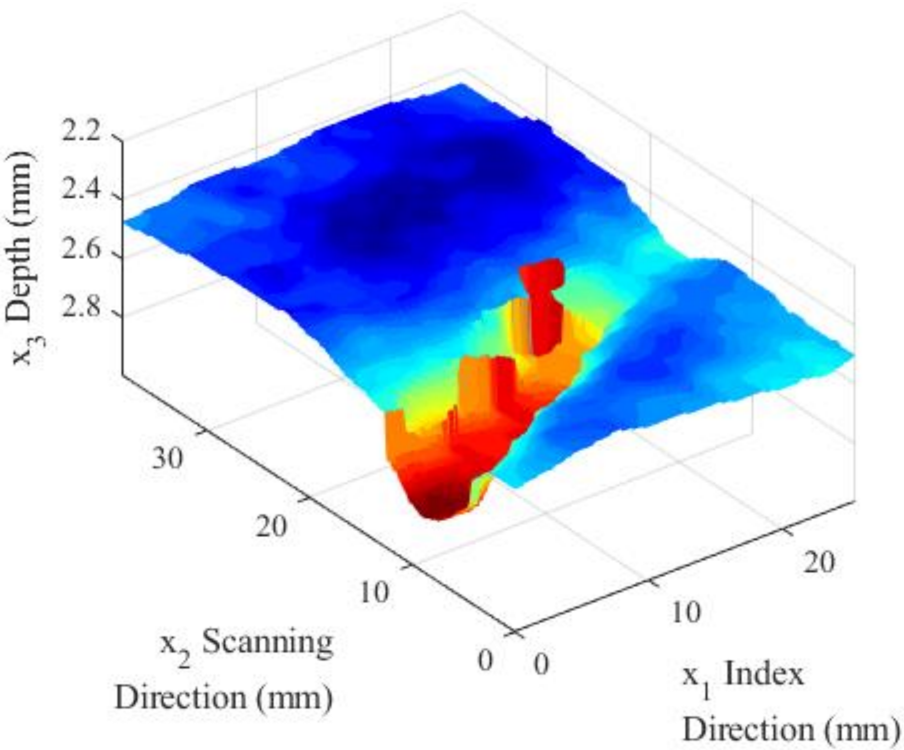

Figure 3.9, Sample lamina plot of a wrinkle within a composite

3.4.1 Automated Lamina Plot Generation with Out-of-Plane Wrinkle

The first step to create the 3D ultrasound lamina plot is to select the individual lamina to be tracked for which the wrinkle geometric features are desired. In order track the lamina the ultrasound data had to be put into a usable form. As mentioned above individual a-scans were taken every 0.2 mm in both the index direction $x_{1,j}$ and scanning direction $x_{2,j}$, and their waveform is defined as $f(t)$. The scan area is defined as $(x_{1,i}, x_{2,j})$ with each point representing the location of a single a-scan. The a-scans and the scan area can be combined to form a three-dimensional representation of the whole scan of the laminate as $f(t, x_{1,i}, x_{2,j})$.

Before using $f(t, x_{1,i}, x_{2,j})$ to investigate the wrinkle the unnecessary echo data recorded at the front of each a-scan needs to be removed. The approach to do this is described in [46] where a detection threshold is determined to catch the time of the first peak of the wave form corresponding to the front surface of the laminate for all $(x_{1,i}, x_{2,j})$. These moments in time that are determined and are used to make a third order polynomial surface, which is used to shift $f(t, x_{1,i}, x_{2,j})$. This shift aligns the start times, t_0, for all of the front wall reflection to be at the same time, $\tilde{t}$, where $\tilde{t} = t - t_0$. The new shifted form of the ultrasound data is defined as $F(\tilde{t}, x_{1,i}, x_{2,j})$ and will be used in the preceding sections.

For determining lamina of interest to be isolated within $F(\tilde{t}, x_{1,i}, x_{2,j})$, averaged b-scans in the x_1 and x_2 directions need to be generated. The process described below is by Blandford (see e.g. [40][41]). The average b-scans for the two directions are formed using the formulas found in those works, where the average is performed over the first 2 mm of b-scans in both directions, this corresponds to $n = m = 10$.

$$F_1(\tilde{t}, x_{1,i}) = \frac{1}{n}\sum_{k=0}^{n-1} F(\tilde{t}, x_{1,i}, x_{2,k}) \tag{3.5}$$

$$F_2(\tilde{t}, x_{2,j}) = \frac{1}{m}\sum_{k=0}^{m-1} F(\tilde{t}, x_{1,k}, x_{2,j}) \tag{3.6}$$

Equation (3.5) is for the formation of the average b-scans in the index direction x_1 and Equation (3.6) is for the scanning direction x_2. Figure 3.10 is the first 10 b-scans averaged across the scanning direction. From this image the lamina of interest is determined and is marked with a green arrow. This lamina also corresponds to where the two halves of the laminate were cured together and is where the 3D microscope scan was taken. The bounding of this lamina is a manual process requiring the user to select the points on the b-scan image above and below the lamina of interest (see e.g. [40][41]). Figure 3.10a shows example points selected above the lamina across the entire b-scan in magenta. After the points are selected, a cubic spline is fit to the points corresponding to the full length of the b-scan, (i.e. for $x_{2,j}$ where $j \in (1, 2, 3, \dots M)$), then the spline would contain M number of elements. The process of selecting points is repeated for the bottom edge side of the lamina of interest.

The resulting two cubic splines can be seen in Figure 3.10b, and they are defined as $\tilde{t}_{L_1,T}, (x_1, 0)$ for the top (T) spline and $\tilde{t}_{L_1,B}, (x_1, 0)$ for the bottom (B) spline, as seen in [41]. In practice a good fit requires extra points to be selected around the curved areas of the wrinkle, as seen in Figure 3.10a. Otherwise the spline will over or undershot the wrinkle, or add extra waves. The above steps are then applied to the average b-scan in the x_1 direction, where the same lamina of interest is bounded resulting in $\tilde{t}_{L_1,T}, (x_2, 0)$ and $\tilde{t}_{L_1,B}, (x_2, 0)$.

In the work from [40][41] a homogenization of the scan area $(x_{1,i}, x_{2,j})$ was implanted to average the a-scans into blocks to form the bond line images in Figure 3.8. This approach was pursued in [40][41] to avoid the added noise interference from the woven carbon fibers. For this current study the homogenization approach was removed, for an individual a-scan averaging approach for each point in $(x_{1,i}, x_{2,j})$. This was done to improve the overall resolution of the 3D lamina and to catch the depth variations caused by the wrinkle. To accomplish this a two dimensional gaussian filter developed in [46] is applied to all of $\left(x_{1,i}, x_{2,j}\right)$ in terms of index location of a-scans as in:

$$\widetilde{F}\left(\tilde{t}, x_{1,i}, x_{2,j}\right) = \frac{1}{2\pi\sigma_{x_1}\sigma_{x_2}} \sum_{p=-m}^{m} \sum_{q=-\mathrm{n}}^{\mathrm{n}} e^{\frac{-p^2}{2\sigma_{x_1}^2}} e^{\frac{-q^2}{2\sigma_{x_2}^2}} F\left(\tilde{t}, x_{1,i+p}, x_{2,j+q}\right) \tag{3.7}$$

The full derivation for the application of the 2D gaussian filter can be found in [46]. For this work a standard deviation σ_{x_1} and σ_{x_2} were set to 3 and a step sizes m and n were set to 9, these values were found to provide adequate results. Increasing the standard deviation did not provide any noticeable difference.

The next step uses these gated points in $\tilde{t}_{L_1,T}, (x_1, 0)$, $\tilde{t}_{L_1,B}, (x_1, 0)$, $\tilde{t}_{L_1,T}, (x_2, 0)$ and $\tilde{t}_{L_1,B}, (x_2, 0)$ to track the lamina across all $\left(x_{1,i}, x_{2,j}\right)$, this following the method was developed by Blandford in [40] and [41]. The gated points are minimums with a peak in the middle which corresponds to the lamina of interest. The maximum values between these two points are taken and used as the starting point for creating the lamina. The maximums down x_1 at $x_2 = 0$ are found as

$$S_{L_1}A\left(x_{1,I}, 0\right) = \underset{\tilde{t} \in \left(\tilde{t}_{L_1,T}, (x_1, 0),\ \tilde{t}_{L_1,B}, (x_1, 0)\right)}{max} \left|F(\tilde{t}, x_{1,I}, 0)\right| \tag{3.8}$$

Similarly, the maximum found down x_2 at $x_1 = 0$ are found as

$$S_{L_1}A\left(0, x_{2,J}\right) = \underset{\tilde{t} \in \left(\tilde{t}_{L_1,T}, (0, x_2),\ \tilde{t}_{L_1,B}, (0, x_2)\right)}{max} \left|F(\tilde{t}, 0, x_{2,\mathrm{J}})\right| \tag{3.9}$$

An example of the selected points down x_2 can be seen in Figure 3.11 highlighted by the black line. The time values related to where the maximums occur for $S_{L_1}A\left(x_{1,I}, 0\right)$ and $S_{L_1}A\left(0, x_{2,J}\right)$ are $\hat{t}_{L_1,T}, (x_{1,\mathrm{I}}, 0)$ and $\hat{t}_{L_1,B}, (x_{1,I=1}, x_{2,J})$ respectively. For $\hat{t}_{L_1,B}, (x_{1,I=1}, x_{2,J})$, x_1 does not start at 0, this is to prevent confusion for the algorithm for determining the maximum value at $(x_1, x_2) = (0,0)$. In Figure 3.12 the values of $\hat{t}_{L_1,T}, (x_{1,\mathrm{I}}, 0)$ and $\hat{t}_{L_1,B}, (x_{1,I=1}, x_{2,J})$ are represented as the magenta circles along the index and scanning directions.

The next step is to use the times in $\hat{t}_{L_1,T}, (x_{1,\mathrm{I}}, 0)$ and $\hat{t}_{L_1,B}, (x_{1,I=1}, x_{2,J})$ as a seed for the time location of the maximum in the next row and column of a-scans over $\left(x_{1,i}, x_{2,j}\right)$, see also [40] and [41]. The process first looks at the times from $\hat{t}_{L_1,T}, (x_{1,\mathrm{I}}, 0)$

and uses this time as a seed value to find the times of the maximums in the next row, $S_{L_1}A\left(x_{1,I}, x_{2,J=2}\right)$. The times for this new maximums are $\hat{t}_{L_1,T}, (x_{1,\mathrm{I}}, x_{2,\mathrm{J}=2})$. The times in $\hat{t}_{L_1,B}, (x_{1,I=1}, x_{2,J})$ along x_2 are seeded next to find the maximum values in the column $S_{L_1}A\left(x_{1,I=2}, x_{2,J}\right)$, resulting in $\hat{t}_{L_1,T}, (x_{1,\mathrm{I}=2}, x_{2,\mathrm{J}})$. This process results in two maximum values for any a-scan after the initial seed times are used for the first row and column. To find the value used for the next a-scan times from the previous points are compared and the time corresponding to the maximum of the two is kept. This process is continued across $\left(x_{1,I}, x_{2,J}\right)$ resulting in $\hat{t}_{L_1}(x_{1,\mathrm{I}}, x_{2,\mathrm{J}})$, which is the time location of all of the maximums for the lamina of interest.

The values in $\hat{t}_{L_1}(x_{1,\mathrm{I}}, x_{2,\mathrm{J}})$ are used to plot the surface of the lamina of interest. Figure 3.13 is an example of 3D ultrasound lamina plot created using the process described above. Highlighted by the yellow circles in the figure are the reflections of the three markers placed at the midplane after the first cure. The locations will be used to algin the 3D ultrasound lamina with the 3D microscope lamina in the following section.

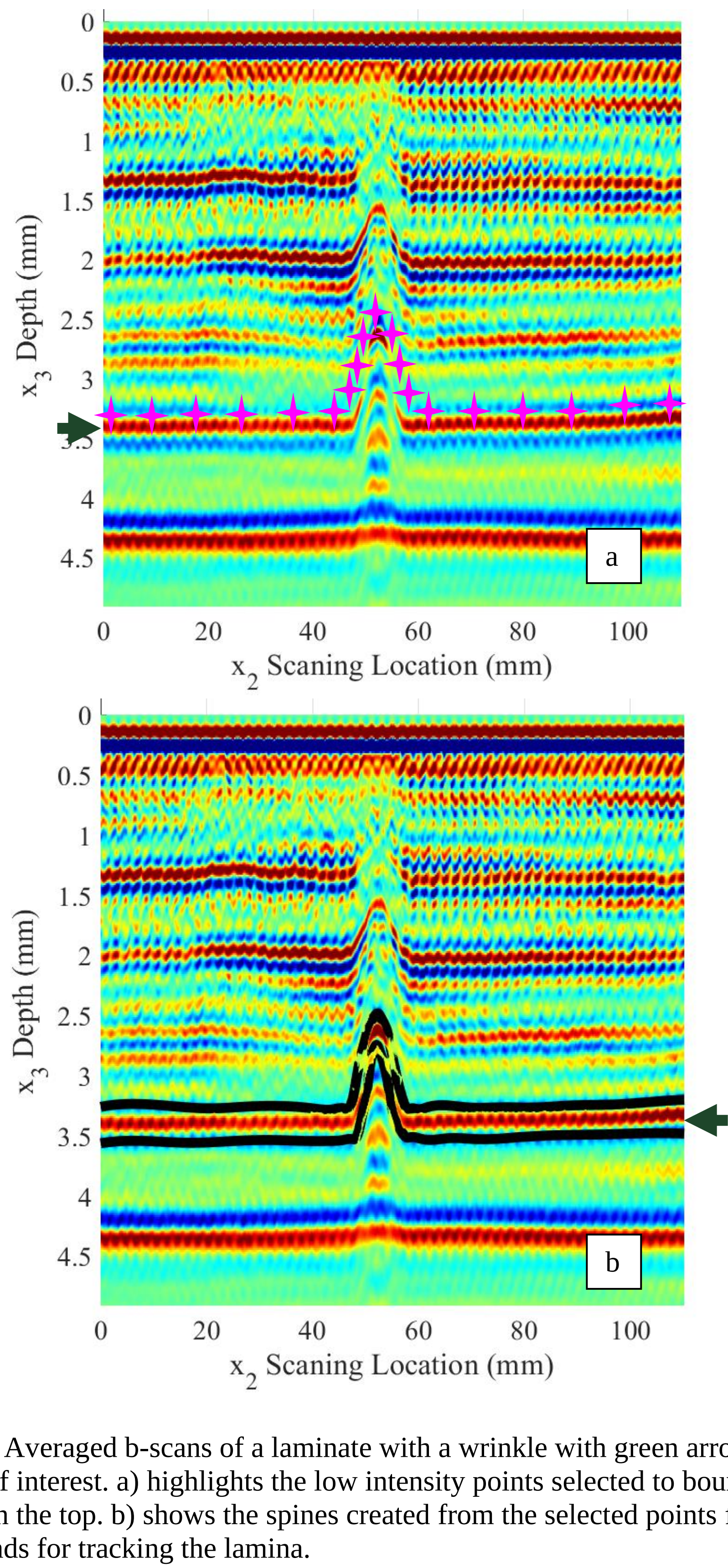

Figure 3.10, Averaged b-scans of a laminate with a wrinkle with green arrow identifying the lamina of interest. a) highlights the low intensity points selected to bound the lamina of interest on the top. b) shows the spines created from the selected points for the top and bottom bounds for tracking the lamina.

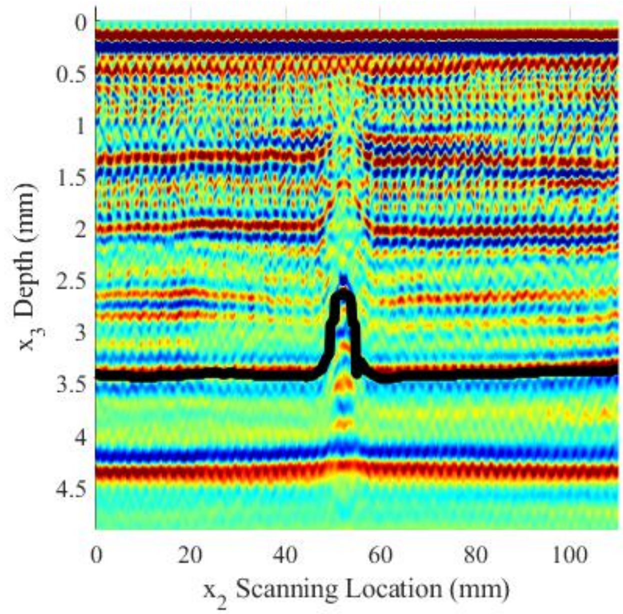

Figure 3.11, B-scan showing the maximums selected from between the bounded lines in Figure 3.10b, represented as $S_{L_1}A\left(0, x_{2,J}\right)$.

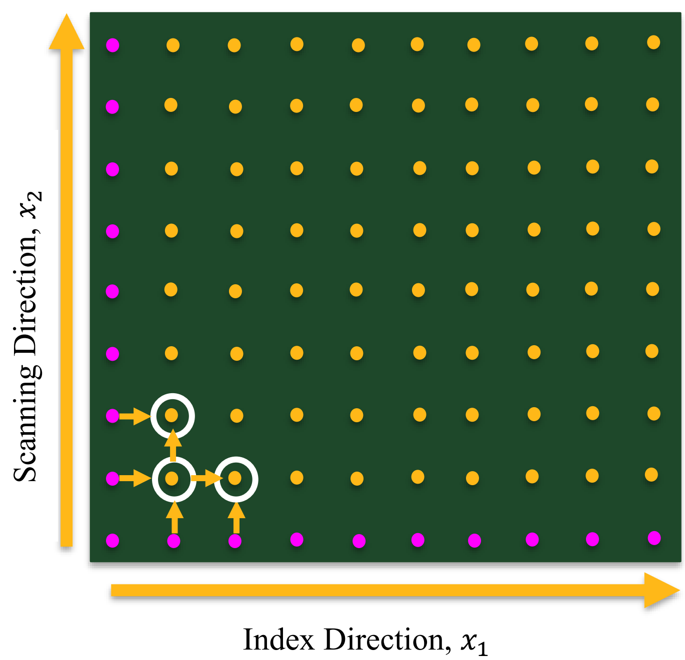

Figure 3.12, Represents all the a-scans for $\left(x_{1,i}, x_{2,j}\right)$. The magenta points are where the maximums are found from the manual selection process, the time locations for these maximums are used to find maximums of the points next to them, as seen by the yellow arrows pointing to the next point.

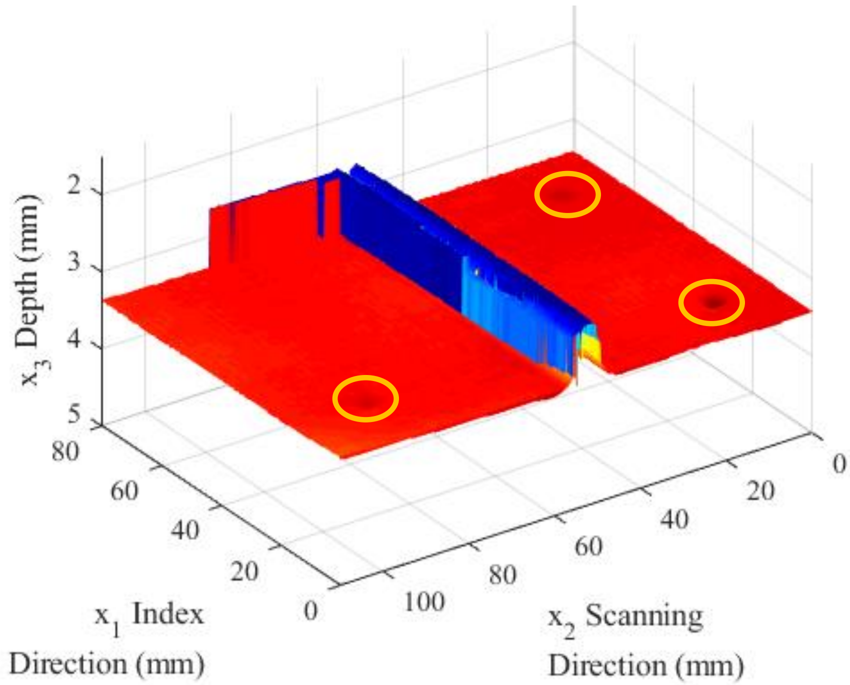

Figure 3.13, 3D ultrasound lamina plot created from the process described above. The three dark spots in the yellow circles correspond to the markers placed after the first cure cycle.

3.5 Lining Up Lamina Plots

In Chapter two samples of the mid surface of the laminate after the first cure cycle were imaged using 3D microscopy, such as in Figure 2.21. The microscopy results are used to validate the ultrasound wrinkle surface from the surface morphology technique in Section 3.4.1. A challenge in the validation is the alignment of the coordinate systems from the microscopy and the ultrasound data sets. This is done in the present study through the use of the markers placed on the interior surface that are offset from the wrinkle but are within each data set. The three markers will allow for the two different plots to be aligned for comparison.

To align these two plots a simplified Euler's rotation theorem was used [47]. Given a point in space, $\mathbf{x}_i$, where the bold face represents a vector in 3-space, and the subscript i indicates the i^th point of interest. This point can be rigidly translated through the point $\mathbf{x}_0$ as

$$\acute{\mathbf{x}}_i = \mathbf{x}_i - \mathbf{x}_0 \tag{3.10}$$

where $\acute{\mathbf{x}}_i$ is the point $\mathbf{x}_i$ in the translated coordinate system that is rigidly translated by $\mathbf{x}_0$.

This coordinate system can then be rotated through a series of angles about the new coordinate axis using Euler's rotation theorem. For example, a rigid body rotation can be expressed by the rotation tensor **A** to rotate from the coordinate system $\acute{\mathbf{x}}$ into the new coordinate system $\hat{\mathbf{x}}$, defined by the basis $(\hat{x}_1, \hat{x}_2, \hat{x}_3)$, as

$$\hat{\mathbf{x}} = \mathbf{A}\acute{\mathbf{x}} \tag{3.11}$$

Any rotation tensor can be formed by the subsequent rotations of three orthogonal rotations, but for simplification in this study the rotations are applied one at a time to align the points into coordinate system $\hat{\mathbf{x}}$**.** For example, a counter-clockwise rotation ϕ about the axis $\acute{x}_3$ is expressed as

$$\mathbf{B} = \begin{bmatrix} \cos\phi & \sin\phi & 0 \\ -\sin\phi & \cos\phi & 0 \\ 0 & 0 & 1 \end{bmatrix} \tag{3.12}$$

Then, a counterclockwise rotation of θ about the $\acute{x}_1$ axis is expressed as

$$\boldsymbol{C} = \begin{bmatrix} 1 & 0 & 0 \\ 0 & cos\theta & sin\theta \\ 0 & -sin\theta & cos\theta \end{bmatrix} \tag{3.13}$$

And finally, a rotation of β about the $\acute{x}_2$ axis is expressed as

$$\mathbf{D} = \begin{bmatrix} cos\beta & 0 & sin\beta \\ 0 & 1 & 0 \\ -sin\beta & 0 & cos\beta \end{bmatrix} \tag{3.14}$$

Depending on the rotation needed for alignment **A** from Equation (3.11) is replaced with ***B***, **C**, or **D**. To identify the angle of rotation from a fixed point in space, the dot product is used. For example, if one wanted to find the angle between the i[th] point in space $\acute{\mathbf{x}}_i$ and the j[th] unit basis vector $\mathbf{e}_j$ along the j[th] axis $\acute{x}_j$, then the angle between the two vectors is simply

$$\acute{\mathbf{x}}_i \cdot \mathbf{e}_j = |\acute{\mathbf{x}}_i||\mathbf{e}_j| \sin(90 - \gamma) \quad \rightarrow \quad \sin(90° - \gamma) = \frac{\acute{\mathbf{x}}_i \cdot \mathbf{e}_j}{|\acute{\mathbf{x}}_i|} \qquad (3.15)$$

where the magnitude of the unit basis $\mathbf{e}_j$ is unity. Equation (3.15) is a rule of cosines using the sine function in place the cosine.

The translation and rotation of both the 3D microscopy and the 3D ultrasound data sets is initiated by first finding the local coordinates for the three markers. For example, the local coordinates for the three markers from the microscopy are shown in Figure 3.12 and are defined as the points $\mathbf{x}_1^{3D}$, $\mathbf{x}_2^{3D}$, and $\mathbf{x}_3^{3D}$. The points are all translated, using Equation (3.11) to the coordinate system $\acute{\mathbf{x}}^{3D}$ by setting $\mathbf{x}_0 = \mathbf{x}_1^{3D}$. Next, the point $\acute{\mathbf{x}}_2^{3D}$, the point $\mathbf{x}_2^{3D}$ but given in terms of the translated system, is pulled in alignment with the $\hat{x}_1$ axis (notice that the superscript $3D$ is no longer necessary as this is the desired global coordinate system) by rotating about the $\acute{x}_3$ axis using Equation (3.13) where the angle of rotation is found using Equation (3.15) or (3.16). This new point $\acute{\mathbf{x}}_2^{3D}$, aligns along $\hat{x}_1$, and is pulled into the $\hat{x}_1 - \hat{x}_2$ plane using a rotation about the new $\hat{x}_2$ axis through Equation (3.14). Lastly, the point $\acute{\mathbf{x}}_3^{3D}$ is then pulled down onto the $\hat{x}_1 - \hat{x}_2$ plane by a rotation about the $\hat{x}_1$ axis using Equation (3.13). The code written within the MATLAB environment first places the 3D microscopy image into the global coordinates using the points $\mathbf{x}_1^{3D}$, $\mathbf{x}_2^{3D}$, and $\mathbf{x}_3^{3D}$. Then the three markers in the ultrasound local coordinate system, denoted by the points $\mathbf{x}_1^{US}$, $\mathbf{x}_2^{US}$, and $\mathbf{x}_3^{US}$ are rotated into the global coordinate system $\hat{\mathbf{x}}$ in a similar fashion where the rotation angles will be different than those of rotation angles for the microscopy image. But once both are expressed in the global coordinate system they are aligned and the surfaces can be directly compared point-by-point.

The three points were chosen by clicking on the center inner edge of the three markers on the surface plot. The reason for this is there is a height difference of the markers between the 3D microscope data and the ultrasound data. Choosing points on the main lamina plane eases the leveling of the lamina in the $\hat{x}_1 - \hat{x}_2$ plane. The index locations for these points are then manually coded into the program for a given data set. An example of the selected points for the 3D microscopy data can be seen in Figure 3.12 and for the 3D ultrasound data set they are shown for the same system in Figure 3.13. It is important to note that the microscopy image is taken relative to what will be the back surface of the part, whereas the ultrasound data is taken relative to the front of the part, but this is easily addressed by selecting the same three points $\mathbf{x}_i$ from both the microscopy and the ultrasound imaging. It is also to note that after selecting the points from the microscopy or the ultrasound data, they will not necessarily be orthogonal to each other. This is not essential, but the closer to orthogonal the points are, the higher will be the confidence in the analysis.

Once the microscopy surface and the 3D ultrasound lamina data set are aligned and placed in the same coordinate system, they are superimposed as in Figure 3.14. As can be observed in the figures the ultrasound surface and the microscopy surface are in alignment. There are subtle differences between the two data sets due to resolution quality, but the key feature is the clear overlap of the identified wrinkle between the two vastly different methods of characterization for the surface morphology. The quantification between these two data sets will be explored in detail in Chapter 4.

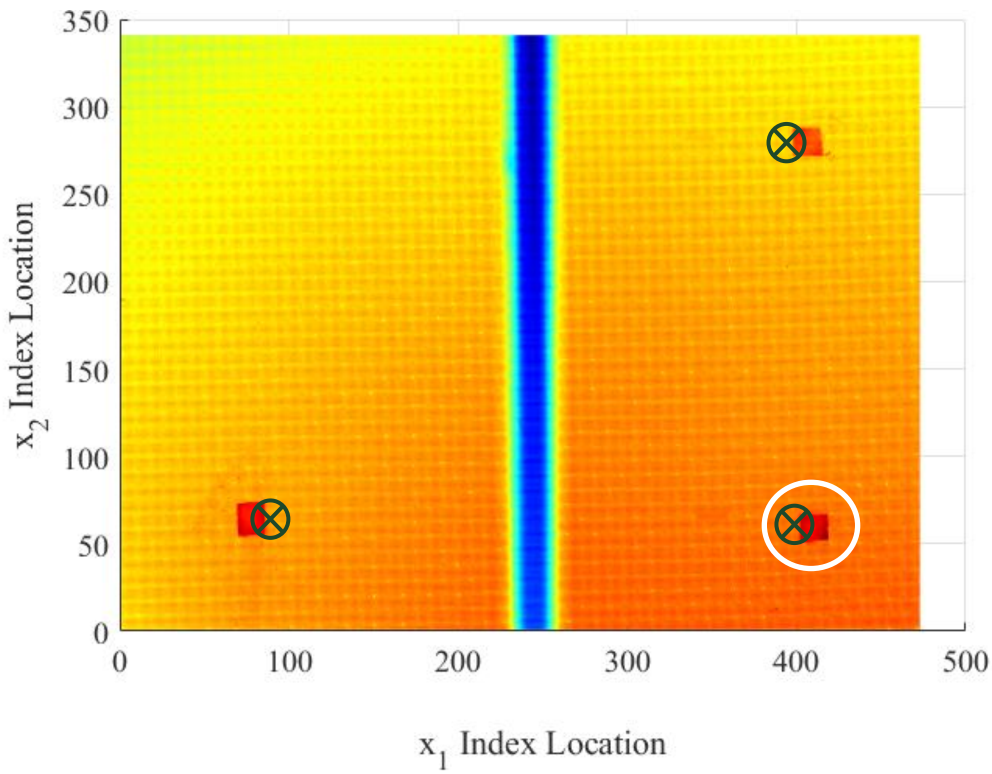

Figure 3.12, 3D microscope plot showing the index locations in the $\mathbf{x}_1$ and $\mathbf{x}_2$ directions. The three points chosen for alignment are shown with the green x's.

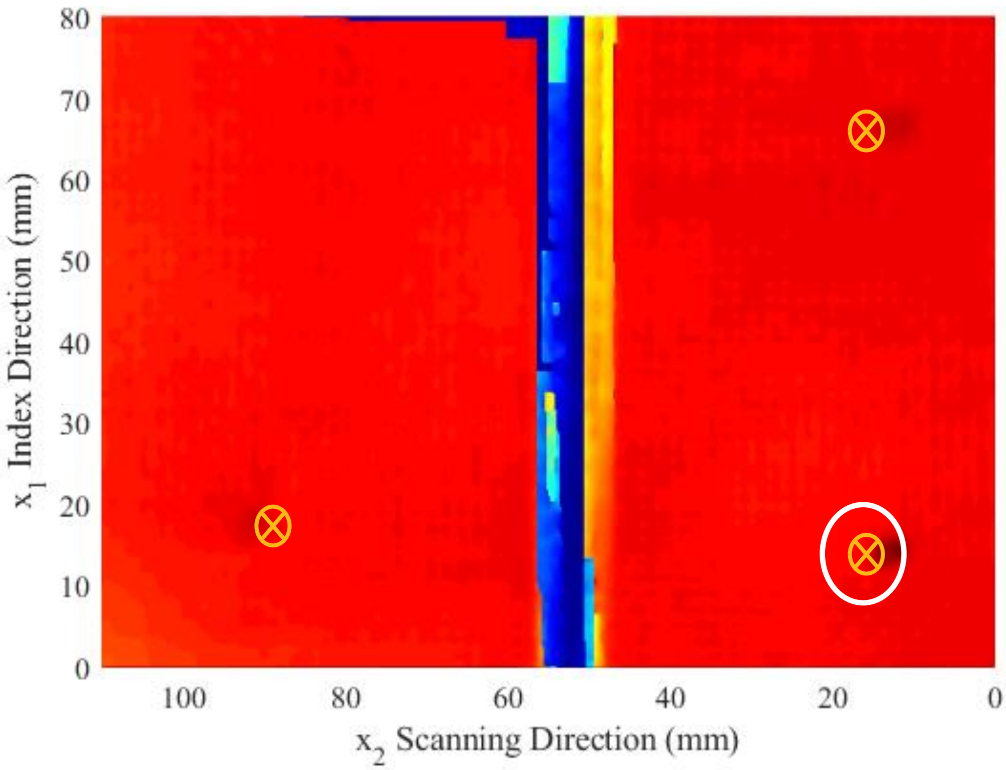

Figure 3.13, The selection of the three alignment points on the ultrasound lamina data plot.

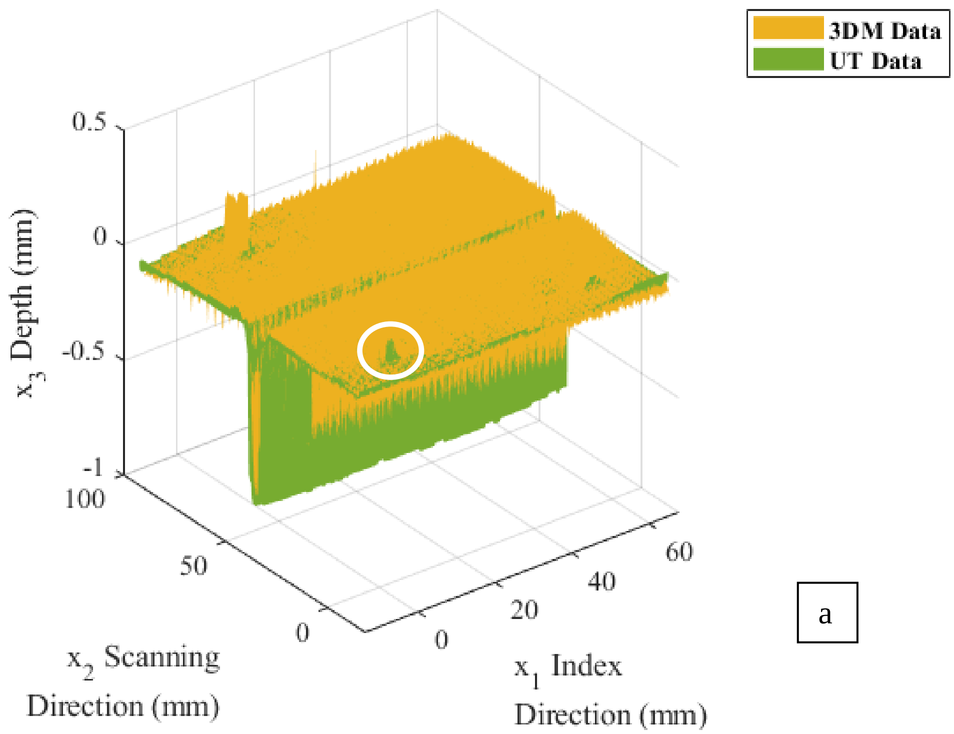

a

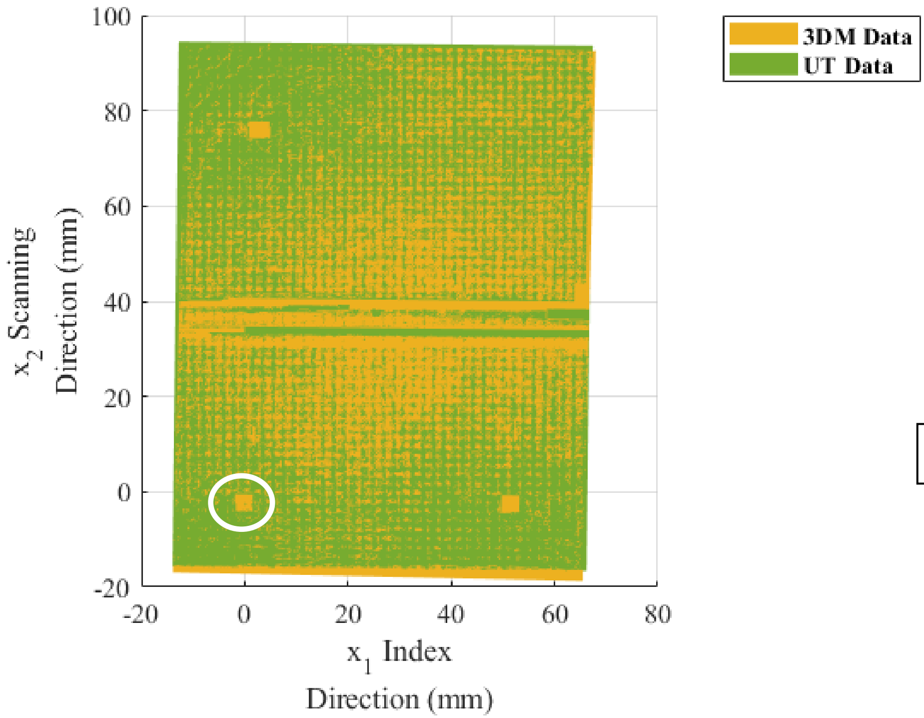

b

Figure 3.14, Figures a) and b) show the aligned data sets from the 3D microscope and the ultrasound dat. The white circle points out the origin.

CHAPTER FOUR

Results

4.1 Introduction

In this Chapter the processed ultrasound scan data for a plain weave carbon fiber composites will be discussed. Using the techniques developed in the last chapter 3D images of the wrinkle will be shown from the ultrasound data. The ultrasound data is then compared to the data collected from the 3D microscope to validate the data collected using ultrasound scanning techniques.

Three laminates will be compared in this chapter, two 18 lamina and one 25 lamina. All three laminates had the same layup of 0°/90° for each lamina. The two 18 layer laminates were both made using the two-step hot press curing process as discussed in Chapter Two. The first half of the laminate was 14 lamina thick with the wrinkle on one surface. The wrinkle wedge mold size used was 6.35 mm by 0.79 mm (0.25 in by 0.03 in), see Figure 2.11. The second half of the part was made with 4 lamina placed on the wrinkle side of the first half of the part. The main difference between the two 18 layer laminates is that one was made with having a delay for gelation and the other was made without the delay, called Part 1 and Part 2 respectively. The last laminate, Part 3, was made using the VARTM process and the wrinkle was induced by using the fold method, where the fold was placed on the fourth lamina layer. This part is presented as to show a potentially more realistic wrinkle within a laminate, since most industry laminates are not made using a two-step curing process as used in the other examples.

The parts were all scanned using the ultrasonic immersion scanning systems as described in Chapter Three. Part 1's scans were made with two different 10 MHz single element focused transducer and a 10 MHz passed array transducer. The laminate was scanned over the same approximate area each time with each transducer. The scans were all made where the scanning direction is perpendicular to the wrinkle within the part. Each scan was large enough to capture the three markers placed in between curing steps. These are used to align the 3D microscope data and the ultrasound data.

Part 2 and part 3 were both only scanned with the 12.7 mm (0.5 in) diameter 10 MHz transducer. For both parts the wrinkle was perpendicular to the scanning direction. For Part 2 a midplane scan was done using the 3D microscope and it will be compared to the 3D ultrasound lamina plot. The 3D ultrasound lamina plot will be presented for Part 3 but with no validation will be shown since the midplane was not scanned.

For Parts 1 and 2 b-scan images will be presented showing the bounded and tracked points for setting up the 3D lamina plot code. The 3D lamina plot from the ultrasound and the 3D microscope will be shown separately, followed by a figure where the two plots have been aligned with one another. Finally, comparison slices of the wrinkled area will be presented comparing the two data sets. Relative error and absolute error will be found for each data comparison set. These error calculations will then be compared to the error calculations for the work in [6]. These are not a one for one comparison but are a general comparison of results.

For Part 3 the b-scans of the bounded and tracked points for making the 3D lamina will be presented. Followed by the 3D lamina plot and one slice showing the wrinkle size at that location.

4.2 Out-of-Plane Wrinkle 3D Lamina Plot Comparisons

4.2.1 Part 1 Out-of-Plane Wrinkle Study 1

The following plots and figures will be related to Part 1 and the scans performed on it. As mentioned above this was an 18 layer laminate, made using the six hour delay for gelation between cures. As this is still a developing technique for investigating wrinkles within composites there are still some issues with acquiring good scans.

In some of the 3D lamina plots it will be shown that wrinkle is not well tracked across the entire scanning area. The lack of consistent intensities for the entire lamina being tracked cause the tracking algorithm to sometimes get lost and it will not be able to recover. One of the future goals for wrinkle detection should be to improve the resolution of the side walls of the wrinkle arc. The technology used for these ultrasonic scans are good for looking at flat objects below them, but when curved surfaces are introduced difficulties arise. The main reflection off of the slope of the wrinkle arc does not go straight back to the transducer but is shot off in the normal direction of the slope. Therefore, on many of the b-scans shown here they do not have good definition for the wrinkle slopes.

In Figure 4.1 a b-scan of the wrinkle using the 10 MHz 12.7 mm focused transducer is shown. The green box is highlighting the main wrinkle arch of interest, and it can be seen that the majority of the slopes of the wrinkle are missing as discussed above. This is common on most of the scans presented here.

Figure 4.2a presents the bounded lamina of interest for generating the 3D lamina plot. Then in Figure 4.2b the maximum intensity found between the bounded area is shown, and these are the first points used to start making the 3D lamina plot.

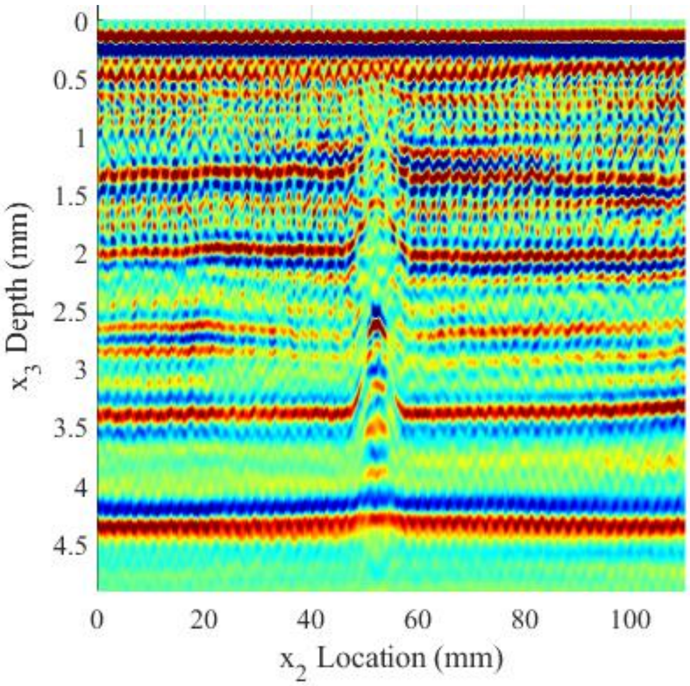

Figure 4.1, B-scan of Part 1 showing the out-of-plane wrinkle. The green box highlights the loss of intensity of the signal between the slopes and the peak of the wrinkle.

The 3D ultrasound lamina plot is presented in Figure 4.3a. As discussed earlier there are issues with the tracking of the wrinkle across the entire scan area. Figures 4.3b and c are closer looks at some of the inconsistencies seen through the tracking process. In Figure 4.4 is the height plot from the 3D microscope scan of the mid plane in between the first and second cures for manufacturing the laminate. This image will be the same for all three scan comparisons of Part 1. The figure has had the middle marker shifted to the origin and it has been leveled in the $x_1 - x_2$ plane.

Figure 4.5 shows the superimposed alignment of the 3D ultrasound lamina with the 3D microscope lamina. From visual inspection of the figures the alignment between the data displays good correlation. Though in reality there are some issues with it because of the missed tracked portions of the lamina in the ultrasound data as seen in Figures 4.3b and c.

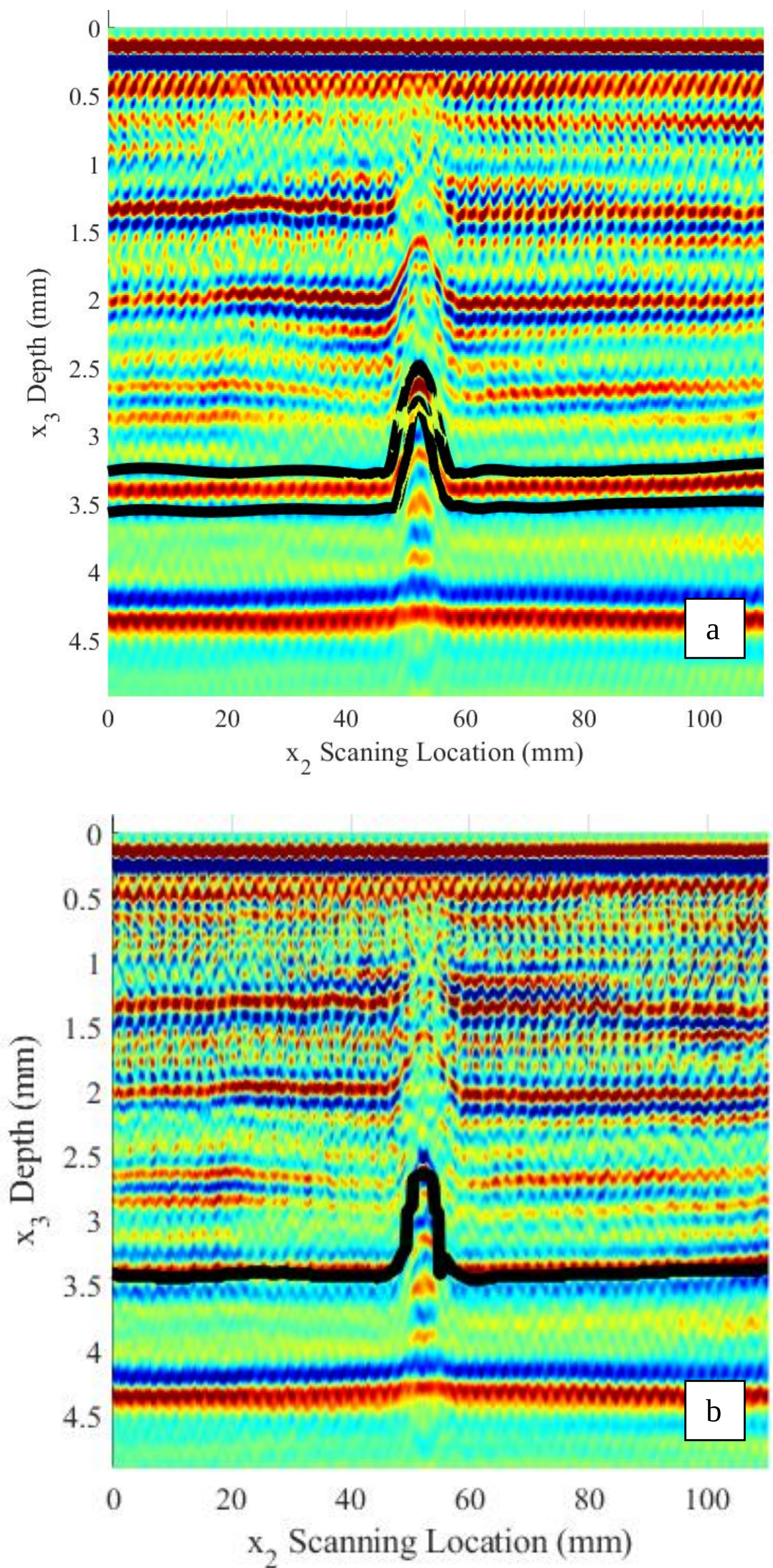

Figure 4.2, a) B-scan of Part 1 showing the bounded lamina of interest, b) b-scan showing the selected maximum intensities between the bounded region.

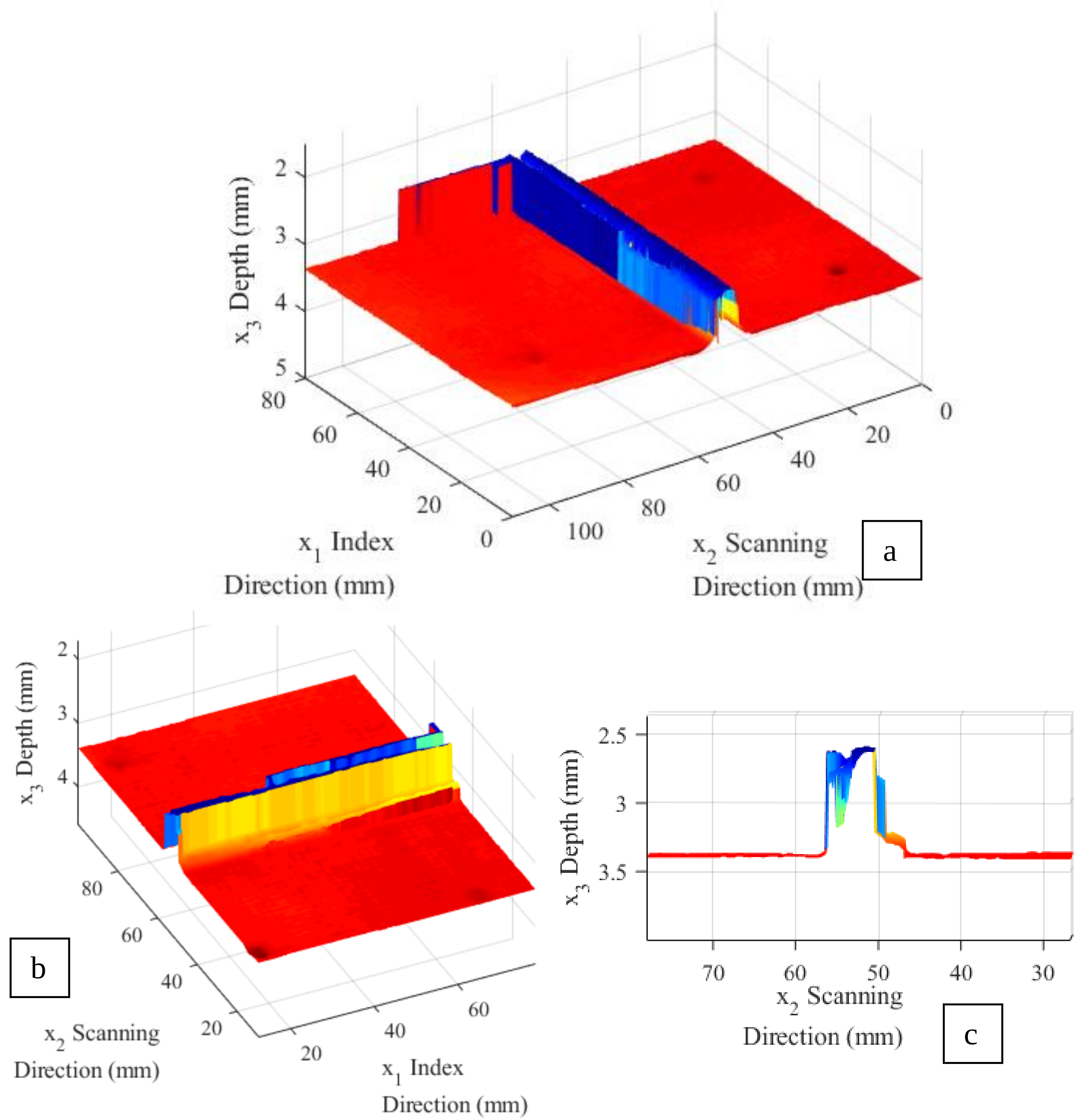

Figure 4.3, a) 3D lamina plot of the out-of-plane wrinkle withing Part 1, b) and c) are closer looks at some of the issues with the wrinkle tracking across the laminate.

In Figures 4.6a and b two slices of data are taken from the comparison plots shown in Figure 4.5. These plots are taken at approximately the same location, but because of the difference between step sizes for the data sets they are not exact. The first sample is taken at about 20 mm and the second is at about 40 mm. The code for plotting the slices finds the minimum of the curves which can be used to find the height of the wrinkle. The width of the wrinkle is found by selecting the points where the slope of the wrinkle begins to change towards the minimum point and where it begins to level back out. These points are manually selected at this current time.

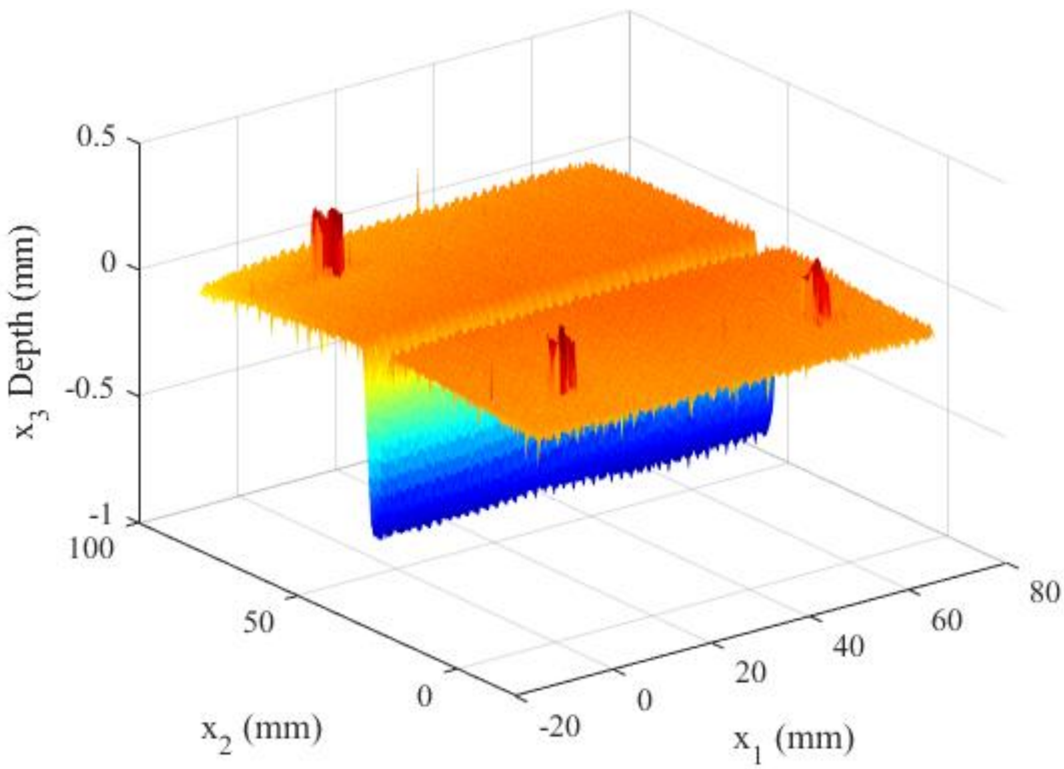

Figure 4.4, 3D microscope height map of the midplane of the laminate after the first cure.

For calculating the height of the wrinkle the minimum value found is subtracted from the y values found for the width dimensions. The average of these two differences is the approximate height of the wrinkle. The width of the wrinkle is found by taking the difference of the two width points selected. The intensity is found by using Equation 1.2 with the calculated height and width values. This process is applied to both data sets for the ultrasound and the 3D microscope. The results of these calculations can be found in Table 4.1.

The relative error and the absolute error are found for each slice comparison. The relative error (RE) is found by taking the absolute value of the measured value (MV) minus the actual value (AV), dividing by the AV, and multiplying by 100 as in

$$RE = \frac{|MV - AV|}{AV} \times 100 \quad (4.1)$$

The absolute error (AE) is found by taking the absolute value of the difference between the measured value and the actual value, as in

$$AE = |MV - AV| \quad (4.2)$$

The error values for each comparison can be found in Table 4.1. From the error values calculated for this comparison there appears to be good agreement between the data sets.

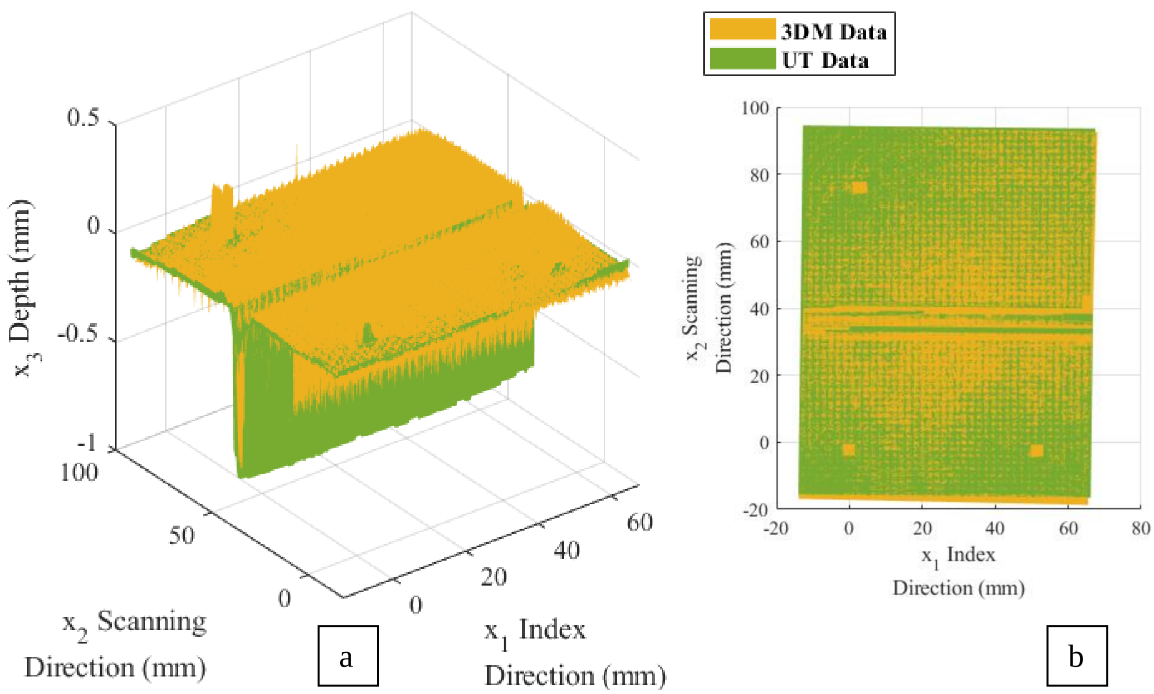

Figure 4.5, a) and b) show the superimposed alignment of the 3D ultrasound lamina with 3D microscope lamina.

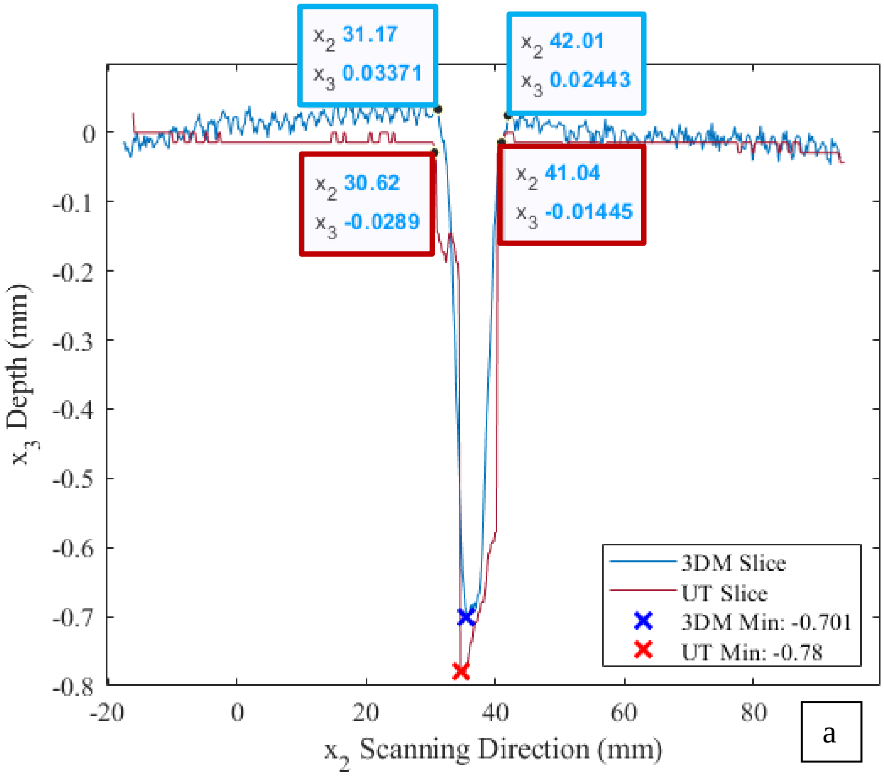

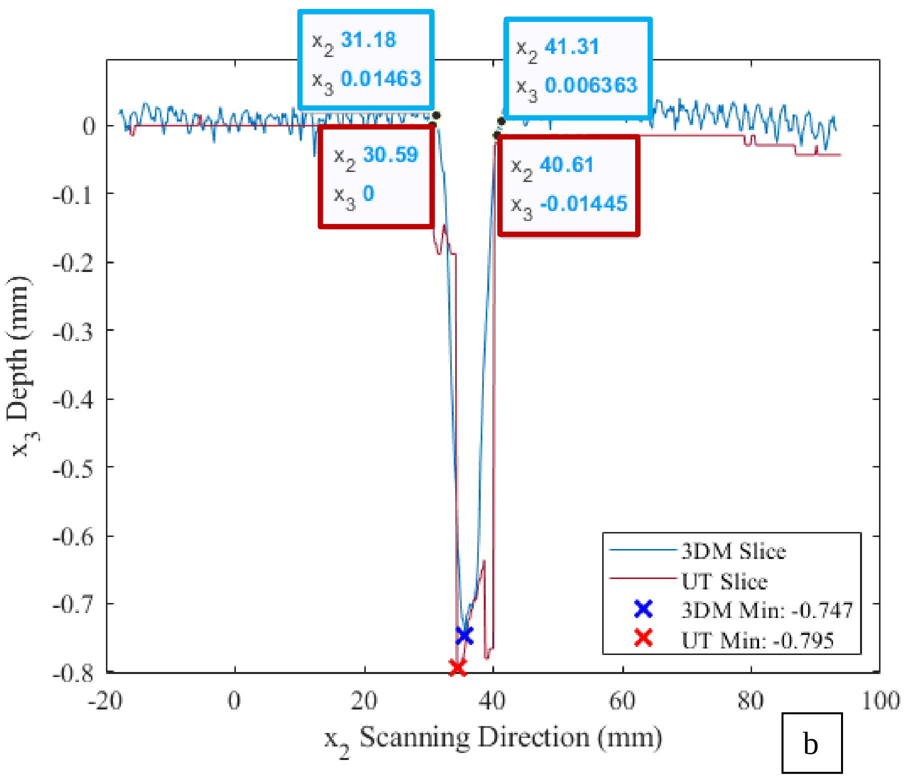

Figure 4.6, a) Slice comparison of the wrinkle at 20 mm, and b) slice comparison of the wrinkle at 40 mm. The minimum values represent the height of the wrinkle and the other points are used to find the width.

Table 4.1 Measured Values of the Out-of-Plane Wrinkles Study 1

Slice Position	Dimension	3D Microscope (mm)	Ultrasound (mm)	Relative Error (%)	Absolute Error
20 mm Slice	Height	0.73	0.758	3.87	0.0283 mm
	Width	10.84	10.42	3.87	0.42 mm
	Intensity	0.0337	0.0364	8.057	0.0027
40 mm Slice	Height	0.758	0.788	3.99	0.0303 mm
	Width	10.13	10.02	1.09	0.11 mm
	Intensity	0.0374	0.0393	5.14	0.0019

4.2.2 Part 1 Out-of-Plane Wrinkle Study 2

The scans done for this section used the single element focused 10 MHz transducer with a 6.35 mm (0.25 in) diameter element. The results for these scans are similar to the ones presented in the last section, though there are still issues with tracking the slopes of the wrinkles and with the tracking algorithm going out of alignment.

Figure 4.7a is the b-scan showing the bounds being applied to start the wrinkle tracking. One noticeable difference in the b-scan is there is even less definition of the wrinkle slope as compared to Figure 4.1. Figure 4.7b is the maximum values found in between the bounded area being used by the tracking algorithm.

Figure 4.8a is the 3D ultrasound lamina plot that was created. An issue can be clearly seen at the back of the lamina where the peak of the wrinkle has dropped off significantly, Figure 4.8b is a closer look at this region. This is another example of how the algorithm can get off course and not be able to recover. There is a potential need to work on improving the tracking of the algorithm, but there may also be improvement gain when there is better wrinkle definition within the ultrasound scan data.

The 3D ultrasound lamina plot and the 3D microscope plot are superimposed upon each other in Figure 4.9a and b. The laminas have already been aligned together.

The same procedure that was done above will be implemented on this plot. Two slices will be taken again at about 20 mm and 40 mm. Figure 4.10 shows the two slices, and the measurement results are in Table 4.2. The relative error and the absolute error are calculated and are in the same table. These values show good correlation between the two data sets despite the poor tracking of the algorithm.

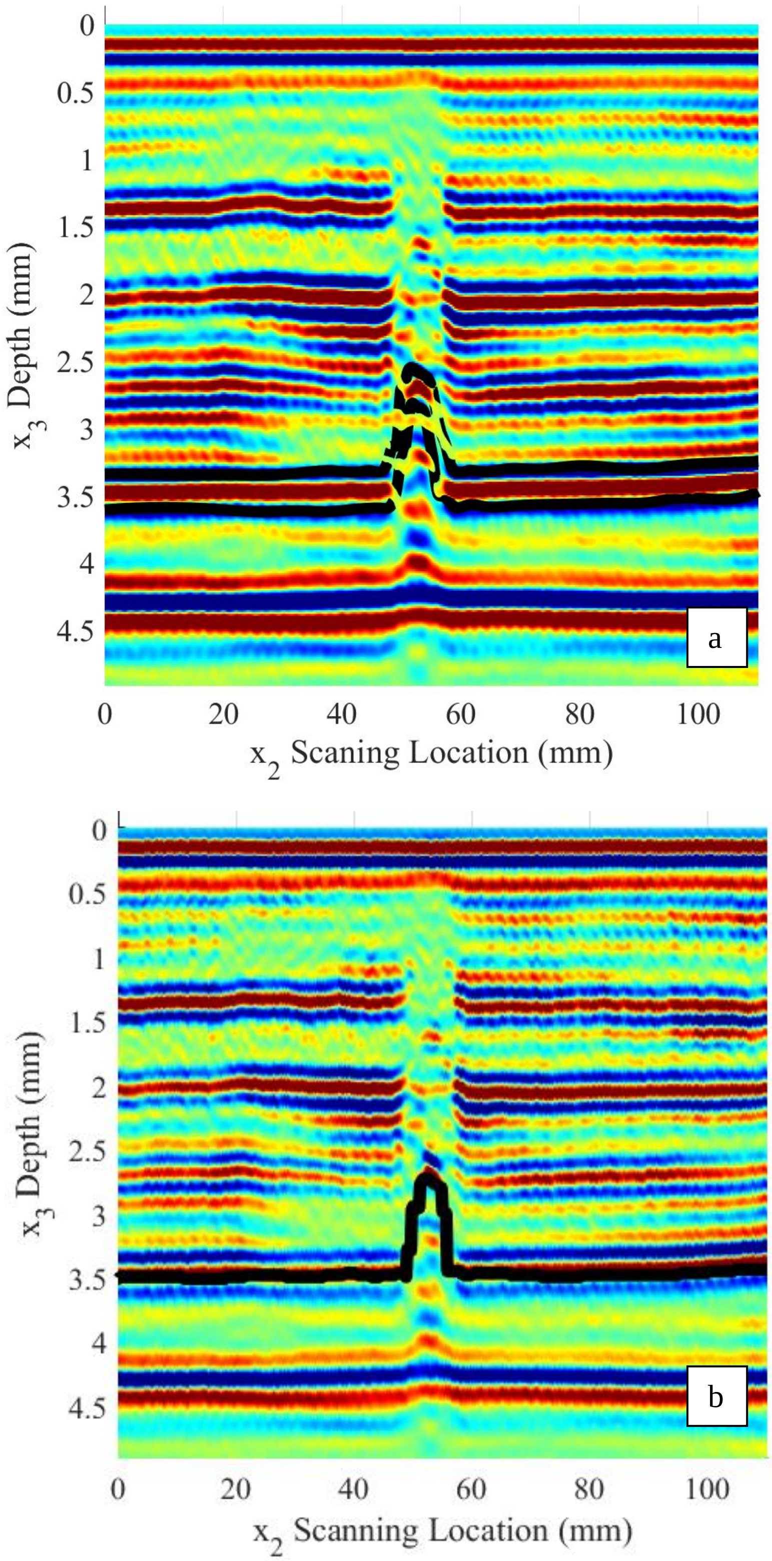

Figure 4.7, a) B-scan of Part 1 showing the bounded lamina of interest, b) b-scan showing the selected maximum intensities between the bounded region.

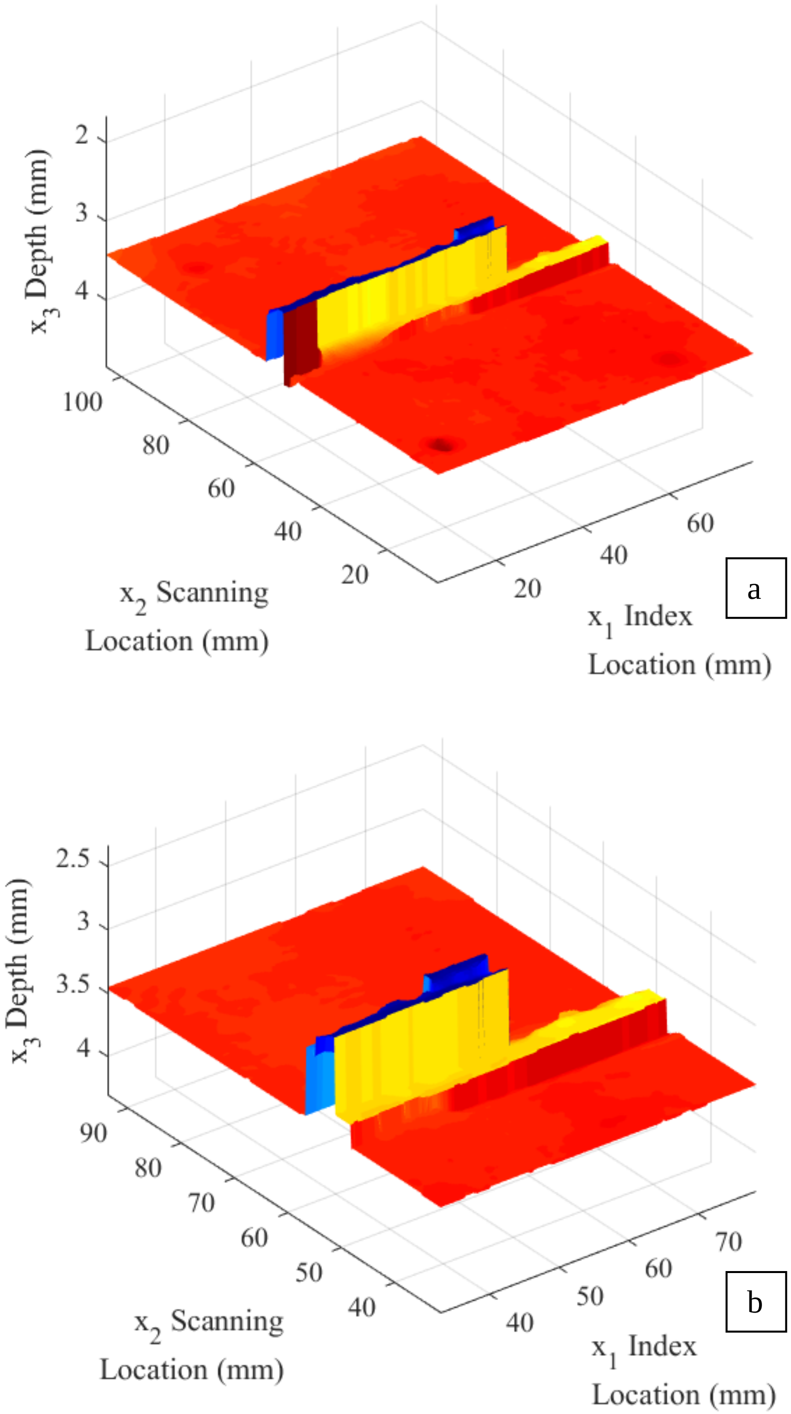

Figure 4.8, a) is the full 3D ultrasound lamina plot form the data using the 6.35 mm diameter transducer, b) is a zoomed in section of the 3D lamina where the tracking algorithm gets lost.

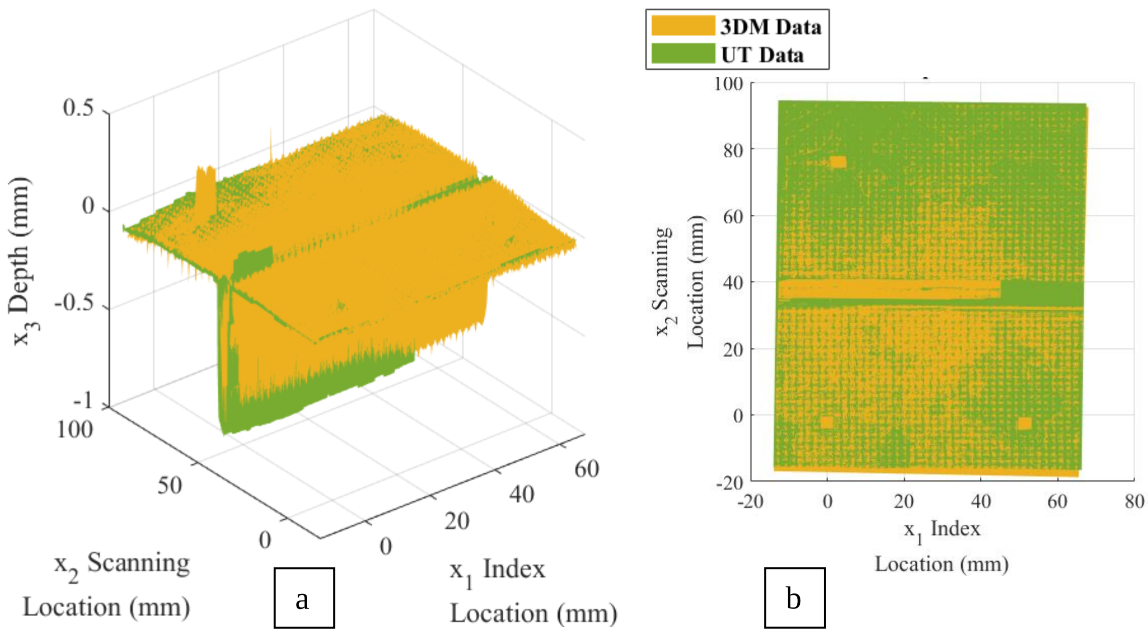

Figure 4.9, Superimposed alignment of the 3D ultrasound lamina with 3D microscope lamina, a) isometric view, and b) top view.

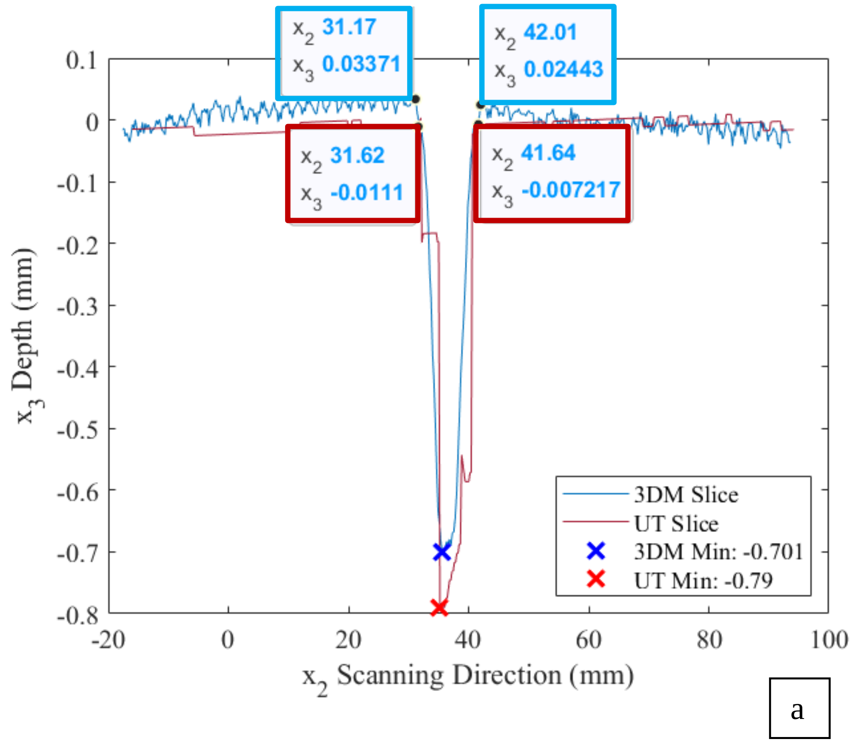

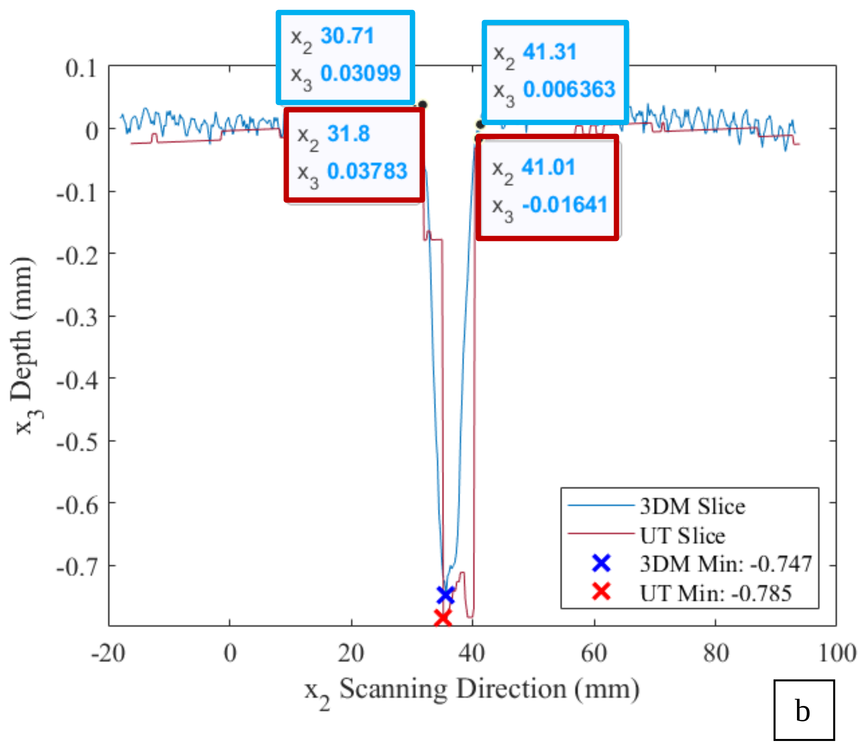

Figure 4.10, a) Slice comparison of the wrinkle at 20 mm, and b) slice comparison of the wrinkle at 40 mm. The minimum values represent the height of the wrinkle and the other points are used to find the width.

Table 4.2 Measured Values of the Out-of-Plane Wrinkles Study 2

Slice Position	Dimension	3D Microscope (mm)	Ultrasound (mm)	Relative Error (%)	Absolute Error
20 mm Slice	Height	0.73	0.781	6.95	0.051 mm
	Width	10.84	10.02	7.56	0.82 mm
	Intensity	0.0337	0.039	15.71	0.0053
40 mm Slice	Height	0.767	0.796	3.92	0.03 mm
	Width	9.6	9.21	4.06	0.39 mm
	Intensity	0.0399	0.0416	4.23	0.0017

4.2.3 Part 1 Out-of-Plane Wrinkle Study 3

The final analysis of Part 1 is conducted using the 10 MHz phased array immersion transducer. The transducer has 64 elements, but only 12 were used to create the focused beam for this scan. The phased array system was acquired close to the end of this study, therefore the results shown here are only preliminary. The results for this scan fall more in line with the results from the 10 MHz 12.7 mm diameter transducer over the 6.35 mm diameter transducer. This may be the result of the fact that the larger diameter transducer is closer to 12 element phased array aperture. The same set of figures will be presented here as with the past two studies.

Figure 4.11a is the bounded lamina of interest for the 3D lamina plot and 4.11b is the maximum intensities found in the bounded region. As with the larger diameter transducer the wrinkle slopes are more defined, but there are still gaps along the slopes.

In Figure 4.12 the 3D ultrasound lamina plat of the wrinkle is shown, this lamina still has some issues but is better than what was seen in study 2. The lamina tracking is still not perfect like the other two studies, but the peak and the width are tracked decently across the scan area. The tracking algorithm at the end drifted off course following the lamina at the peak of the wrinkle, the cause of this is unclear.

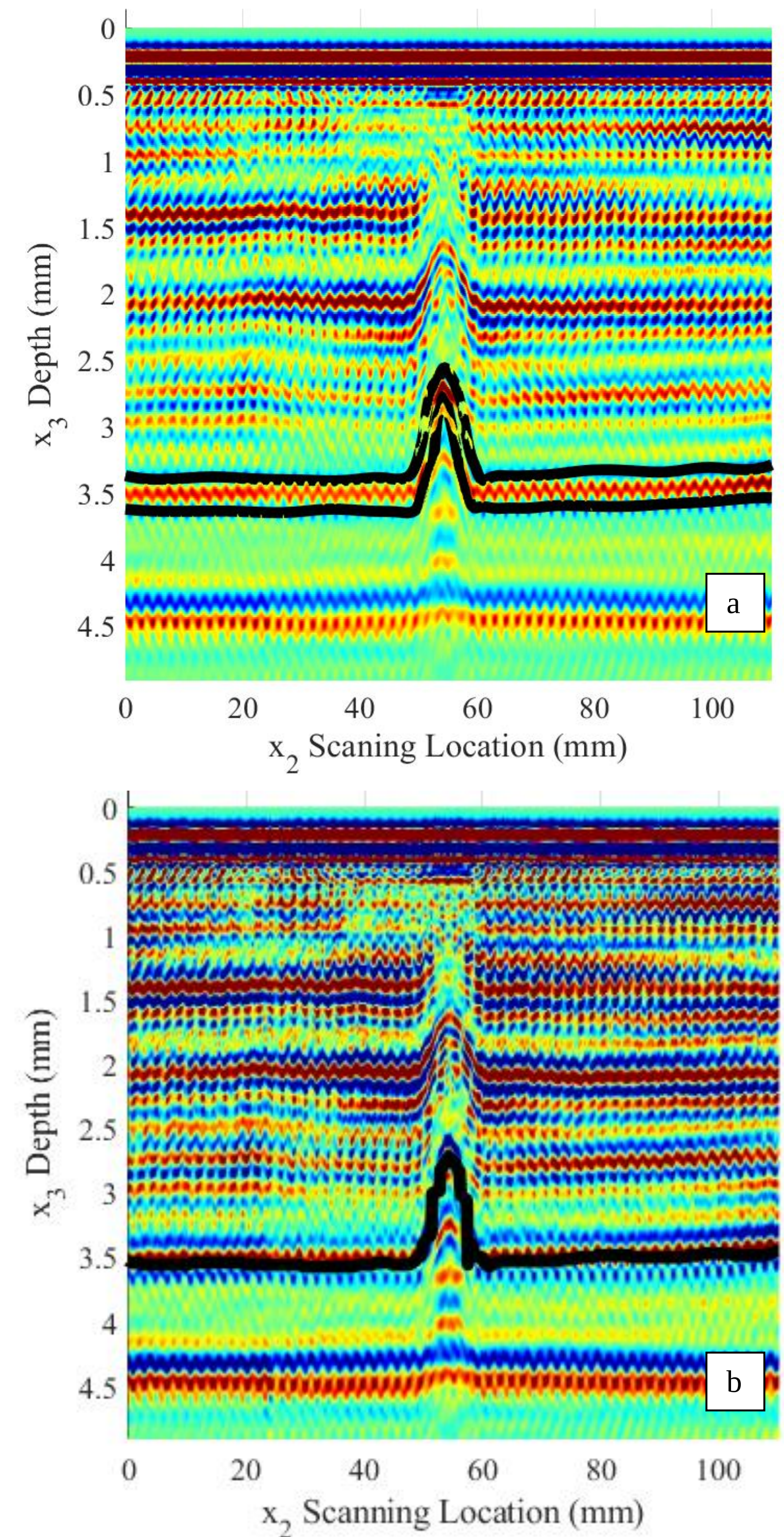

Figure 4.11, a) B-scan of Part 1 showing the bounded lamina of interest, b) b-scan showing the selected maximum intensities between the bounded region.

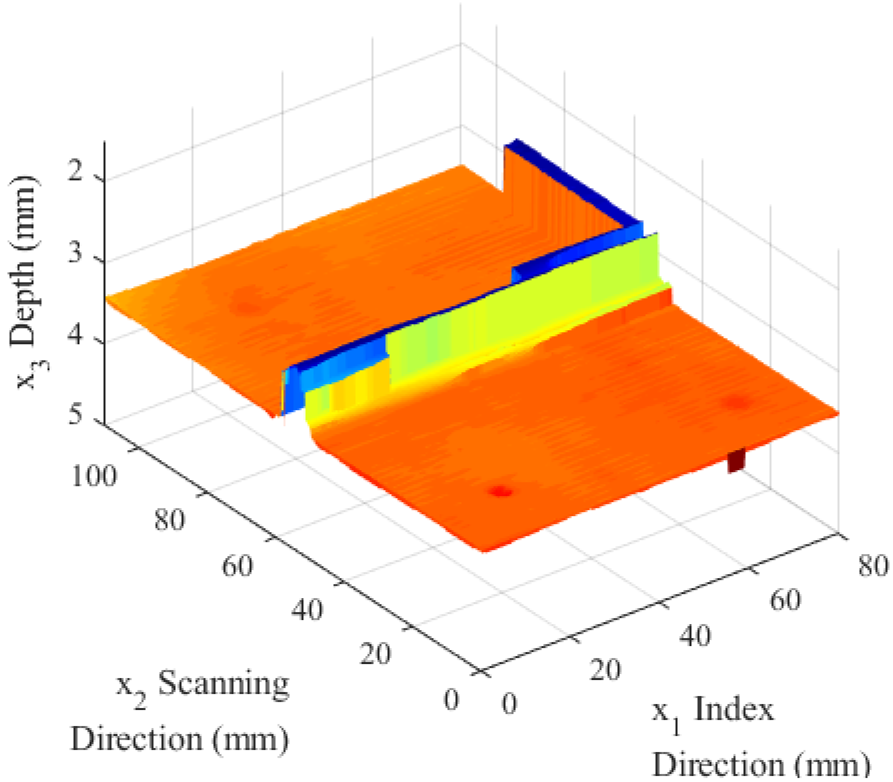

Figure 4.12, The full 3D ultrasound lamina plot from the data using the phased array transducer.

The superposition and alignment for 3D ultrasound lamina and the 3D microscope lamina was less accurate since the third marker on side of its own did not show up clearly. A faint image of the marker can be seen in Figure 4.12, and a manual approximation was used to select the point in the area of the marker. The two lamina plots together can be seen in Figure 4.13a and b. Despite the difficulty in finding the marker the figures show good alignment between the two data sets.

The slice comparison presented here is the same as the previous two studies, where slices are compared at 20 mm and 40 mm. Figure 4.14a and b shows the two slices and the data points used for the calculations. The results for the comparison can be found and the error calculations can be found in Table 4.3. Again, good agreement between these two data sets is presented.

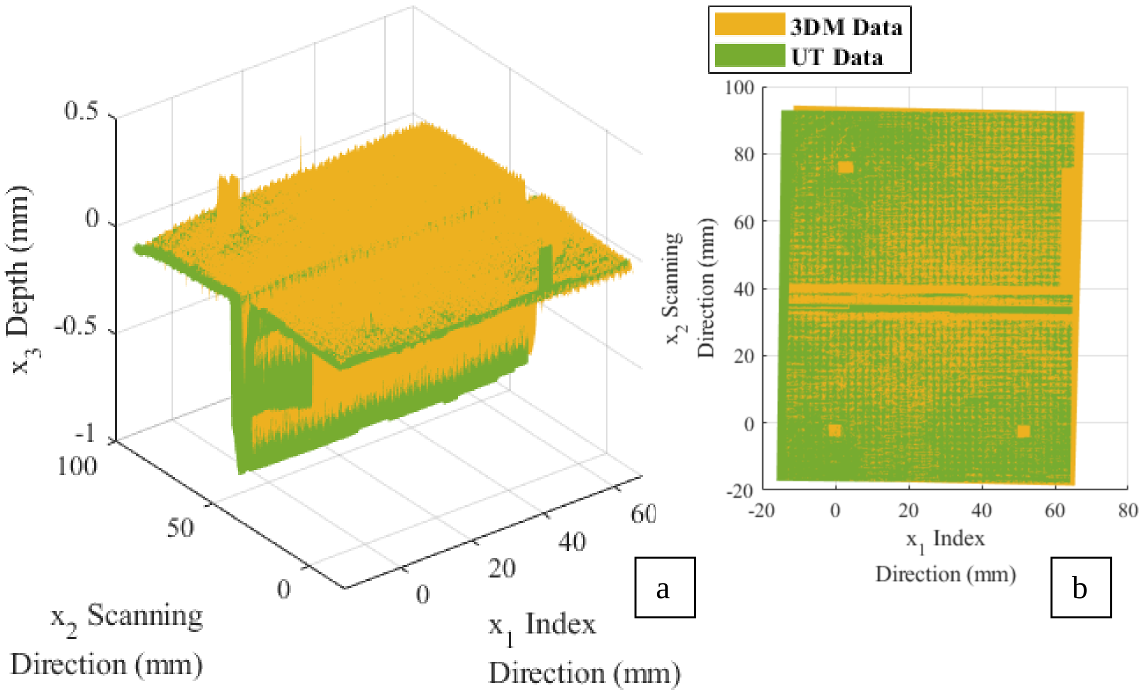

Figure 4.13, Superimposed alignment of the 3D ultrasound lamina with 3D microscope lamina, a) isometric view, and b) top view.

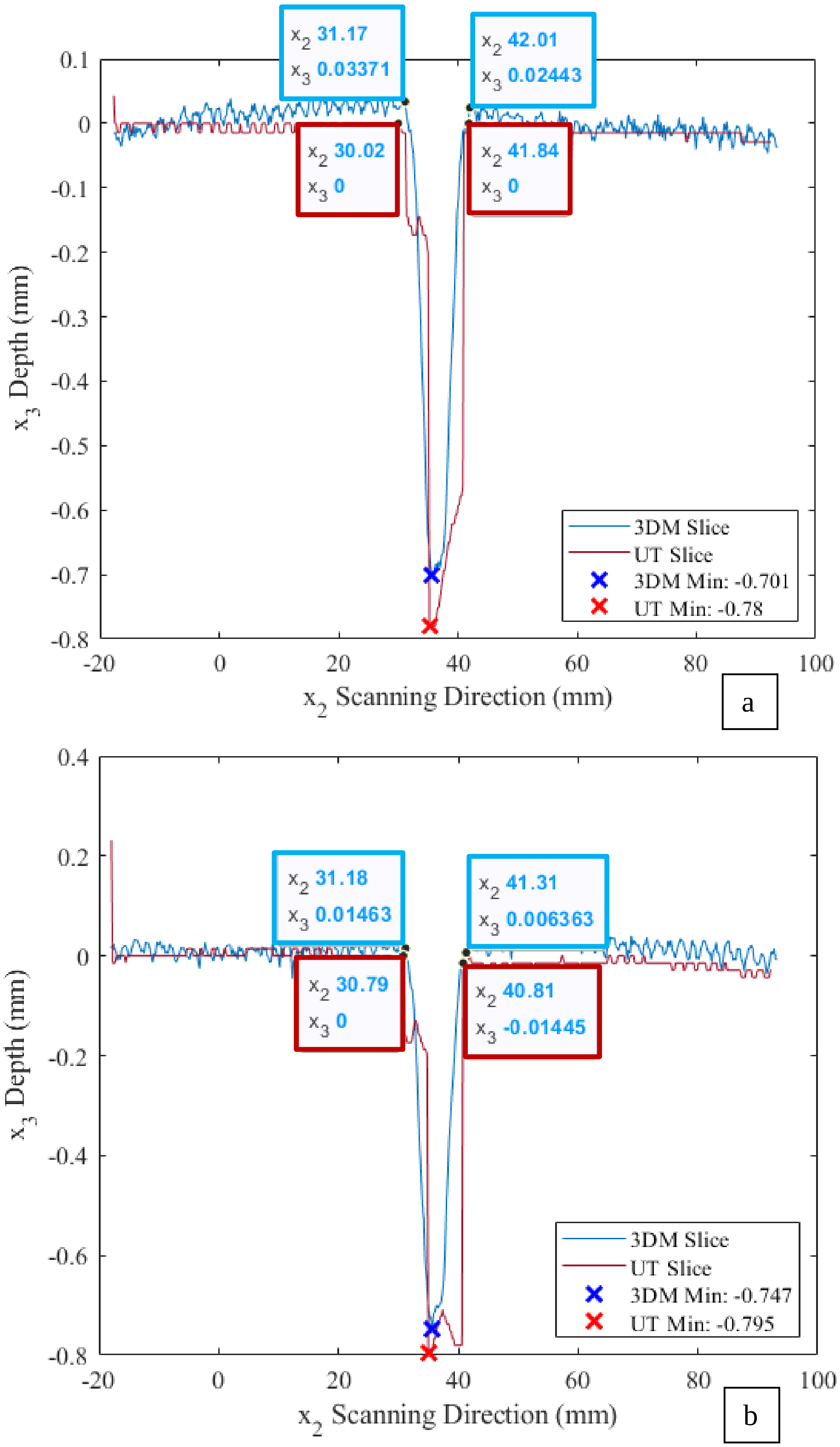

Figure 4.14, a) Slice comparison of the wrinkle at 20 mm, and b) slice comparison of the wrinkle at 40 mm. The minimum values represent the height of the wrinkle and the other points are used to find the width.

Table 4.3 Measured Values of the Out-of-Plane Wrinkles Study 3

Slice Position	Dimension	3D Microscope (mm)	Ultrasound (mm)	Relative Error (%)	Absolute Error
20 mm Slice	Height	0.73	0.78	6.84	0.0499 mm
	Width	10.84	11.82	9.04	0.98 mm
	Intensity	0.0337	0.033	2.02	0.00068
40 mm Slice	Height	0.758	0.788	3.99	0.0303 mm
	Width	10.13	10.02	1.09	0.11 mm
	Intensity	0.0374	0.0378	1.1	0.00041

4.2.4 Part 2 Out-of-Plane Wrinkle Study 4

As stated above, Part 2 was made using the two-step curing process, but the six hour delay for gelation was not implemented. This laminate was manufactured using a an expired laminating resin system designed for opened molding unlike the infusion resin in the part above. The wrinkle for this laminate was made using a wedge mold of the same size as was used for manufacturing Part 1. One noticeable difference for the data that is presented in this section is the tracking of the wrinkle across the lamina is very clean and uniform. There are only a few areas where the tracking algorithm fails, similar to the previous results. The reason for why the signal is clearer for this lamina plot is uncertain and is an opportunity for future work.

The b-scan with bounded lamina of interest can be seen in Figure 4.15a, and the points selected in that bounded region are in Figure 4.15b. Figure 4.16 is the 3D ultrasound lamina plot created using the points selected in the previous figure.

The same 3D microscope scan of the mid plane was preformed on Part 2. In Figure 4.17 the 3D microscope and 3D ultrasound laminas have been superimposed and aligned upon each other. Slices at 20 mm and 40 mm are taken for this study and are compared in the same manner as seen in the previous studies. Figure 4.18a and b are the slices with the data points collected. Table 4.4 displays the results for the comparison and the error calculations. The results do not correlate as well as the data from the first 3 studies, but despite this their absolute errors are still very small.

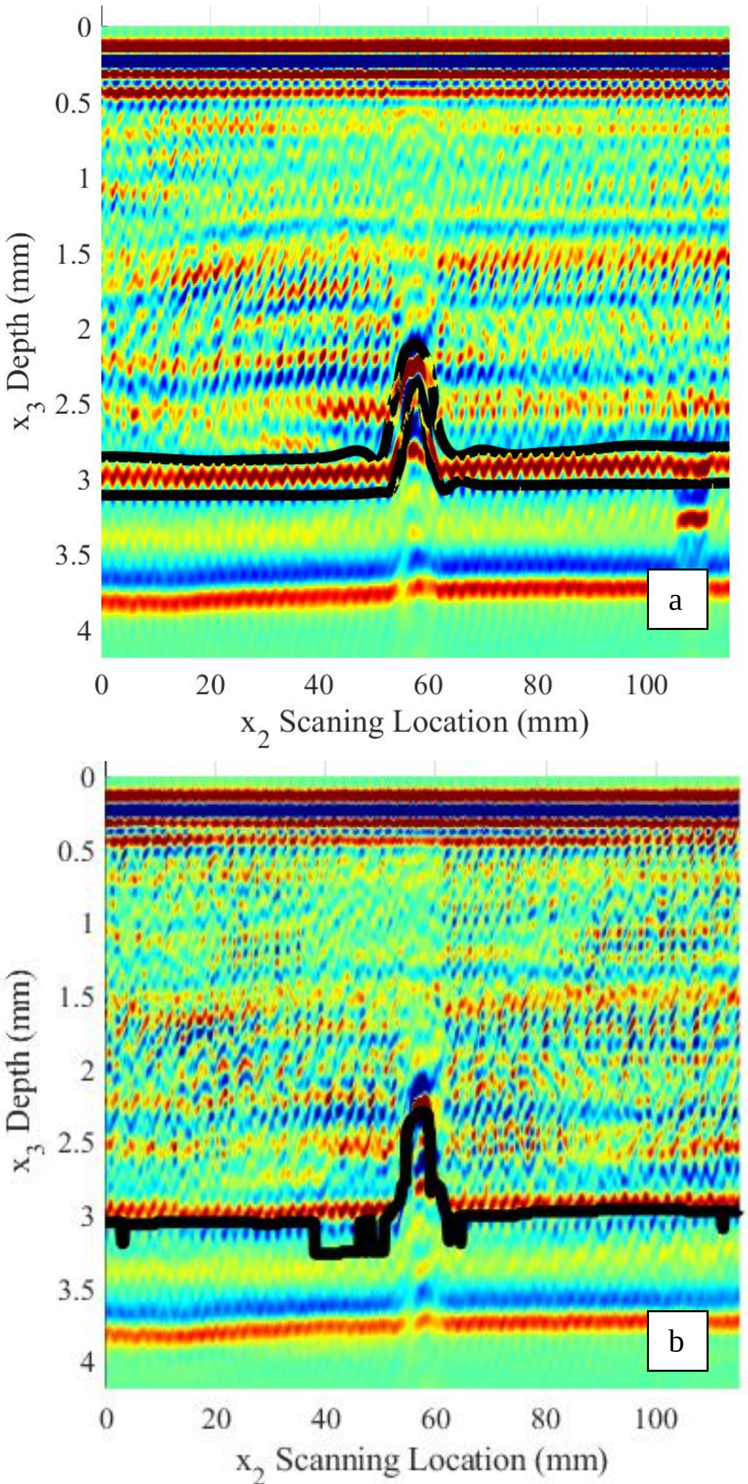

Figure 4.15, a) B-scan of Part 2 showing the bounded lamina of interest, b) b-scan showing the selected maximum intensities between the bounded region. The extra intensity on the right side of a) corresponds to one of the markers placed and shows up because the b-scan is an average of 10 b-scans.

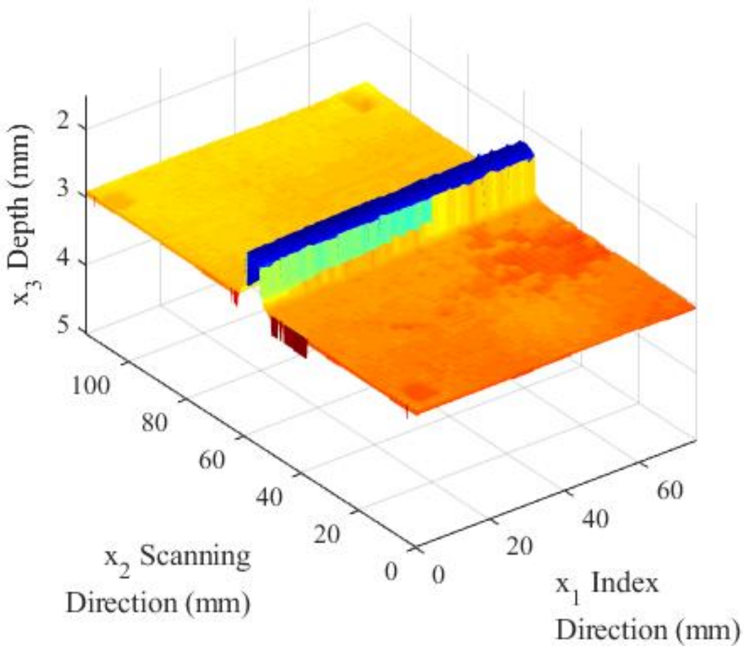

Figure 4.16, Part 2 3D ultrasound lamina plot from the scan data.

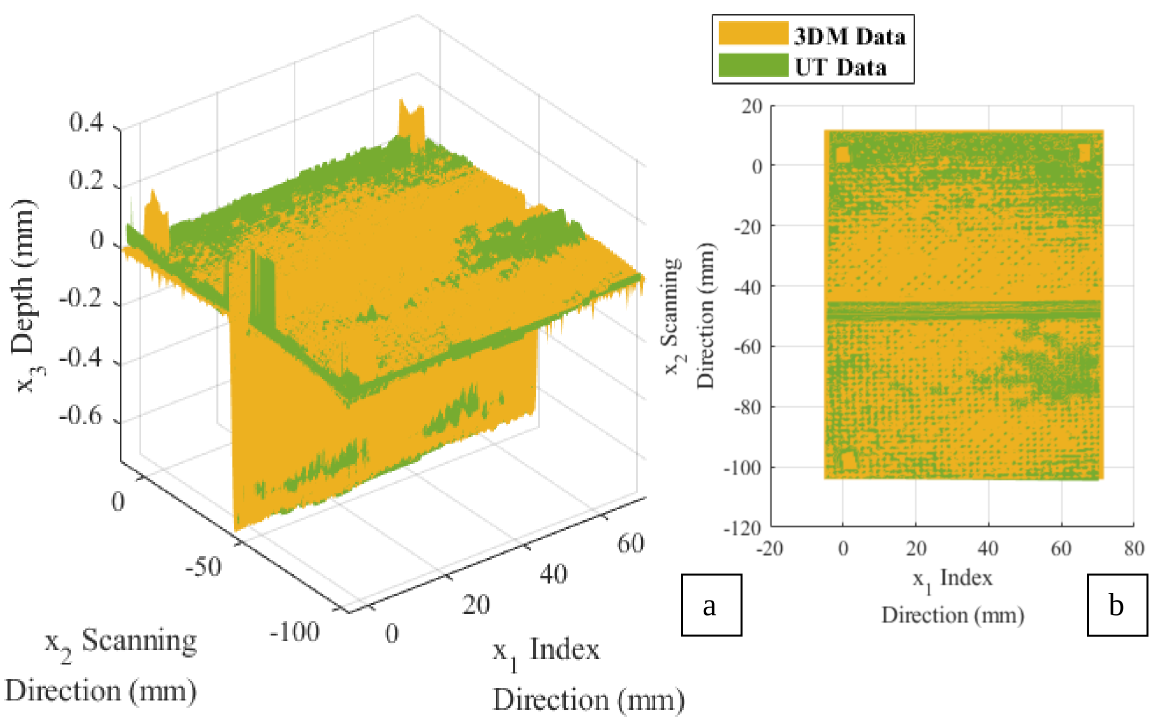

Figure 4.17, Superimposed alignment of the 3D ultrasound lamina with 3D microscope lamina, a) isometric view, and b) top view.

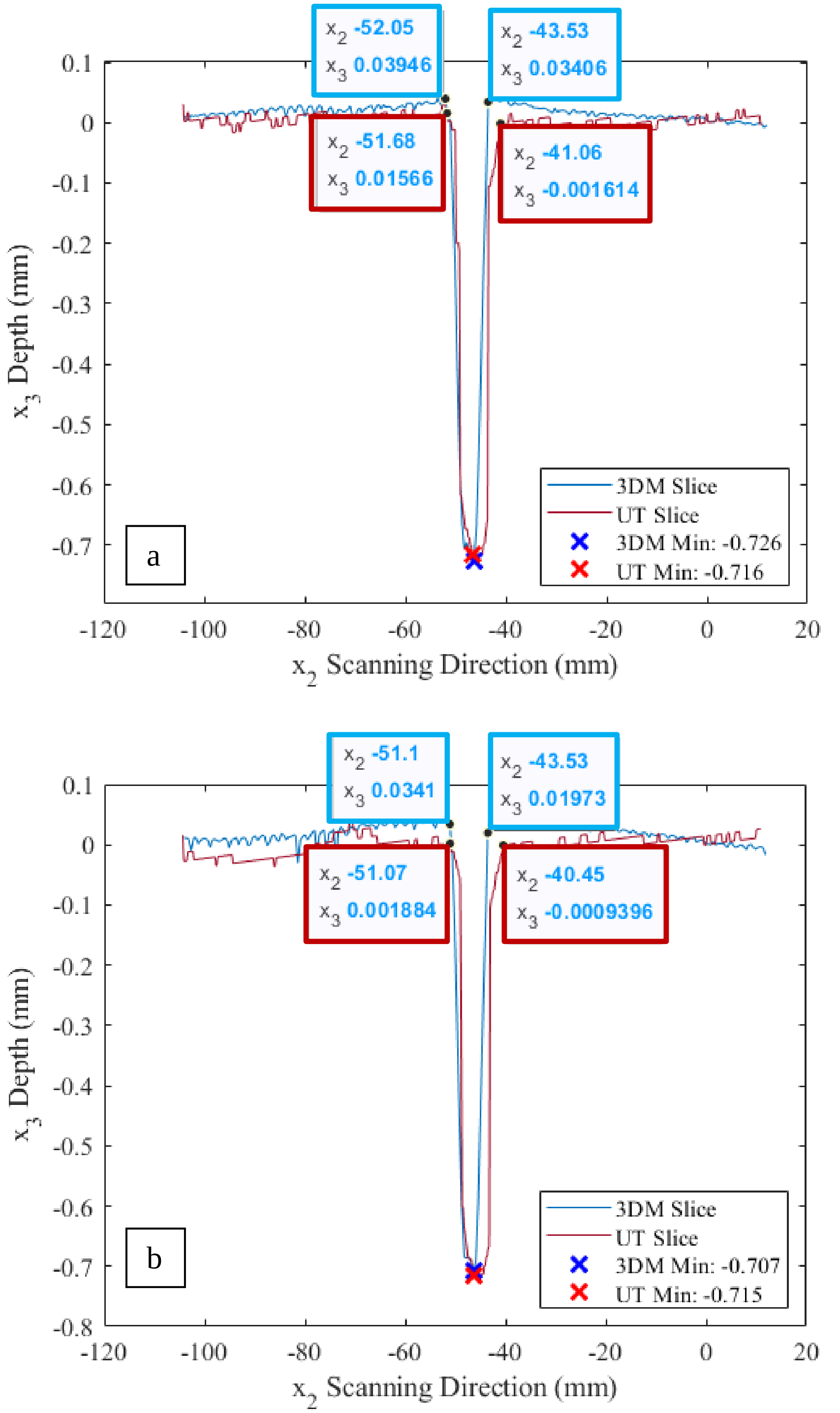

Figure 4.18, a) Slice comparison of the wrinkle at 20 mm, and b) slice comparison of the wrinkle at 40 mm. The minimum values represent the height of the wrinkle and the other points are used to find the width.

Table 4.4 Measured Values of the Out-of-Plane Wrinkles Study 4

Slice Position	Dimension	3D Microscope (mm)	Ultrasound (mm)	Relative Error (%)	Absolute Error
20 mm Slice	Height	0.73	0.78	6.34	0.047 mm
	Width	7.57	10.62	40.3	3.05 mm
	Intensity	0.049	0.038	24.19	0.0117
40 mm Slice	Height	0.76	0.72	5.2	0.04 mm
	Width	8.52	10.82	27	2.3 mm
	Intensity	0.045	0.035	21.3	0.0095

4.2.5 Part 3 Out-of-Plane Wrinkle Study 5

The final study is of Part 3 a laminate made using the VARTM process and the wrinkle was made using the fold method in one layer. The reason for showing Part 3 is that it does not have the slightly resin rich region where the two cured halves came together as in Part 1 and 2. This region provides an unrealistically strong ultrasonic reflection, which allows for easy detection of the wrinkle. Composites used in industry are not typically made with a two-step curing process as done in this work, but the two-step method does provide a good means to create a wrinkle of a known size that can be measured without destroying the laminate.

Part 3 is scanned with the 10 MHz 12.7 mm diameter focused. Figure 4.19 is a b-scan showing the bounded wrinkle of interest within the laminate with the strongest intensity. The wrinkle is tracked using the same process as was used for the last four studies. Figure 4.20 is the 3D ultrasound lamina plot of the wrinkle across the scanning area. A unique feature of this wrinkle is that it tapers off midway through the scan, this is different from the other wrinkles which were consistent across the scan area. There are still issues with the tracking algorithm, but most of them are not near the wrinkle itself.

A slice of the wrinkle was taken at 10 mm, Figure 4.21, and the approximate height was 0.304 mm and the width was 15.45 mm. From this an approximate intensity can be found for the wrinkle of 0.01. These values cannot be validated without another means of authentication either by CT or by cutting the sample and using microscopy. Though based on the first three studies of this chapter the confidence in these results is strong for them representing the size of the wrinkle within the laminate. Figure 4.22 shows the downward slope of the wrinkle intensity across the scan area. There is a little spike at 20 mm which is the result of a small spike at that location, but overall it captures the fading of the wrinkle through the laminate.

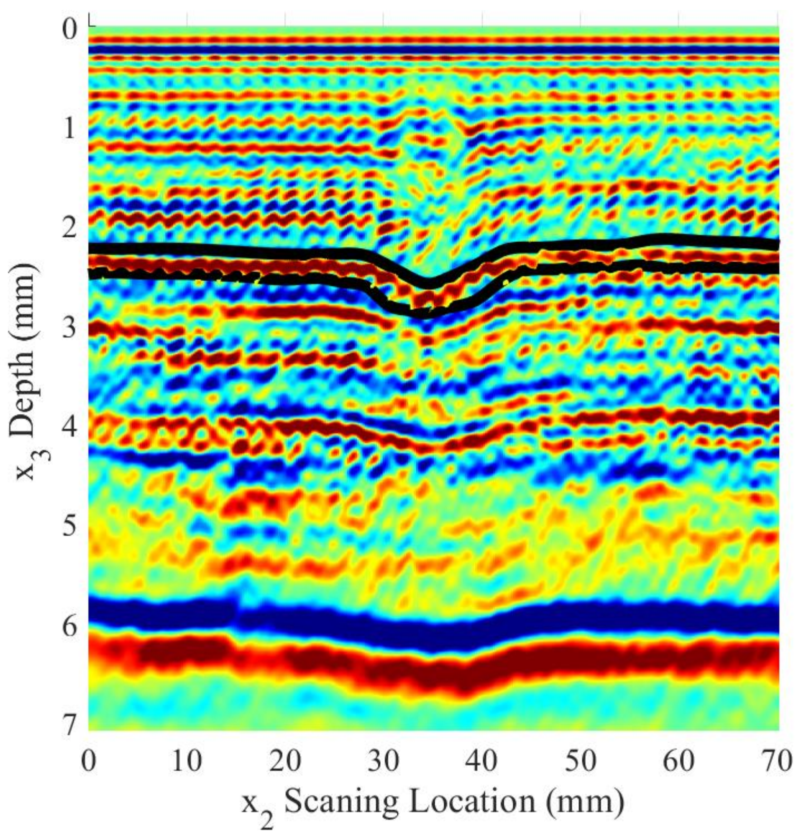

Figure 4.19, B-scan of Part 3 showing the bounded lamina of interest containing the out-of-plane wrinkle.

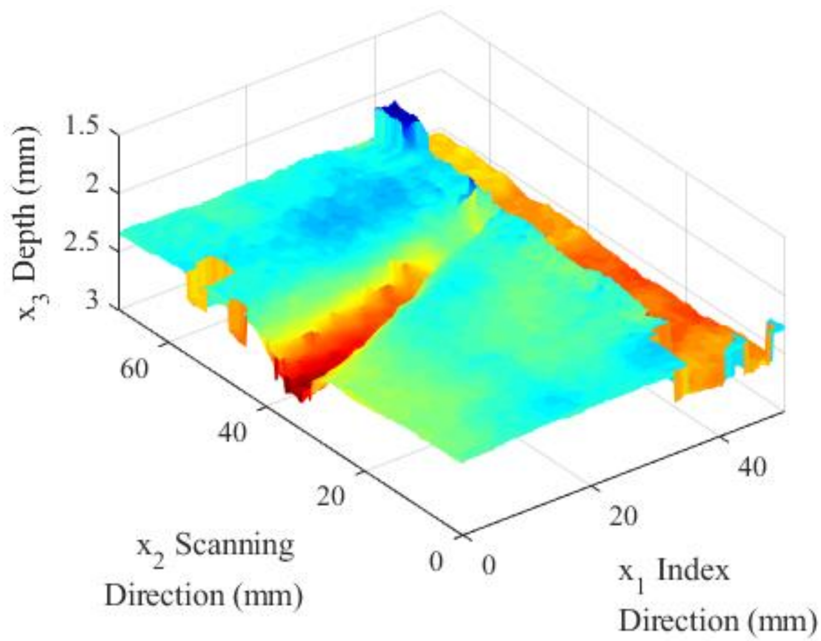

Figure 4.20, Part 3 3D ultrasound lamina plot from the scan data.

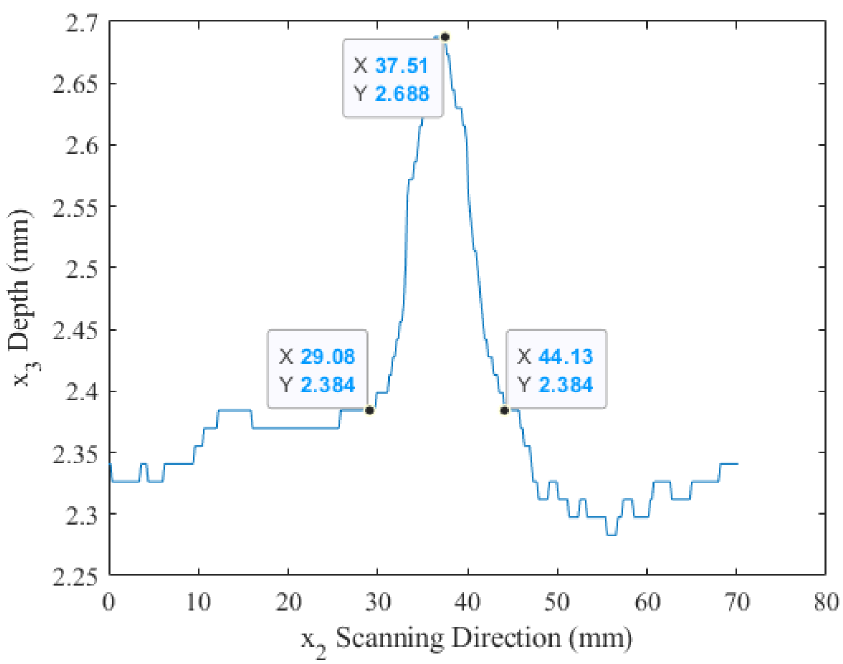

Figure 4.21, Slice of the 3D ultrasound lamina plot of the wrinkle at 10 mm, with the selected points to measure the wrinkle.

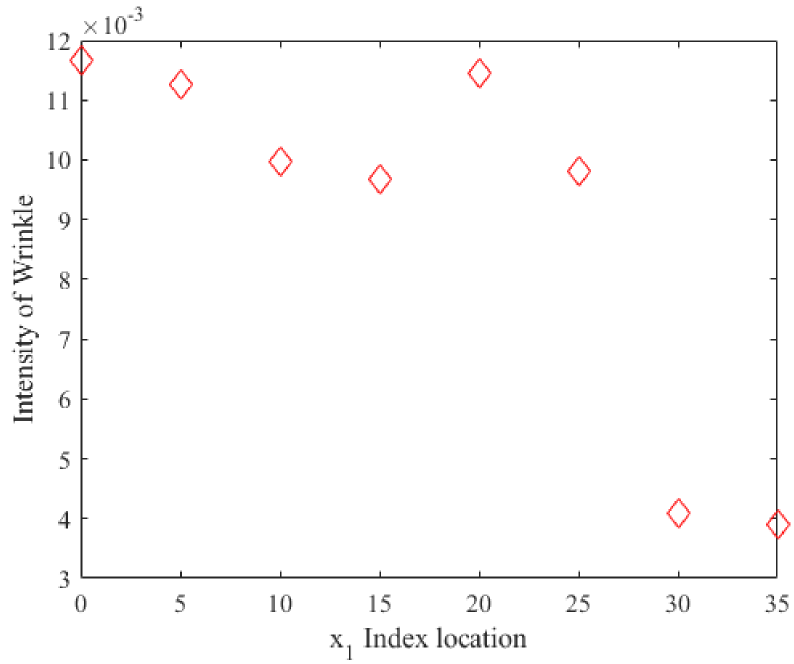

Figure 4.22 Plot of the intensity at various points along the wrinkle as it disappears

4.3 Results Comparison to Similar Research

There are not many works of research out demonstrating their ability characterize a wrinkle with its height, width, and intensity except for the work in [6]. In this section a simple comparison of their results to ours will be shown. An average relative and average absolute error are found for the data presented in [6]. Table 4.5 displays the errors for the height (H), width (W) and intensity (I) for the first three studies done in this chapter with the errors from [6].

From this comparison the data collected is in good standing with that of current research. A one for one comparison cannot be made between the two data sets as the results from [6] come from a different material system and some different postprocessing techniques are used. A notable difference would be the scale of the absolute error in this study as compared to the work in [6], for the height it is under 1 mm as compared to 5.75

mm in [6]. This work used an automated process to track the wrinkle across the scan area in order to characterize it, in [6] a manual process was used to measure the wrinkle off of b-scans. The automated tracking method provides quicker wrinkle size approximation over a scan area rather manually comparing b-scans. Another difference between the works is that they reported the max angle of the wrinkle, and this was not considered in this work.

Table 4.5 Relative Error (RE) and Absolute Error (AB) Comparison for Height (H), Width (W) and Intensity (I) from the Current Work and the Work in [6]

	Study 1		Study 2		Study 3		Data [6]	
	RE (%)	AE	RE (%)	AE	RE (%)	AE	RE (%)	AE
H	3.87	0.0283 mm	6.95	0.051 mm	6.84	0.0499 mm	10.8	0.575 mm
W	3.87	0.42 mm	7.56	0.82 mm	9.04	0.98 mm	13.5	5.75 mm
I	8.057	0.0027	15.71	0.0053	2.02	0.00068	16.3	0.013
H	3.99	0.0303 mm	3.92	0.03 mm	3.99	0.0303 mm	-	-
W	1.09	0.11 mm	4.06	0.39 mm	1.09	0.11 mm	-	-
I	5.14	0.0019	4.23	0.0017	1.1	0.00041	-	-

4.4 Approximate Stiffness Reductions

In Chapter One the stiffness reduction caused by out-of-plane wrinkles in a sample composite were discussed. A similar discussion will be presented here using the wrinkle intensity sizes found from studies 1 to 3. As in the Chapter One discussion the Hsaio-Daniel model for effect of fiber wrinkles on stiffness will be used [5][9]. This model is based on unidirectional composites unlike the woven composites in this work. The intensities found will be plotted to show how much they could potentially reduce the stiffness in the fiber direction of a unidirectional composite.

Figure 4.23 is the normalized stiffness verses the intensity as found in the Hsiao-Daniel model. The intensities found for the first three studies above ranged from 0.034 to 0.04. These two values will be plotted along with the mean value of 0.0365 on the normalized E11 curve in Figure 4.23. From this figure and these values there is a potential 55 to 60 % stiffness reduction in the fiber direction with wrinkles of the same intensity as were found in this study. This is an approximation and helps to give a good idea as to the affect small wrinkles can have on a composite structure.

In [7] wrinkle intensity versus normalized stiffness is modeled for a cross ply laminate, which means alternating 0°/90° unidirectional layers. This is closer to the layups used in this study as the plain weave fabric has fibers in both directions. When the intensities that were used above are compared with the plots in [7] about a 2 to 5 % reduction in stiffness is seen. In [8] a model for wrinkle stiffness versus wrinkle intensity is plotted for quasi-isotropic laminates. Using the intensities from above results in approximately 15 to 20% stiffness reduction. The models from these to works provide a closer approximation of the potential stiffness reduction for a composite with an out-of-plane wrinkle of similar size as is found in this work.

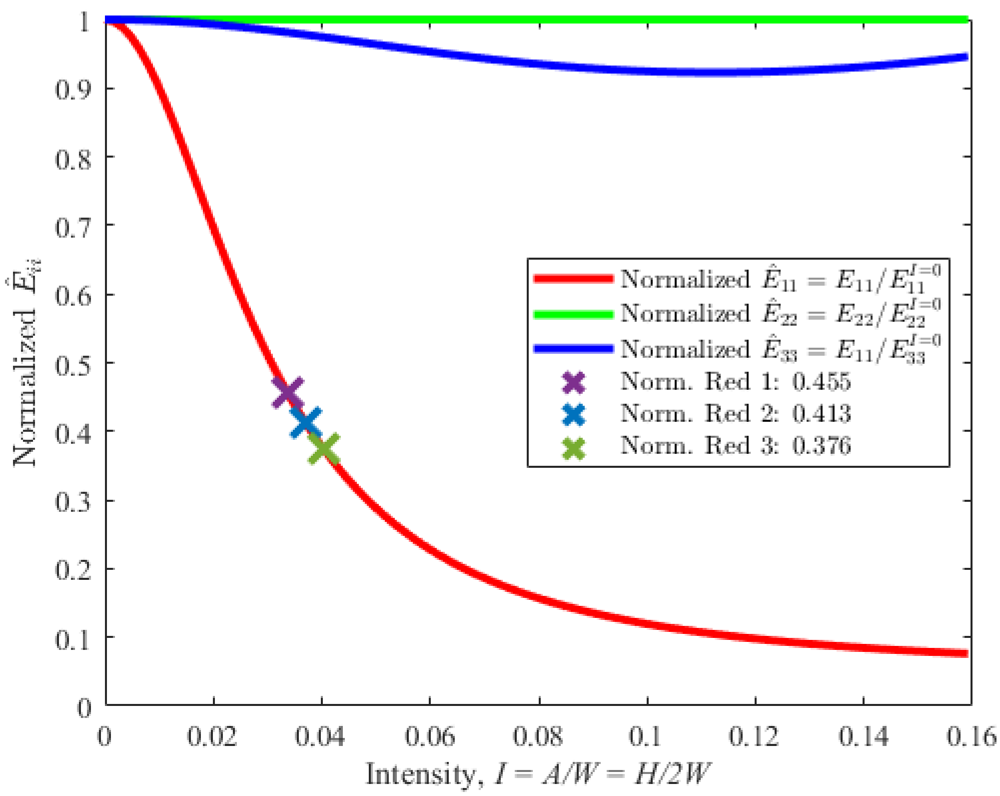

Figure 4.23, Hsiao-Daniel model for stiffness reduction for composites with out-of-plane wrinkles. Three values of intensity for the wrinkles found in the above studies have been plotted, showing the potential reductions from wrinkles of this size.

CHAPTER FIVE

Conclusion

5.1 Conclusion

The research within this work focused on the development of ultrasonic characterization of out-of-plane wrinkles within woven composites with 3D microscopy validation. Out-of-plane wrinkles and the ability to characterize them is a key interest to industry, see e.g. [2][3][4]. Characterization of wrinkles would improve the ability to approve and fail laminates used in industry. Though there is still more work needing to be done on determining the acceptable threshold for the wrinkle intensities and in improving manufacturing processes to reduce the occurrence of wrinkles.

The fist main accomplishment of this work involved the manufacturing of woven carbon fiber laminates with embedded out-of-plane wrinkles. This process was developed over many iterations of experimentation with different manufacturing methods. One of the challenges was how to embed a wrinkle of a known size, this was achieved by development of the two-step hot press manufacturing process. The process enables the creation of an out-of-plane wrinkle during the first cure stage, which can then be measured using a 3D microscope. The 3D microscope data provides an accurate characterization of the wrinkle which was used to validate the ultrasound data acquired.

The second accomplishment of this work is the modification of the bond line detection algorithm for use with wrinkle detection. The algorithm was developed by Ben Blandford and was modified in this work to incorporate an individual a-scan tracking of the wrinkle lamina across the scan area. The previous work took averages over sections of scans. The result of this modification was a detailed 3D ultrasound lamina representing the out-of-plane wrinkle within the laminate. As mentioned in [40][41] and in Chapter Four the tracking algorithm has some issues with tracking the desired lamina across the scan area. Despite this limitation a 3D representation of the wrinkles could be generated with good detail.

The final accomplishment of this work was to validate the out-of-plane wrinkle size as was characterized by the 3D ultrasound lamina. This validation was done by aligning the 3D microscope lamina with the 3D ultrasound lamina and then comparing slices at selected points. From the investigation of three different ultrasonic transducers the avg relative errors for the height, width, and intensity were 4.92%, 4.45% and 6.04% respectively. The average absolute errors were 0.0366 mm, 0.4717 mm and 0.0021, respectively.

These results show good correlation between the two sets of scan data of the wrinkle. Providing a promising future for the method discussed in this work to be used in the study and characterization of out-of-plane wrinkles. The method is not perfect and has room for improvement and refining.

5.2 Future Work

The potential for future work in regard to wrinkle detection is very open with many opportunities to pursue. The main areas of focus should be in improved fabrication of laminates with wrinkles, improved ultrasonic scanning techniques, and improved post processing of the scan data.

5.2.1 Improved Fabrication of Laminates with Out-of-Plane Wrinkles

For improvements in the fabrication of laminates with out-of-plane wrinkles there are few avenues to pursue. One is in the use unidirectional prepregs to make the laminates instead of the dry woven fabric, this would provide an opportunity for the work to be better correlated to other research in this area. The use of prepregs is also cleaner than wet layup fabrication. Changing the resin system used in the wet layup process from an infusion resin to a resin designed for open molding should be considered. There are differences in these resin systems, but as to their effect on the detection and fabrication of wrinkles it is uncertain.

A second area interest would be to improve the two-step manufacturing process and possibly remove it all together. A potential improvement could be to have the two halves of the wet lamina approach gelation at the same time. Then around the six hour mark apply the wrinkle mold to one lamina stack to induce the waviness for a short time. Remove the wrinkle mold and set the second stack of lamina on top and cure in the hot press together. The thought behind this approach would be the removal of the slightly resin rich region in between the two-step cure process which stands out in the b-scans. Another consideration is to manufacture a wrinkled composite as described in this work, but instead of using the 3D microscope to scan the midplane scan the entire part with the new CT system that is available. Varying the wrinkle wedge used to embed the wrinkle should be considers as they can come in a variety of shapes and sizes.

A final manufacturing consideration would be to make molds for making curved composite panels, as molds seem to be a major cause of wrinkles forming. Molds would be compatible with the VARTM and hot press manufacturing methods. They would help to simulate more realistic parts as seen in industry as well similar to Figure 1.5 the curved part from NDE labs. The future integration of robotics into the ultrasonic scanning process will improve the accessibility to scan curved composites removing the limitations of freedom in the current immersion system.

5.2.2 Improved Ultrasonic Scanning Techniques

Phased array scanning has huge potential for improving wrinkle detection within composites. This technology was not fully investigated for this work because of the late addition of it during the research. A current researcher within the team has been investigating the use sectoral scanning using phased array and the result with wrinkles is very impressive. One of the struggles of this work was the detection of the slopes of the wrinkles, in his preliminary results he is showing almost full definition of the slopes of the wrinkle. The b-scans show a consistent intensity for the lamina of interest containing the wrinkle.

Another area of focus with phased array would be the integration of full matrix capture (FMC) and the total focusing method (TFM). These two methods were talked about in Chapter One and have been shown by other researchers as good tools for investigating composites and wrinkles. These two methods were used in conjunction in the work by Larrañaga-Valsero showing good results for wrinkle characterization [6]. The difficulty for integrating these techniques will be developing the codes needed to fire the phased array in the FMC configuration and for handling the postprocessing of the data using the TFM. There are other works out there about these methods which can be used as starting points, see e.g. ([6] [27][37][49]).

5.2.3. Improving the Post Processing Techniques

Along with incorporating the TFM into the post processing of the ultrasonic scans, there should be some focus on improving the algorithm that tracks a bounded intensity across the scan area. As noted in Chapter Four this is an area of improvement for the wrinkle tracking work presented here. Applying some of the techniques from the previous section to improve the ultrasound scans could improve the quality of the 3D ultrasound lamina generated.

5.3 Concluding Remarks

The study of wrinkles within composites is an important topic of interest to researchers and those in industry. The ability to detect wrinkles and accurately characterize them is important for moving forward with how to handle composites affected by them. Knowing the actual size of a wrinkle could help to prevent parts in industry that have small wrinkles from being scrapped providing potential cost savings to manufacturers. This work presented preliminary research on detecting and characterizing out-of-plane wrinkles within woven composites using ultrasonic nondestructive evaluation with validation using 3D microscopy. The technology in this work is a building block to improving the detection of wrinkles within composites.

BIBLIOGRAPHY

[1] Barbero EJ. Introduction to Composite Materials Design. Milton, UNITED KINGDOM: Taylor & Francis Group; 2017.

[2] Georgeson GE, Bingham JP, HONG HT, Wu Y-J, Pryor JM, FIENI SL, et al. Wrinkle Characterization and Performance Prediction for Composite Structures Using Ultrasonic and Optical Inspection. EP3315961A1, 2018.

[3] Thompson JG, Georgeson GE, Holmes TM, Tat HH. Infrared Thermographic Methods for Wrinkle Characterization in Composite Structures. US9519844B1, 2016.

[4] Grewal NS, Georgeson GE, Bingham JP, Morris JD, Basu S. Methods for Measuring Out-of-Plane Wrinkles in Composite Laminates. US10605781B2, 2020.

[5] Hsiao HM, Daniel IM. Elastic properties of composites with fiber waviness. Composites Part A: Applied Science and Manufacturing 1996;27:931–41. https://doi.org/10.1016/1359-835X(96)00034-6.

[6] Larrañaga-Valsero B, Smith RA, Tayong RB, Fernández-López A, Güemes A. Wrinkle Measurement in Glass-Carbon Hybrid Laminates Comparing Ultrasonic Techniques: A Case Study. Composites Part A: Applied Science and Manufacturing 2018;114:225–40. https://doi.org/10.1016/j.compositesa.2018.08.014.

[7] Zhu J, Wang J, Zu L. Influence of Out-of-Plane Ply Waviness on Elastic Properties of Composite Laminates Under Uniaxial Loading. Composite Structures 2015;132:440–50. https://doi.org/10.1016/j.compstruct.2015.05.062.

[8] Takeda T. Micromechanics Model for Three-Dimensional Effective Elastic Properties of Composite Laminates With Ply Wrinkles. Composite Structures 2018;189:419–27. https://doi.org/10.1016/j.compstruct.2017.10.086.

[9] Zhang C. Modeling of Flexible Fiber Motion and Prediction of Material Properties. Thesis. 2011.

[10] Kulkarni P, Mali KD, Singh S. An Overview of The Formation of Fibre Waviness and its Effect on the Mechanical Performance of Fibre Reinforced Polymer Composites. Composites Part A: Applied Science and Manufacturing 2020;137:106013. https://doi.org/10.1016/j.compositesa.2020.106013.

[11] Weber TA, Englhard M, Arent J-C, Hausmann J. An Experimental Characterization of Wrinkling Generated During Prepreg Autoclave Manufacturing Using Caul Plates. Journal of Composite Materials 2019;53:3757–73. https://doi.org/10.1177/0021998319846556.

[12] Krumenacker N, Madra A, Hubert P. Image-Based Characterization of Fibre Waviness in a Representative Vacuum-Bagged Corner Laminate. Composites Part A: Applied Science and Manufacturing 2020;131:105774. https://doi.org/10.1016/j.compositesa.2020.105774.

[13] Wu C, Gu Y, Luo L, Xu P, Wang S, Li M, et al. Influences of In-Plane and Out-of-Plane Fiber Waviness on Mechanical Properties of Carbon Fiber Composite Laminate. Journal of Reinforced Plastics and Composites 2018; 37:877–91. https://doi.org/10.1177/0731684418765981.

[14] Wang J, Potter K, Hazra K, Wisnom M. Experimental Fabrication and Characterization of Out-of-Plane Fiber Waviness in Continuous Fiber-Reinforced Composites. Journal of Composite Materials 2012;46:2041–53. https://doi.org/10.1177/0021998311429877.

[15] Pham DC, Cui X, Karuppiah A, Lua J. Compressive Failure Modeling of Composites with Defects. AIAA Scitech 2019 Forum, American Institute of Aeronautics and Astronautics; n.d. https://doi.org/10.2514/6.2019-1544.

[16] Bender JJ, Hallett SR, Lindgaard E. Parametric Study of The Effect of Wrinkle Features on The Strength of a Tapered Wind Turbine Blade Sub-Structure. Composite Structures 2019;218:120–9. https://doi.org/10.1016/j.compstruct.2019.02.065.

[17] Guzman-Maldonado E, Wang P, Hamila N, Boisse P. Experimental and Numerical Analysis of Wrinkling During Forming of Multi-Layered Textile Composites. Composite Structures 2019;208:213–23. https://doi.org/10.1016/j.compstruct.2018.10.018.

[18] Moezzi M, Haji-Badali A, Barez F. Analysis of the Wrinkle Geometry of the Woven Fabrics During Uniaxial Bias Extension Test Using Ricker Wavelet Algorithm. Composites Part A: Applied Science and Manufacturing 2021;141:106230. https://doi.org/10.1016/j.compositesa.2020.106230.

[19] Farnand K, Zobeiry N, Poursartip A, Fernlund G. Micro-Level Mechanisms of Fiber Waviness and Wrinkling During Hot Drape Forming of Unidirectional Prepreg Composites. Composites Part A: Applied Science and Manufacturing 2017;103:168–77. https://doi.org/10.1016/j.compositesa.2017.10.008.

[20] Lightfoot JS, Wisnom MR, Potter K. A New Mechanism for the Formation of Ply Wrinkles Due to Shear Between Plies. Composites Part A: Applied Science and Manufacturing 2013;49:139–47. https://doi.org/10.1016/j.compositesa.2013.03.002.

[21] Hsiao HM, Daniel IM. Effect of Fiber Waviness on Stiffness and Strength Reduction of Unidirectional Composites Under Compressive Loading. Composites Science and Technology 1996;56:581–93. https://doi.org/10.1016/0266-3538(96)00045-0.

[22] Mizukami K, Mizutani Y, Todoroki A, Suzuki Y. Detection of In-Plane and Out-of-Plane Fiber Waviness in Unidirectional Carbon Fiber Reinforced Composites Using Eddy Current Testing. Composites Part B: Engineering 2016;86:84–94. https://doi.org/10.1016/j.compositesb.2015.09.041.

[23] Mizukami K, Mizutani Y, Kimura K, Sato A, Todoroki A, Suzuki Y. Detection of In-Plane Fiber Waviness in Cross-Ply CFRP Laminates Using Layer Selectable Eddy Current Method. Composites Part A: Applied Science and Manufacturing 2016; 82:108–18. https://doi.org/10.1016/j.compositesa.2015.11.040.

[24] Wu D, Cheng F, Yang F, He W. Non-Destructive Testing of Carbon-Fiber-Reinforced Plastics with a PCB-Based T-R Probe. Composite Structures 2020;240:112080. https://doi.org/10.1016/j.compstruct.2020.112080.

[25] Smith RA, Nelson LJ, Mienczakowski MJ, Wilcox PD. Ultrasonic Analytic-Signal Responses from Polymer-Matrix Composite Laminates. IEEE Transactions on Ultrasonics, Ferroelectrics, and Frequency Control 2018;65:231–43. https://doi.org/10.1109/TUFFC.2017.2774776.

[26] Nelson LJ, Smith RA, Mienczakowski M. Ply-Orientation Measurements in Composites Using Structure-Tensor Analysis of Volumetric Ultrasonic Data. Composites Part A: Applied Science and Manufacturing 2018;104:108–19. https://doi.org/10.1016/j.compositesa.2017.10.027.

[27] Pain D, Drinkwater BW. Detection of Fibre Waviness Using Ultrasonic Array Scattering Data. J Nondestruct Eval 2013;32:215–27. https://doi.org/10.1007/s10921-013-0174-z.

[28] X3000 Industrial 3D X-Ray Inspection System | North Star Imaging n.d. https://4nsi.com/systems/x3000 (accessed June 24, 2021).

[29] Tayong RB, Mienczakowski MJ, Smith RA. 3D Ultrasound Characterization of Woven Composites, Provo, Utah, USA: 2018, p. 130008. https://doi.org/10.1063/1.5031603.

[30] Zardan JP, Gueudré C, Corneloup G. Study of Induced Ultrasonic Deviation for the Detection and Identification of Ply Waviness in Carbon Fibre Reinforced Polymer. NDT & E International 2013;56:1–9. https://doi.org/10.1016/j.ndteint.2013.02.001.

[31] Zhang Z, Guo S, Li Q, Cui F, Malcolm AA, Su Z, et al. Ultrasonic Detection and Characterization of Delamination and Rich Resin in Thick Composites with Waviness. Composites Science and Technology 2020;189:108016. https://doi.org/10.1016/j.compscitech.2020.108016.

[32] Ambrozinski L, Mrowka J, O'Donnell M, Pelivanov I. Detection and Imaging of Local Ply Angle in Carbon Fiber Reinforced Plastics Using Laser Ultrasound and Tilt Filter Processing. Composites Part A: Applied Science and Manufacturing 2019;126:105581. https://doi.org/10.1016/j.compositesa.2019.105581.

[33] Smith RA, Nelson LJ, Mienczakowski MJ, Challis RE. Automated Analysis and Advanced Defect Characterisation From Ultrasonic Scans of Composites. Insight: Non-Destructive Testing & Condition Monitoring 2009;51:82–7. https://doi.org/10.1784/insi.2009.51.2.82.

[34] Fernández-López A, Larrañaga-Valsero B, Guemes A. Wrinkle Characterization In Composite Laminates Using Phased Array. n.d. 6th International Symposium on NDT in Aerospace 2014. https://www.ndt.net/search/docs.php3?id=16970&msgID=0&rootID=0 (accessed June 19, 2021).

[35] Smith RA, Nelson LJ, Mienczakowski MJ, Wilcox PD. Ultrasonic Tracking of Ply Drops in Composite Laminates. AIP Conference Proceedings 2016;1706:050006. https://doi.org/10.1063/1.4940505.

[36] Nelson LJ, Smith RA. Three-Dimensional Fibre-Orientation Characterisation in Monolithic Carbon-Fibre Composites. 11th European Conference on Non-Destructive Testing (ECNDT 2014), October 6-10, 2014, Prague, Czech Republic.

[37] Holmes C, Drinkwater BW, Wilcox PD. Post-Processing of The Full Matrix of Ultrasonic Transmit–Receive Array Data for Non-Destructive Evaluation. NDT & E International 2005;38:701–11. https://doi.org/10.1016/j.ndteint.2005.04.002

[38] Xie N, Smith RA, Mukhopadhyay S, Hallett SR. A Numerical Study on The Influence of Composite Wrinkle Defect Geometry on Compressive Strength. Materials & Design 2018;140:7–20. https://doi.org/10.1016/j.matdes.2017.11.034.

[39] Hsiao K-T, Heider D. 10 - Vacuum Assisted Resin Transfer Molding (VARTM) in Polymer Matrix Composites. In: Advani SG, Hsiao K-T, editors. Manufacturing Techniques for Polymer Matrix Composites (PMCs), Woodhead Publishing; 2012, p. 310–47. https://doi.org/10.1533/9780857096258.3.310.

[40] Blandford B. Nondestructive Inspection and Quantification of Carbon Fiber Laminates for Barely Visible Impact Damage and Adhesive Layer Thickness Measurements. Dissertation. 2020.

[41] Blandford B. Analysis of Adhesive Bond Thickness Between Carbon Fiber Laminated Composites Using an Ultrasonic C-scan Technique. Journal Paper, Pending Review.

[42] Schemerr Jr LW. Fundamentals of Ultrasonic Nondestructive Evaluation: A Modeling Approach. 2nd ed. Springer International Publishing; 2016. https://doi.org/10.1007/978-3-319-30463-2.

[43] Olympus, Ultrasonic Transducers Technical Notes. 2019.

[44] What is an Array? | Olympus IMS n.d. https://www.olympus-ims.com/en/ndt-tutorials/transducers/what-array/ (accessed June 14, 2021).

[45] Olympus. Focus PC UT and Phased Array Data Acquisition and Analysis Software, Advanced User’s Manual, Software Version 1.0. Revision B, February 2017.

[46] Blackman NJ, Jack DA, Blandford BM. Improvement in the Quantification of Foreign Object Defects in Carbon Fiber Laminates Using Immersion Pulse-Echo Ultrasound. Materials 2021;14:2919. https://doi.org/10.3390/ma14112919.

[47] Weisstein EW. Euler Angles n.d. https://mathworld.wolfram.com/EulerAngles.html (accessed June 14, 2021).

[48] Weisstein EW. Direction Cosine n.d. https://mathworld.wolfram.com/DirectionCosine.html (accessed June 14, 2021).

[49] Grager J-C, Schrapp M, Mooshofer H, Sause MGR, Zelenyak A-M, Große CU. Ultrasonic Imaging of Carbon Fiber-Reinforced Plastics Using the Full Matrix Capture Data Acquisition Technique. 19th World Conference on Non-Destructive Testing 2016 https://www.ndt.net/search/docs.php3?id=19483&msgID=0&rootID=0 (accessed June 23, 2021).